

LONG WAVES IN NARROW ENCLOSED BASINS

A THESIS SUBMITTED TO  
THE GRADUATE SCHOOL OF NATURAL AND APPLIED SCIENCES  
OF  
MIDDLE EAST TECHNICAL UNIVERSITY

BY

ONUR BARAN TEKİN

IN PARTIAL FULFILLMENT OF THE REQUIREMENTS  
FOR  
THE DEGREE OF MASTER OF SCIENCE  
IN  
CIVIL ENGINEERING

SEPTEMBER 2012

Approval of the thesis:

**LONG WAVES IN NARROW ENCLOSED BASINS**

submitted by **ONUR BARAN TEKİN** in partial fulfillment of the requirements for the degree of **Master of Science in Civil Engineering Department, Middle East Technical University** by,

Prof. Dr. Canan Özgen \_\_\_\_\_  
Dean, Graduate School of **Natural and Applied Sciences**

Prof. Dr. Güney Özcebe \_\_\_\_\_  
Head of Department, **Civil Engineering**

Prof. Dr. Ahmet Cevdet Yalçiner \_\_\_\_\_  
Supervisor, **Civil Engineering Dept., METU**

**Examining Committee Members:**

Prof. Dr. Ayşen Ergin \_\_\_\_\_  
Civil Engineering Dept., METU

Prof. Dr. Ahmet Cevdet Yalçiner \_\_\_\_\_  
Civil Engineering Dept., METU

Assoc.Prof. Dr. Utku Kanoğlu \_\_\_\_\_  
Engineering Sciences Dept., METU

Dr. Işıkhan Güler \_\_\_\_\_  
Civil Engineering Dept., METU

Civil Engineer Dr. Bergüzar Öztunalı \_\_\_\_\_  
Ministry of Transport, Maritime Affairs and Communications

**Date:** 14.09.2012

**I hereby declare that all information in this document has been obtained and presented in accordance with academic rules and ethical conduct. I also declare that, as required by these rules and conduct, I have fully cited and referenced all material and results that are not original to this work.**

Name, Last name : Onur Baran Tekin

Signature :

## **ABSTRACT**

### **LONG WAVES IN NARROW ENCLOSED BASINS**

Tekin, Onur Baran

M.S., Department of Civil Engineering

Supervisor: Prof. Dr. Ahmet Cevdet Yalçın

September 2012, 94 pages

In this study, numerical modeling of landslide generated tsunami waves in closed basins and their mechanisms are presented. Historical landslide generated tsunamis are investigated and also the governing parameters affecting impulse wave parameters are studied. The numerical model is based on the solution of nonlinear form of the long wave equations with respect to related initial and boundary conditions. In order to validate the outputs of the modeling by NAMIDANCE, empirical formulation is applied to the same cases as the numerical model and the results are discussed. The numerical model is then applied to Pervari Dam artificial reservoir as a case study to investigate the effects of potential landslide into the reservoir. The outputs of the numerical model are compared with empirical formulation results for different approaches of modeling the landslide effect in water body. The critical sections are observed for overtopping and maximum wave amplitude values and the results are discussed.

Keywords: Tsunami, subaerial landslide, tsunami modeling, tsunami simulation, NAMIDANCE

## ÖZ

### DAR KAPALI HAVZALARDA UZUN DALGALAR

Tekin, Onur Baran

Yüksek Lisans, İnşaat Mühendisliği Bölümü

Tez Yöneticisi: Prof. Dr. Ahmet Cevdet Yalçiner

Eylül 2012, 94 sayfa

Bu çalışmada, kapalı havzalarda heyelan sonucunda oluşan depreşim dalgalarının sayısal modellemeleri ve mekanizmaları sunulmaktadır. Tarihte oluşan heyelan kaynaklı depreşim dalgaları incelenmiş ve ayrıca dalga parametrelerini etkileyen ana parametreler çalışılmıştır. Sayısal model doğrusal olmayan uzun dalga denklemlerinin başlangıç ve sınır koşulları içerisinde çözümü üzerine kurulmuştur. NAMI-DANCE ile yapılan modellemenin doğrulanması için, sayısal modelin uygulandığı bütün durumlara ampirik yöntem de uygulanmış ve sonuçlar tartışılmıştır. Sayısal model daha sonra durum çalışması olarak Pervari Baraj gölüne, gölde oluşan bir potansiyel heyelanın etkilerini çalışmak için uygulanmıştır. Sayısal modelin çıktıları, heyelanın su kütlesi üzerindeki etkisini modellemek için yapılan farklı yaklaşımlar için ampirik yöntem sonuçlarıyla karşılaştırılmıştır. Kritik noktalar incelenerek, barajın üzerinden aşma ve maksimum dalga yüksekliği değerleri ve sonuçlar tartışılmıştır.

Anahtar Kelimeler: Tsunami, heyelan, modelleme, benzetim, NAMI DANCE

*To my family.*

## ACKNOWLEDGEMENTS

I would like to express my sincere gratitude to my supervisor Prof. Dr. Ahmet Cevdet Yalçın for his guidance, encouragement, sharing his knowledge and experience throughout the study.

I would also like to thank my colleagues and supervisors at Enerjisa Enerji Üretim A.Ş for sharing their knowledge, expertise, data and giving their support on and off the study.

Dr. Andrey Zaytsev and Dr. Anton Chernov are kindly acknowledged for their efforts and success on development of the simulation and visualization code NAMI-DANCE.

Last, but not least, I would like to express my deepest thanks to my parents, my sister and especially my love Ekin for their patience and endless support.

## TABLE OF CONTENTS

ABSTRACT .....	iv
ÖZ.....	v
ACKNOWLEDGEMENTS .....	vii
TABLE OF CONTENTS .....	viii
LIST OF TABLES .....	x
LIST OF FIGURES.....	xi
LIST OF SYMBOLS .....	xiv
CHAPTER 1 INTRODUCTION .....	1
CHAPTER 2 LITERATURE REVIEW .....	4
CHAPTER 3 HISTORICAL EVENTS .....	19
CHAPTER 4 SUBAERIAL LANDSLIDE GENERATED TSUNAMIS .....	27
CHAPTER 5 COMPARISON OF NUMERICAL MODEL WITH EMPIRICAL FORMULATIONS.....	32
5.1 Model Set – Up.....	33
5.2 Empirical Formulation.....	34
5.3 Numerical Modeling.....	35
5.3.1 Numerical modeling with NAMI-DANCE without Flux .....	36
5.3.2 Numerical modeling with NAMI-DANCE with Flux .....	39
5.3.3 Numerical modeling with NAMI-DANCE with vertical coastal slope ( $\alpha =90^\circ$ ) .....	42
5.4 Determination maximum wave amplitude with empirical formulation .	47

5.5	Comparison of maximum wave amplitudes obtained from numerical modeling.....	47
5.6	Comparison of maximum wave amplitudes obtained from numerical modeling and empirical formulation.....	49
5.7	Alternative Flux & Initial Wave Conditions .....	50
CHAPTER 6 A CASE STUDY: LANDSLIDE IN PERVARI DAM RESERVOIR .....		55
6.1	History of Earthquakes in the Region.....	57
6.2	Landslide into the Pervari Dam Reservoir .....	58
6.3	Modeling with NAMI-DANCE.....	60
6.3.1	Bathymetry & Mapping .....	60
6.3.2	Modeling of the landslide case for Pervari Dam.....	61
6.3.3	Simulation & discussion of the results.....	64
6.4	Comparison of model outputs with empirical formula results .....	74
6.5	High resolution simulation of Landslide at Pervari Dam.....	77
CHAPTER 7 DISCUSSIONS AND CONCLUSIONS .....		84
REFERENCES.....		88

## LIST OF TABLES

Table 5-1 - Input data of the bathymetry & landslide, used for comparison .....	36
Table 5-2 - Maximum wave amplitudes by empirical formulation .....	47
Table 5-3 – $H_{\max}$ Value from Modeling & Empirical Formulation for each case.	49
Table 5-4 - $\varepsilon$ of maximum wave amplitude values .....	50
Table 6-1 - List of nearby earthquakes in the last century ( <a href="http://www.sayisalgrafik.com.tr/deprem">http://www.sayisalgrafik.com.tr/deprem</a> ) .....	58
Table 6-2 – Estimated landslide and determined coastal slope parameters .....	59
Table 6-3 - Gauge Point Coordinates and their Water Depth .....	61
Table 6-4 – Determined initial water surface parameters .....	63
Table 6-5 – Comparison of model outputs with empirical relation results .....	75
Table 6-6 - $\varepsilon$ of maximum wave amplitude values .....	75
Table 6-7 – Gauge points used in 1m grid size simulation .....	78

## LIST OF FIGURES

Figure 3-1 - Map of the North Atlantic Ocean showing the location of the 1929 Grand Banks earthquake epicenter (Fine et al., 2005). .....	20
Figure 3-2 - Picture of the Pontesei dam and artificial reservoir, the 1959 landslide is clearly visible in the upper part of the picture (Panizzo et al., 2005).....	21
Figure 3-3 - Sections of the Vajont valley before and after 9 October 1963 landslide (Semenza, 2002). .....	22
Figure 3-4 - Map of south-central Alaska with the rupture zone of the MW 9.2 1964 Great Alaska earthquake (Plafker, 1969). .....	23
Figure 3-5 - Photographs of the building site before and after the accident (Assier-Rzadkiewicz et al., 2000). .....	24
Figure 3-6 - Geographic map of central-southern Italy, showing the location of the Aeolian archipelago (Tinti et al., 2005). .....	26
Figure 4-1 – Principal phases in the phenomenon of subaerial landslide generated waves (Panizzo, 2004).....	28
Figure 4-2 – Landslide generated tsunami parameters (Heller & Hager, 2010)...	29
Figure 4-3 – Different types of impulse waves (Noda, 1970).....	30
Figure 5-1 - Cross-section of the inclined coastal slope (1/3) set-up.....	33
Figure 5-2 - Cross-section of the vertical coastal slope set-up .....	33
Figure 5-3 – Top view of the set-ups .....	34
Figure 5-4 - The layout of the experiments. (Panizzo et. al., 2005).....	35
Figure 5-5 - Sketch of the physical model used to study the run up of landslide generated water waves on plane slopes. (Panizzo et. al., 2005).....	35
Figure 5-6 – Change of $H_{max}$ along propagation distance for different initial wave lengths without flux.....	37

Figure 5-7 - Change of $H_{\max}$ along propagation distance for different initial wave lengths without flux.....	38
Figure 5-8 - Change of $H_{\max}$ along propagation distance for different initial wave lengths without flux.....	39
Figure 5-9 - Change of $H_{\max}$ along propagation distance for initial wave amplitudes with flux.....	40
Figure 5-10 - Change of $H_{\max}$ along propagation distance for initial wave amplitudes with flux.....	41
Figure 5-11 - Change of $H_{\max}$ along propagation distance for the case of vertical coastal slope ( $\alpha =90^\circ$ ).....	43
Figure 5-12 - Change of $H_{\max}$ along propagation distance for the case of vertical coastal slope ( $\alpha =90^\circ$ ).....	44
Figure 5-13 - Change of $H_{\max}$ along propagation distance for the case of vertical coastal slope ( $\alpha =90^\circ$ ).....	45
Figure 5-14 - Change of $H_{\max}$ along propagation distance for the case of vertical coastal slope ( $\alpha =90^\circ$ ).....	46
Figure 5-15 - Change of $H_{\max}$ along propagation distance for alternative initial wave conditions without flux .....	52
Figure 5-16 - Change of $H_{\max}$ along propagation distance for alternative initial wave conditions with flux .....	53
Figure 6-1 - Project Location .....	56
Figure 6-2 – Project Layout (Intertechne & Temelsu, 2009).....	56
Figure 6-3 - Cross-Section of the Dam Body.....	57
Figure 6-4 - Location of nearby Earthquakes ( <a href="http://www.sayisalgrafik.com.tr">www.sayisalgrafik.com.tr</a> ) .....	58
Figure 6-5 – Landslide layout from Google Earth View .....	59
Figure 6-6 – The locations of the Gauge points to observe time histories of water level fluctuations at different locations of the dam reservoir.....	60
Figure 6-7 – Initial water surfaces for cases (a), (b), (c) & (d).....	64
Figure 6-8 – Maximum wave amplitude distributions along the reservoir for the four cases.....	66

Figure 6-9 - Maximum wave amplitude distributions near dam body location for the four cases .....	67
Figure 6-10 – Location of chosen gauge points .....	68
Figure 6-11 – Time histories of water surface fluctuations at gauge points .....	69
Figure 6-12 – Time histories of water surface fluctuations at gauge points .....	70
Figure 6-13 – Time histories of water surface fluctuations at gauge points .....	71
Figure 6-14 – Time histories of water surface fluctuations at gauge points .....	72
Figure 6-15 – Time histories of water surface fluctuations at gauge points .....	73
Figure 6-16 – Map of 1m resolution domain .....	77
Figure 6-17 – Location of the gauges used in 1m grid size simulation .....	78
Figure 6-18 - Time change of wave amplitude at the gauges for 1m grid size simulations .....	79
Figure 6-19 – Time change of wave amplitude at the gauges for 1m grid size simulations .....	80
Figure 6-20 – Time change of current speeds at selected gauge points.....	81
Figure 6-21 – Time change of wave amplitude at the current speeds at selected gauge points.....	82

## LIST OF SYMBOLS

$t_s^*$	non dimensional time of underwater landslide motion
$w$	landslide width
$h$	landslide height
$v$	impact velocity
$d$	local water depth
$\alpha$	ramp inclination angle
$H_{\max}$	maximum wave height/amplitude
$\theta$	angle from landslide velocity vector
$r$	distance from landslide impact point
$T_{\max}$	wave period of maximum wave
$r_u$	runup
$\gamma$	slope inclination angle
$g$	gravitational acceleration
$T$	wave period
$H$	wave height/amplitude
$V$	landslide volume
$\rho$	density of the fluid
$Fr$	Froude number
$s$	slide thickness
$L_p$	the distance of slope from the impact point

Other parameters are clearly defined whenever applicable.

## **CHAPTER 1**

### **INTRODUCTION**

Tsunamis are large water waves triggered by a sudden disturbance of the ocean floor or the ocean surface, which is usually caused by earthquakes, landslides or volcanic eruptions (Panizzo, 2004).

The term tsunami comes from the Japanese, meaning "harbor" (tsu) and "wave" (nami) combined "harbor waves". Tsunami waves can travel at speeds up to 800 kilometers per hour with wave periods varying from minutes to hours and wave lengths up to several hundreds of kilometers. As they propagate through shallow water their wave heights increase and they become very destructive.

Although tsunamis are generated mostly by earthquakes, landslides are the second most common causes of tsunamis, and landslides generated by subaerial landslides will be investigated in this study.

Creation of a reservoir against an unstable or potentially unstable slope may both affect its stability and increase the consequences of failure. With the reservoir full, or being filled, the risk increases from that of slope failure into a valley to that of failure into a body of water. In the event of rapid failure, impulse waves from reservoir landslides may overtop and damage the dam, and can have effects beyond the confines of the reservoir. This can endanger public safety over a large area adjacent to the reservoir and downstream from it. (ICOLD Bulletin 124, 2002).

Artificial reservoirs are particularly susceptible to the damaging effects of landslide generated impulse waves. A prediction method for their characteristics is, therefore, vital for hazard assessment for existing and planned reservoirs (Bruggemann, 2012). The tragedy caused by Vajont landslide on October 9, 1963 proved that landslide generated tsunamis are one the most important hazards. 270 million cubic meters, slide with 30m/s slide velocity entered into newly filled Vajont reservoir resulting in a maximum wave height of nearly 210 meter, which overtopped the dam and destroyed most of the town Longarone and parts of other towns in Piave Valley. The concrete arch dam survived with little damage but the incident killed over 2000 people. (ICOLD Bulletin 124, 2002).

There are a number of methods that can be used to predict the effects of potential landslides, which are briefly explained in Chapter 4 of this study. Numerical modeling using computer programs seems to be the most efficient and economical way for determining the wave parameters of impulse waves. Code named NAMI-DANCE ver. 5.6 which simulates and animates tsunami generation and propagation based on the solution of nonlinear form of the long wave equations with respect to related initial and boundary conditions is used in Chapter 5 & 6 of this study to predict the effects of a potential landslide in an artificial, closed basin.

This study consists of 7 chapters. In Chapter 1 an introduction and brief information about the landslide generated tsunamis is given.

In Chapter 2, literature survey giving information about previous efforts of understanding the landslide generated tsunamis is presented.

In Chapter 3, some of the important historical tsunamis and their catastrophic effects are mentioned.

In Chapter 4, information is given about the subaerial landslide generated tsunamis and parameters affecting this are presented.

In Chapter 5, the numerical model which is generated by NAMI-DANCE is tried to be verified by an empirical formulation and the outputs of this effort is given. A number of trial simulations are performed and the outputs are compared between themselves and with empirical formulation.

In Chapter 6, the model is applied to the artificial reservoir of Pervari Dam for the determination of wave parameters at critical points and the possibility of overtopping is observed. Four cases are taken into account for the modeling of the tsunami and again the results are discussed.

In Chapter 7, conclusion and the general discussions are presented.

## **CHAPTER 2**

### **LITERATURE REVIEW**

Tsunamis can occur from different sources such as; landslides, rock falls, snow avalanches, ice falls and glacier calvings and these waves can be a threat for a dam as they may overtop the dam crest or cause floods in upstream and downstream. In this thesis, a landslide generated tsunami in a dam reservoir is studied. In the literature there are a number of studies on the mechanism and the modeling of landslide generated waves which mainly focus on wave generation, wave propagation, wave run-up stages and most of these studies are supported with comparison of results by regenerating past events and experimental studies. Some of these works are mentioned below.

Fritz et. al. (2003), used digital particle image velocimetry (PIV) in a physical model based on Froude similarity to investigate landslide impact and wave generation in landslide generated waves. Velocity vector are recorded using PIV and this data is used for understanding the wave generation. For the modeling of the landslides an artificial granular material is used.

Montagna et al. (2011) used FLOW-3D, a fully three-dimensional Computational Fluid Dynamics commercial code based on the VOF technique for the treatment of the free surface to make a numerical modeling of tsunamis generated by landslides falling along the flank of a conical island. The results of this numerical modeling are compared with experimental data for the validation and the accuracy of the model and computational costs are estimated. The case study is inspired the tsunamis generated by the landslide that took place in the island named “Sciara del Fuoco” and attacked the coast of the island of Stromboli.

The CFD code FLOW-3D solves the Reynolds Averaged Navier-Stokes equations and the continuity equation for incompressible flow along with the true volume of fluid method in order to compute the free surface motion and also consider a very crucial aspect which is the interaction between moving objects and the fluid. Montagna et al. used Renormalization group (RNG) model of FLOW-3D's many techniques of modeling turbulence stresses, to reproduce the experiments of Di Risio et al. (2009). Authors compared these results and concluded that; the model reproduces the typical behavior of the frequency dispersive waves, crest and trough amplitudes, run-up and run-down trends and also the features of wave propagation (i.e. arrival time of the crest, wave height, wave period etc.), especially in the areas that are away from the generation area. The authors also concluded that the computational costs are acceptable.

Italian dam register RID (Registro Italiano Dighe) funded a research program and Panizzo et al. (2005) studied three real cases of subaerial landslides which fell down Italian artificial reservoirs (1959 Pontesei, 1960 and 1963 Vajont). Panizzo et al. (2005) used experimental, numerical and mathematical studies, to forecast the principal parameters of landslide generated waves as a function of assumed parameters of the falling landslide and the water body.

These 4 formulations are derived in Panizzo et al. (2005);

$$t_s^* = 0.43 \left( \frac{wh}{d^2} \right)^{-0.27} \left( \frac{v}{\sqrt{gd}} \right)^{-0.66} (\sin\alpha)^{-1.92} \quad (1)$$

$$\frac{H_{max}}{d} = 0.07 \left( \frac{t_s^*}{A_w^*} \right)^{-0.45} (\sin\alpha)^{-0.88} \exp(0.6 \cos \theta) \left( \frac{r}{d} \right)^{-0.44} \quad (2)$$

$$T_{max} \sqrt{\frac{g}{d}} = 2.50 t_s^{*-0.22} (\sin\alpha)^{-0.25} \left( \frac{r}{d} \right)^{0.17} \quad (3)$$

$$\frac{r_u}{d} = 1.37 \left( \frac{H_{max}}{d} \right)^{1.51} \left( T_{max} \sqrt{\frac{g}{d}} \right)^{0.47} (\sin\gamma)^{0.26} \quad (4)$$

where  $t_s^*$  is the non-dimensional time of underwater landslide motion,  $w$  is the landslide width,  $h$  is the landslide height,  $d$  is the local water depth,  $v$  is the landslide velocity,  $g$  is the gravitational acceleration,  $\alpha$  is the ramp inclination angle,  $H_{\max}$  is the maximum wave height in the distant shore and  $T_{\max}$  is its wave period,  $A_w^*$  is the non-dimensional parameter ( $A_w^* = wh/d^2$ ),  $\theta$  is the angle from landslide velocity vector,  $r$  is the distance from impact point,  $r_u$  is the wave run-up and  $\gamma$  is the slope inclination angle at the distant shore.

By using these formulations, for the first time the period  $T$  of the incident impulse water wave has been considered as influencing factor.

Panizzo et al. (2005) then applied these formulations to the real cases of landslide generated tsunami events in Italy, and compared the results with the real parameters. The study got useful information about the generated impulse waves by using the set of empirical formulations defined by the carried out experimental studies even though the selected real cases presented values of the involved parameters outside the experimented ranges. In the considered three real cases occurred in the Pontesei and the Vajont artificial reservoirs, both the maximum generated wave height  $H_{\max}$  and the wave runup  $r_u$ , estimated by using empirical formulations showed good satisfactorily agreement with the values deduced from the literature.

Geist et al. (2009) used Cornell University Long and Intermediate Wave Modeling package (COULWAVE), a long and intermediate wave modeling package based on the non-linear Boussinesq equations, to stimulate the generation, propagation and run-up of the waves generated by three possible failure scenarios for the Currituck landslide along the North American Atlantic offshore margin. The study is aimed to determine the importance of bottom friction and wave breaking on the wave evolution of tsunamis. In the study; first tsunami generation and propagation are calculated for three possible failure

scenarios, then using each of the scenarios two critical parameters for the local tsunami: duration of landslide failure and bottom friction of the continental shelf a sensitivity analysis is conducted. Also it is determined whether significant energy propagates at oblique angles to the slide axis the regional propagation of the tsunami over a much larger area and finally a very high-resolution 1D propagation and runup model is carried out to accurately model dispersion, nonlinearity, and wave breaking as the tsunami propagates across the continental shelf.

The simulations showed that volume of the landslide, initial acceleration and the duration of the vertical movement are the primary source parameters that affect wave heights whereas variations in failure duration does not has an important effect. It is also understood that, the bottom friction along the continental shelf and near shore region is the primary hydrodynamic parameter. By using the high-resolution 1D simulation; the effect that wave breaking and combined influence of dispersion and nonlinearity (described by the Boussinesq equations) has on near shore propagation and runup are revealed.

In their study, Cecioni and Bellotti (2010) extended a numerical model based on depth integrated mild slope equation (MSE), which is ideal for the small amplitude tsunamis in the far field, to reproduce the generation and propagation of landslide generated waves. The results obtained by the model are compared to experimental data obtained from the physical modeling of the landslide generated tsunamis falling on the flank of Stromboli Island.

The writers concluded that a correct reproduction of wave generation and propagation by using a model is based on the linear MSE is only possible in deep water conditions and for small sea bottom vertical variation. So in the study a modified MSE is derived, which includes a source term achieved by assuming the time variation of the water depth function, induced by a submarine earthquake or landslide and verified this MSE by using the physical model.

To investigate the physical features of a landslide generated tsunami propagating along a plane beach, Sammarco and Renzi (2008) developed a forced two-horizontal-dimension analytical model and compared the results with available experimental data.

The features of the waves are analyzed using the model and it is seen that, the wave motion starts to be trapped at the shoreline and finally only transient long shore travelling edge waves are present. It is also discovered that longer waves travel faster and are followed by a tail of shorter waves, while new crests are created. The writes conclude that; the larger waves in landslide generated and propagating in sloping beach are shifted toward the middle of the wave train unlike transient waves in constant depths. Using the experimental data acquired from the studies of Di Risio et al. (2008), the model is validated.

In the wake of devastating 1998 Papua New Guinea tsunami, Bardet et al. (2003) summarized the state-of-the-art knowledge on underwater landslides and their potential to generate tsunamis from the multidisciplinary perspectives of observational and engineering seismology, geotechnical engineering, marine geology, and hydrodynamics to have a better understanding the hazards from underwater landslides, the extents of their potential damage and to make recommendations on future researches and assist planners in mitigating their risks.

For better understanding of landslide generated tsunamis the critical items are defined as; i) Modeling Earthquake Ground Motions and Source Characteristics, ii) Modeling Landslides in Geotechnical Engineering, iii) Conducting Post-tsunami Field Surveys, iv) Making studies on Past, Present, and Future Potential Tsunamis and v) To have a better understanding on the Mechanism of Tsunami Generation by Landslides.

In the study it is concluded that; underwater landslide tsunamis are definite hazards to the world coastlines, no comprehensive model covers all aspects of landslide induced tsunamis from source mechanism to coastal inundation, research must be carried out urgently so as to reduce the risks on the population and industrial developments and landslide tsunamis require multidisciplinary studies.

Assier-Rzadkiewicz et al. (2000) used a numerical model on the basis of the shallow water approximation to simulate the tsunami generated by a 10 million m<sup>3</sup> landslide in Nice new harbor extension on 16th of October 1979 during land filling operations. The authors investigated previous models applied to this specific event and concluded that these previous analyses used rough approximate methods and produced models which did not conveniently fit data. They also compared the results of the modeling with the observed data from witnesses.

In the study two numerical models developed, one for the tsunami propagation, the other for the landslide considered as the flow of a viscous fluid. The characteristic wavelengths are considerably larger than the water depth and that the slide thickness is much smaller than the characteristic slide length. In the model, the sea-bottom deformation is used as input data.

To model the tsunami, depth-averaging the equations of mass and momentum conservation leads to the following governing equations:

$$\frac{\partial h}{\partial t} + \frac{\partial}{\partial x} (hu) + \frac{\partial}{\partial y} (hv) \quad (5)$$

$$\frac{\partial}{\partial t} (hu) + \frac{\partial}{\partial x} (hu.u) + \frac{\partial}{\partial y} (hu.v) = -\frac{1}{2} \frac{\partial}{\partial x} (gh^2) + gh \frac{\partial d}{\partial x} \quad (6)$$

$$\frac{\partial}{\partial t} (hv) + \frac{\partial}{\partial x} (hv.u) + \frac{\partial}{\partial y} (hv.v) = -\frac{1}{2} \frac{\partial}{\partial y} (gh^2) + gh \frac{\partial d}{\partial y} \quad (7)$$

where  $u(u, v)$  is the depth-averaged horizontal velocity, where  $d(x, y, t)$  is the bathymetry and is related to  $h$  by  $h(x, y, t) = d(x, y, t) + \eta(x, y, t)$ ,  $\eta(x, y, t)$  being the water surface elevation.

For landslide modeling, it is assumed that the whole mass suddenly loses its equilibrium and for simplicity, the landslide is considered as a viscous fluid flowing down the slope under gravity forces without dilution, erosion and deposition.

The results of the model showed that inundation observed in front of the airport could be created by an underwater landslide of about 10 millions of  $m^3$  but using witnesses' observations and the negative wave recorded by tide gages, it seems impossible that this landslide is responsible of the entire observed tsunami. The total involved volume of the 1979 slide has been estimated at about 150 millions of  $m^3$ .

Poisson and Pedreros (2010) used a modified version of GEOWAVE, which can take properly into account the decreasing tsunami wavelength near shore through a system of nested grids, to model the generation and propagation of two historical landslide-induced tsunamis that reached the coasts of the French Lesser Antilles. A tsunami hit the Martinique coast down the western flank of Montagne Pel'ee at the beginning of the big eruption of May 1902 and then more recently, the northeastern coast of Guadeloupe was affected by a tsunami that had been generated around Montserrat by pyroclastic flows entering the sea, during the July 2003 eruption of the Soufriere Hills volcano. In the study, two source hypotheses are considered for each case and reported tsunami height data are used to verify the results obtained from the numerical modeling.

Parameters like; landslide entry location, width, strike and velocity; landslide volume reaching the sea; run out length and time in water are used to compute the initial tsunami in the near-field zone through the generation model TOPICS. Then, a model based on fully nonlinear Boussinesq equations accounting for frequency dispersion (FUNWAVE) is used to model the propagation and inundation of tsunami waves. Also for better approximation of wavelength especially in near shore zone a nesting system is introduced to the model.

In the first case study (Martinique), two simulations are performed. In the first simulation, the whole volume of fallen debris is considered as a single lahar of 5 million m<sup>3</sup>, whereas it is subdivided in three distinct flows in Simulation 2, thus entering the sea during 1 min and not instantaneously. When both simulated tsunamis are compared with reported wave amplitudes at Saint-Pierre, a fair agreement is obtained. In the second case study (Montserrat), 98% of the 200 million m<sup>3</sup> of collapsed material reached the sea. However, both the Mattioli et al. (2007) simulation and the authors' simulation showed that a limited source volume can indeed generate a tsunami as was observed in Montserrat and in Guadeloupe. This shows clearly that it is wrong to identify the volume of a potential huge landslide as a direct tsunami source, as it would collapse and enter the sea during a non-instantaneous time sequence instead of considering the potential peak debris flow.

The results showed the importance of temporal progression of the landslides on the generated waves and for better modeling effects on coasts as far as possible from the source should be taken into account to better constrain the tsunami source.

According to Ashtiani and Ramshe (2011), landslide-generated wave's characteristics are of the utmost importance in the dam engineering and water reservoir planning. They used a two-dimensional depth-integrated fourth-order

Boussinesq-type numerical model called LS<sub>3</sub>D, which is extended for sub-aerial landslides and validated using available three-dimensional experimental data to estimate the impact of landslide-generated waves in dam reservoirs. By using this numerical model the impact of landslide-generated waves in two real cases, the Maku and Shafa-Roud dam reservoirs in the northwestern and the north of Iran are investigated.

In the study it is emphasized that four distinct stages can be distinguished in simulating landslide-generated waves in dam reservoirs: the generation, the propagation, the overtopping, and the run-up stages.

The main concern in numerical modeling is defined as the accuracy of approximate equations to describe the nonlinearity effects and frequency dispersion of waves. According to the authors the Boussinesq-type models are more efficient than models developed based on NSW waves or potential flow equations. The LS<sub>3</sub>D model has fourth order accuracy in considering the nonlinearity effects and frequency dispersion of waves.

In the comparison of the experimental data with the results of the numerical model a time phase difference of 10-15 % and an error of 5 % in the wave amplitudes are observed. The effects of the shape of the sliding mass are also considered and the maximum computational error is found as 3 %. Finally the wave amplitudes in propagation and generation stages are compared and 5 % difference is observed. In the light of these results the model is proven itself.

The generated wave heights, wave run-up, maximum wave height above the dam crest, and the dam overtopping volume have been evaluated in the case studies. For the Maku dam reservoir a maximum positive near-field wave height of 18 m, maximum wave run-up of 30.7 m, and maximum downstream flood volume of 4,500 m<sup>3</sup> although the dam has a notable freeboard of 9 m. At the Shafa-Roud

dam site have been a maximum wave height of 31 m, maximum wave run-up of 21.2m, and maximum dam flood volume of 80,000 m<sup>3</sup> are calculated which is a big threat for the downstream area.

Mazzanti and Bozzano (2011), reproduced the tsunami that hit the village of Scilla (Southern Calabria, Italy) on February 6th, 1783 killing 1,500 habitants, caused by a  $5 \times 10^6$  m<sup>3</sup> landslide which is triggered by a 5.8 M earthquake, using the three dimensional DAN3D model for simulating the landslide propagation both in the subaerial and in the submerged parts of the slope and a simple linear shallow water model for both tsunami generation and propagation. The outputs of the numerical simulation of the landslide are used as input parameters for tsunami modeling in the study. The results are compared with the recorded historical documents.

The writers emphasize that tsunamis generated by rock slides and rock avalanches are determined by the volume, shape, velocity profile and run out length of the landslide for a given bathymetry. Sub-critical ( $Fr < 1$ ) landslide velocities imply that the generated waves will propagate ahead of the moving landslide, and for super-critical ( $Fr > 1$ ) landslide velocities, the landslide will move faster than the waves and goes ahead. But for both cases, the build-up of the wave is limited whereas the most efficient generation is when  $Fr \approx 1$ . Since the Froude number varies along the path due to the change in landslide velocity and change in the water depth during the travel down the slope, wave speed is not constant. Using DAN3D and the Froude number analysis the high tsunamigenic potential of the Scilla landslide is inferred.

After the landslide is modeled, tsunami generation and propagation is reproduced with a linear shallow water model. In the model the landslide is described as a flexible box with a pre-defined velocity progression. The travel distance of the slide  $s(t)$  at time  $t$  is described in three phases:

Acceleration phase:

$$s(t) = R_a \left(1 - \cos \frac{U_m}{R_a} t\right), 0 < t < T_a \quad (8)$$

Constant speed phase:

$$s(t) = R_a + U_m (t - T_a), T_a < t < T_c + T_a \quad (9)$$

Deceleration phase:

$$s(t) = R_a + R_c + R_d \sin \left( \frac{U_m}{R_d} (t - T_a - T_c) \right), T_c + T_a < t < T_c + T_a + T_d \quad (10)$$

where  $U_m$  is the maximum slide velocity,  $T_a$  is the acceleration time,  $R_a$  is the acceleration distance,  $T_c$  is the constant speed time,  $R_c$  is the constant speed distance,  $T_d$  is the deceleration time, and  $R_d$  is the deceleration distance. The total travel time is  $T = T_a + T_c + T_d$ , while the run-out distance of the slide is  $R = R_a + R_c + R_d$ .

The comparison of the wave run-up reported in historical documents with the values computed by the numerical simulation, showed that a good correspondence in most of the locations, but it gave overestimated wave run-ups in the locations characterized by gentle slopes. This discrepancy is thought to be because of the linear shallow water model which ignores the effects of dispersion and wave breaking.

Murty (2003) stated that the amplitude of a landslide generated tsunami depends on the total volume of the landslide but there are other side factors that must be taken into account such as; depth of the slide, angle of the slide, distance moved by the slide, duration of the slide, density of the slide material, coherent nature of the slide, grain size and spectrum and characteristic speed of the slide, etc. In his study, Murty, tried to establish a relationship between the volume of the slide ( $V$ , in millions of  $m^3$ ) and maximum amplitude ( $H$ , in meters) by using the worldwide observational data found in the literature and to compare this relationship with the

results of some numerical models. In the study the main parameter is the slide volume and the relationship that is derived is phenomenological.

To derive a relationship, a regression line was fitted making use of observational data alone and a result two equations are obtained;

$$H= 0.3945V \tag{11}$$

or

$$V= 2.3994H \tag{12}$$

In the study there is a poor agreement between observations and the results of some numerical simulations which do not explicitly use the volume of the slide as one of the input parameters.

Suleimani et al. (2011) used a numerical model to investigate both the tectonic and landslide-generated tsunami caused after the Mw 9.2 earthquake in Alaska. Tsunami propagation and inundation simulation is achieved with a nonlinear shallow water model that is formulated for depth-averaged water fluxes and also takes into account the temporal position of the shoreline by using a free surface moving boundary. The outputs of the model for both the local landslide generated waves hit the shore one minute after the earthquake and the tectonic waves that come 30 minutes after that are compared with observed tsunami amplitudes, arrival times and inundation areas. The comparison is found to be consistent and the model is verified.

As indicated by Watts et al. (2003) integration of marine geology data and interpretations into numerical simulations is required for recreating landslide

tsunami generation and propagation of past events. In their study, 1946 Unimak, Alaska, the 1994 Skagway, Alaska, and the 1998 Papua New Guinea events are taken as case studies and modeled with GEOWAVE combining Tsunami Open and Progressive Initial Conditions System (TOPICS) with the fully nonlinear Boussinesq water wave model FUNWAVE. The importance of submarine mass failures (SMFs) is emphasized as they add to the effects of the earthquake tsunamis and lead to higher amplitude waves. Watts et al. (2003) divide their modeling strategy into three parts: (i) Wavemaker model: a model for the center of mass motion of SMFs (slides or slumps) and possible deformation rate around this center, as a function of material, geometrical, and hydrodynamic parameters, (ii) Tsunami generation model: a model for tsunami generation due to the specified SMF shape and motion, based on results of both two- and three-dimensional fully nonlinear potential flow models and (iii) Tsunami propagation and inundation model: a model for tsunami propagation and inundation, based on extended fully nonlinear Boussinesq equations. The case studies' results are compared with tsunami observations and records and it is concluded that GEOWAVE can successfully model previous event when sufficient geological inputs are provided.

In their study Fritz et al. (2009) investigated the  $30.6 \times 10^6$  m<sup>3</sup> landslide that was generated by the Mw 8.3 earthquake in Lituya Bay on July 10, 1958 and the 524 meter run up tsunami it created. For the study a physical model with a scale of 1:675 based on the generalized Froude similarity with a pneumatic landslide tsunami generator is used with laser measurement techniques such as particle image velocimetry (PIV) and laser distance sensors (LDS) is used for landslide impact, wave generation and run up on the headland. Also the landslide is modeled in three-dimension with a 1:400 scale physical model. The results show that the landslide generates a large air cavity and an extremely nonlinear wave that remains nonbreaking and that is because of the short propagation distance to the

headland run up. Fritz et al. (2009) shows that predicted tsunami amplitudes by previous studies are in correspondence with the experimentally measured values also the destructed forest area is in accordance with the results.

Fritz et al. (2004) defined four different types of landslide generated waves using a two-dimensional physical model equipped with laser distance sensors (LDS), particle image velocimetry (PIV), and capacitance wave gauges (CWG) based on Froude similarity: (i) weakly nonlinear oscillatory wave, (ii) non-linear transition wave, (iii) solitary-like wave and (iv) dissipative transient bore, most of which are located in intermediate wave regime. Wave profiles, propagation behaviors, wave parameters and the factors affecting them are investigated and Fritz et al. (2004) and the physical model results are compared with the waves generated in Lituya Bay tsunami.

The Great Banks landslide-generated tsunami on November 18<sup>th</sup> 1929 is modeled by Fine et al. (2005) using a shallow water numerical model. A  $M_w$  7.2 earthquake caused a 200 km<sup>3</sup> submarine landslide which lead to a tsunami with waves 3 – 8 m in amplitude and run-up up to 13 m in some places. The modeling results show good accordance with visual observation and tide gauge records in terms of arrival times and the amplitudes of tsunami waves.

For defining the influence of subaerial component of slides on surface wave generation, Fine et. al. (2003) carried out numerical experiments and compared the efficiency of viscous and rigid-body slide models. Their investigations showed that higher tsunami waves are generated in rigid body slides than viscous slides since subaerial slides displace a considerable volume of water at relatively high

speed (roughly four times higher). Slide volume, slide type (rigid-body or viscous), slide density, position, slope angle, Froude number (Fr) are found to be the most critical parameters affecting the generation of surface waves. The most efficient wave generation is observed for  $Fr = 1.0$ .

Fine et. al (2003) argues that, “most realistic” slide model must be chosen for correct evaluation and this model should be a viscous physical model in most cases. They also indicate that for rigid-body slides, higher waves are observed for higher initial position of the slide, but in viscous slides there is an optimal slide position that creates largest tsunami waves. In rigid-body slides the added volume of landslide always leads into an increase in leading wave height. Finally, Froude number (the ratio between the slide and wave speeds) is defined as the critical parameter in determining the generation of surface waves. The most efficient generation occurs near resonance when  $Fr = 1.0$  and for submarine slides with a density of  $2 \text{ g/cm}^3$ , this number is always less than unity and this is the main reason that subaerial slides are much effective.

## CHAPTER 3

### HISTORICAL EVENTS

Throughout the history, many landslide induced tsunamis are present. Some of these tsunamis are listed and briefly explained below.

- **1783, February 6<sup>th</sup> – Scilla**

30 minutes after 5.8  $M_w$  earthquake in the village of Scilla, an earthquake triggered landslide of about  $5 \times 10^6 \text{ m}^3$  in the form of a rock avalanche occurred. The landslide produced a tsunami with a run-up as high as 16 m that hit the Marine Grande beach 30 – 60 seconds after and killed about 1,500 people.

- **1888, April 23<sup>th</sup> – Trondheimsfjorden, Norway**

The landslide and tsunami along the shore of the bay of Trondheim, central Norway, killed one person and caused major damage to port facilities (L'Heureux et al., 2011).

- **1929, November 18<sup>th</sup> – The Grand Banks**

According to Fine et al. (2005), the most catastrophic tsunami in Canadian history occurred on November 18, 1929, due to a  $M=7.2$  earthquake at the southern edge of the Grand Banks, 280 km south of Newfoundland. The earthquake triggered a  $200 \text{ km}^3$  submarine slope failure and this generated a tsunami that killed 28 people. Tsunami waves had amplitudes of 3–8 m and runup of up to 13 m along the coast of the Burin Peninsula.

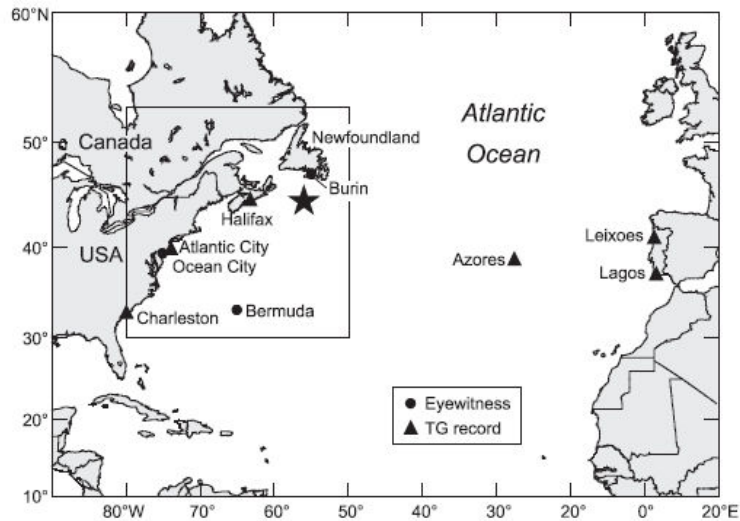


**Figure 3-1** - Map of the North Atlantic Ocean showing the location of the 1929 Grand Banks earthquake epicenter (Fine et al., 2005).

- **1946, April 1<sup>st</sup> – Unimak, Alaska Tsunami**

The earthquake with a magnitude of 7.4 caused a tsunami was catastrophic both in the near field, where it eradicated the Scotch Cap lighthouse on Unimak Island and in the far field, where it killed 159 people in Hawaii, inflicted severe damage in the Marquesas Islands, and reportedly caused destruction as far away as Antarctica (Okal et al., 2003).

- **1958, July 10<sup>th</sup> – Lituya Bay, Alaska**

July 10, 1958, an earthquake Mw 8.3 along the Fairweather fault triggered a major subaerial landslide into Gilbert Inlet at the head of Lituya Bay on the southern coast of Alaska and generated a giant tsunami and run-up of 524 m (highest wave run-up in recorded history) that caused total forest destruction and erosion down to bedrock on a spur ridge in direct prolongation of the slide axis (Hermann et al., 2009)

- **1959, March 22<sup>th</sup> – Pontesei Reservoir**

A 5 million m<sup>3</sup> landslide fell to the artificial reservoir of Pontesei Dam in Italy, caused an impulse wave with approximately 20 m run-up (Panizzo et al., 2005). The wave did not damage the dam but the basin capacity lowered from 9.09 million m<sup>3</sup> to 5.8 million m<sup>3</sup>.



**Figure 3-2** - Picture of the Pontesei dam and artificial reservoir, the 1959 landslide is clearly visible in the upper part of the picture (Panizzo et al., 2005).

- **1960, November 4<sup>th</sup> – Vajont Reservoir**

When the Vajont reservoir while the artificial basin was filling up for the first time, a 700.000 m<sup>3</sup> rock landslide fell into reservoir which was at 652 m over the m.s.l., water depth of 160 m and containing 40.000.000 m<sup>3</sup> of water. The landslide caused an impulse water wave which was 2.0m high and generated a 10m wave run-up on the dam (Semenza, 2002).

- **1961 – Zaxi Reservoir, China**

While the reservoir was 50 – 70 m deep, the 20 m/s landslide produced impulse waves with wave heights up to 21 m and resulted in 3.6 m high waves overtopping the dam (Jing and Wang, 1988). Wave heights of 1.2 – 1.5 m are observed 8 km upstream of the dam.

- **1963, October 9<sup>th</sup> – Vajont Reservoir**

One of the most catastrophic landslide-generated tsunami events occurred in Vajont artificial reservoir when a 270 million m<sup>3</sup> landslide detached from Mountain Toc and fell to the reservoir which was 700.42 m over the m.s.l, water depth of 200 m and containing about 120.000.000 m<sup>3</sup> of water. The wave reached a height of 235 m, overtopped the dam, flooded the city of Longarone and killed 2.000 people (Panizzo et al., 2005). The concrete arch dam survived with very little damage.

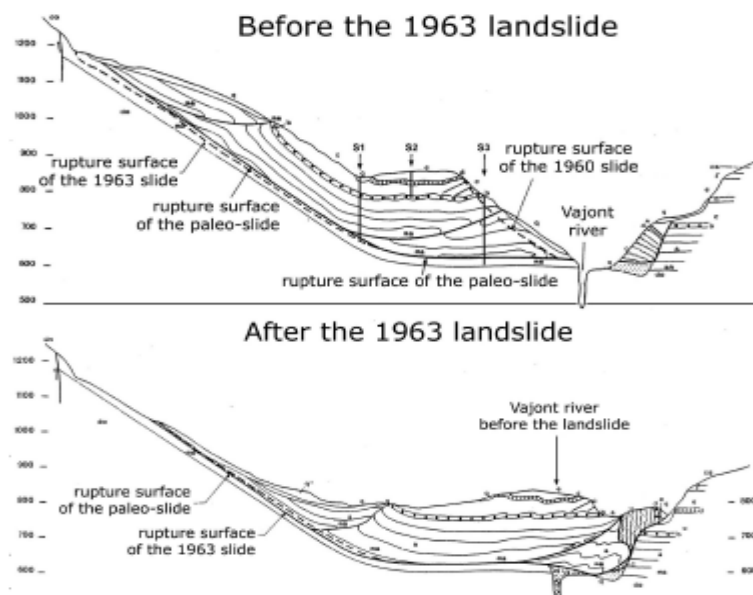


**Figure 3-3** - Sections of the Vajont valley before and after 9 October 1963 landslide (Semenza, 2002).

- **1964, March 27<sup>th</sup> - The Prince William Sound**

According to Plafker (1969), the largest instrumentally recorded earthquake in North America which has a magnitude of Mw 9.2 ruptured an 800-km long section of the Aleutian megathrust, producing vertical displacements over an area of about 285,000 km<sup>2</sup>. Haeussler et al. (2007) estimated the landslide volume as 211 million m<sup>3</sup> and the village of Seward in Resurrection Bay suffered from local landslide generated tsunamis 1 minute after the earthquake and from tectonic waves 30 minutes after that.

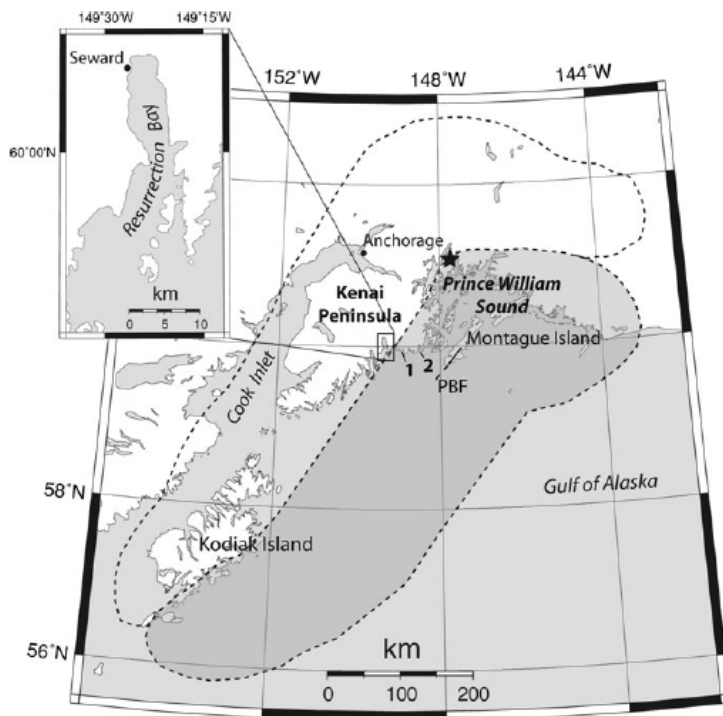


**Figure 3-4** - Map of south-central Alaska with the rupture zone of the MW 9.2 1964 Great Alaska earthquake (Plafker, 1969).

- **1979 – Lomblen Island**

According to Soloviev (1992), a spontaneous landslide produced a tsunami with heights of 7 – 9m and inundation distances of up to 1500 m which killed 539

people and another 700 missing. A characteristic first negative wave has been reported followed by a large positive second wave.

- **1979, October 16<sup>th</sup> – Nice**

During land-filling operation a part (10 million m<sup>3</sup>) of the Nice new harbor extension which is near to the Nice international airport, slumped into the Mediterranean Sea that caused a tsunami which was observed in Antilles city 10 km away from the origin (Assier-Rzadkiewicz et al., 2000).

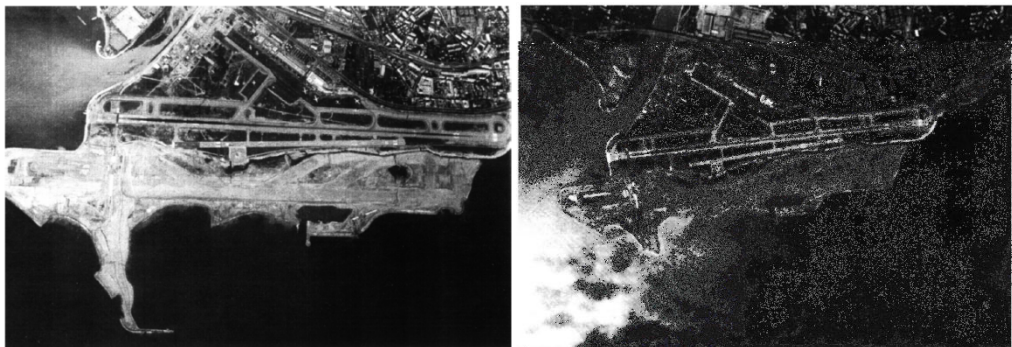


**Figure 3-5** - Photographs of the building site before and after the accident (Assier-Rzadkiewicz et al., 2000).

- **1985 – Xintan Slide, China**

According to Liu (1988), Xintan Slide into Yangtze River created 49m high impulse waves which affected 20 km away. The town of Xiangxi is flooded with 7 meter high waves.

- **1994, November 3rd – Skagway, Alaska Tsunami**

A landslide caused a tsunami that destroyed the railway dock and claimed the life of one construction worker. The tsunami most likely occurred after low tide which triggered the movement of loose alluvial sediment. The waves reached to 9m at the railway dock, 3m at the ore dock, and 11m at the ferry dock (Watts et al., 2003).

- **1998, July 17<sup>th</sup> – Papua New Guinea tsunami**

Although firstly the origin of Papua New Guinea tsunami is thought to be an earthquake, modeling attempts resulted in too small amplitudes and too late arrival times which made clear that the reason of the tsunami is a slump. 20 km of the coast affected by waves with run-up heights up to 15 m and 2200 people were killed (Harbitz et al., 2006).

- **1999, August 17<sup>th</sup> – İzmit Bay**

After the catastrophic Earthquake 11 km southeast of Koceli with a magnitude of Mw 7.4 tsunami waves are observed in an area of 18 km between Tütünciflik and Hereke with a run-up of 2.6m. Although there are opinions stating that no tsunami waves occurred after the earthquake, tsunami waves in İzmit bay show similarities with the 1994 Skagway and 1998 Papua New Guinea tsunami waves (Alpar et al, 2000).

- **2002, December 30<sup>th</sup> - Island of Stromboli in South Tyrrhenian sea, Italy**

On 30 December 2002 the coast of the volcanic island of Stromboli, in the Tyrrhenian Sea, Italy, was attacked by two tsunamis generated by landslides that took place on the north-west flank of the volcano (Tinti et al., 2005).

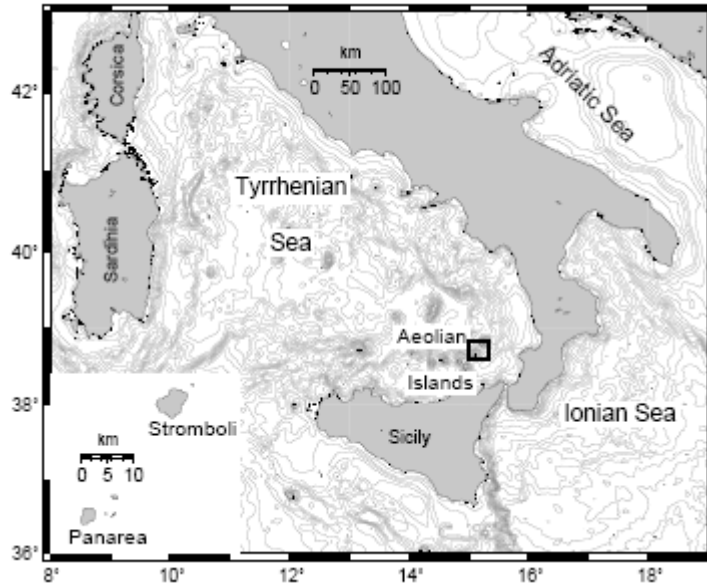


**Figure 3-6** - Geographic map of central-southern Italy, showing the location of the Aeolian archipelago (Tinti et al., 2005).

- **2003, July 13<sup>th</sup> – Montserrat**

The eruption of the Soufrière Hills volcano on Montserrat began in 1995 and on 13 July 2003, a major dome collapse occurred and delivered large pyroclastic flows into the sea, thus leading to the generation of a tsunami (Pelinovsky et al., 2004). The tsunami waves with crest amplitudes of 1m mainly affected mainly the eastern uninhabited shore of Montserrat, Antigua and Guadeloupe (Poisson and Pedreros, 2010).

- **2007, December 4<sup>th</sup> – Chehalis Lake**

During a period of heavy rain, a 2 million m<sup>3</sup> landslide produced a tsunami with a maximum wave height in excess of 10 m in the vicinity of the landslide area and of 4–10 m throughout the lake which destroyed a number of camp grounds that were empty at the time (Stephenson and Rabinovich, 2009).

## CHAPTER 4

### SUBAERIAL LANDSLIDE GENERATED TSUNAMIS

Tsunamis generated by subaerial landslides in closed basins like artificial reservoirs created by dams or lakes etc. pose distinctive problems for hazards assessment because the domain of interest is commonly the “near field,” beyond the zone of complex splashing but close enough to the source that wave propagation effects are not predominant (Walder et. al., 2003).

Panizzo (2004) summarizes principal phases in the phenomenon of subaerial landslide generated waves in his PhD thesis similar to Huber & Hager (1997) as follows;

- a) The landslide starts moving, accelerates and then falls into water which is mainly related with geology and soil mechanics.
- b) The impact of the landslide into water. Due to the energy exchange mechanism between the landslide and the water, the principal landslide parameters are determining the generation of the impulse waves.
- c) The propagation of impulse waves into the reservoir or in the open sea, where wave energy dispersion occurs and refraction, diffraction and shoaling affect wave characteristics.
- d) Final step is the interaction of waves with shorelines or structures. Runup may cause the flood of coastal areas, and overtopping of the dam can be observed in artificial reservoirs.

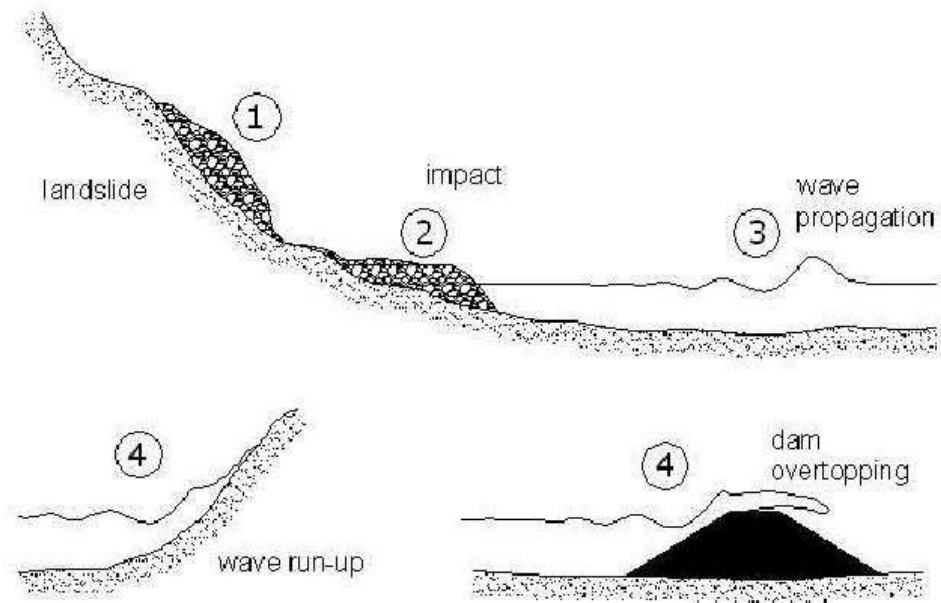


**Figure 4-1** – Principal phases in the phenomenon of subaerial landslide generated waves (Panizzo, 2004)

According to Heller & Hager (2010), the seven governing parameters affecting the wave characteristics such as maximum wave height ( $H_{max}$ ), maximum wave amplitude ( $a_{max}$ ) of period  $T_{max}$  and wave length ( $L_{max}$ ) are;

- a) Still water depth ( $d$ )
- b) Slide impact velocity ( $v$ )
- c) Landslide height ( $h$ )
- d) Bulk slide volume
- e) Bulk slide density ( $\rho_s$ )
- f) Slide impact angle ( $\alpha$ )
- g) Grain diameter ( $d_g$ )

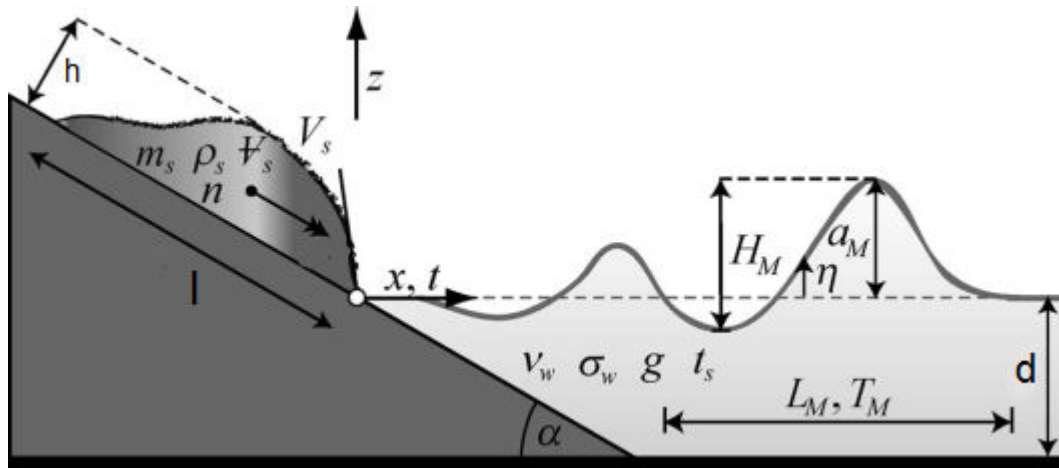


**Figure 4-2** – Landslide generated tsunami parameters (Heller & Hager, 2010)

Fritz et. al., (2004), classified the impulse waves generated by a landslide into 4 groups based on the slide Froude number ( $Fr = v / (gd)^{0.5}$ ) and the dimensionless landslide height ( $H = h/d$ ) such as;

- a) weakly non-linear oscillatory wave
- b) non-linear transition wave
- c) solitary-like wave
- d) dissipative transient bore

Their study implied that in near-field cases, the slide Froude number is the dominant parameter for maximum wave envelope crest and trough amplitudes, period and wavelength of the leading and the second wave, volume of the leading wave crest, leading wave crest energy. Wave type and characteristics have an effect on wave attenuation, wave height whereas the propagation velocity of the leading wave crest follows closely the theoretical approximations for a solitary wave. Finally, it is observed that the wavelength of the leading wave strongly depends on the subaqueous slide run-out.

A similar classification of landslide generated waves was done by Noda (1970) with the use of physical experiments which involve vertical fall of a box. Their classification as function of landslide volume and landslide velocity is given in Figure 4-3.

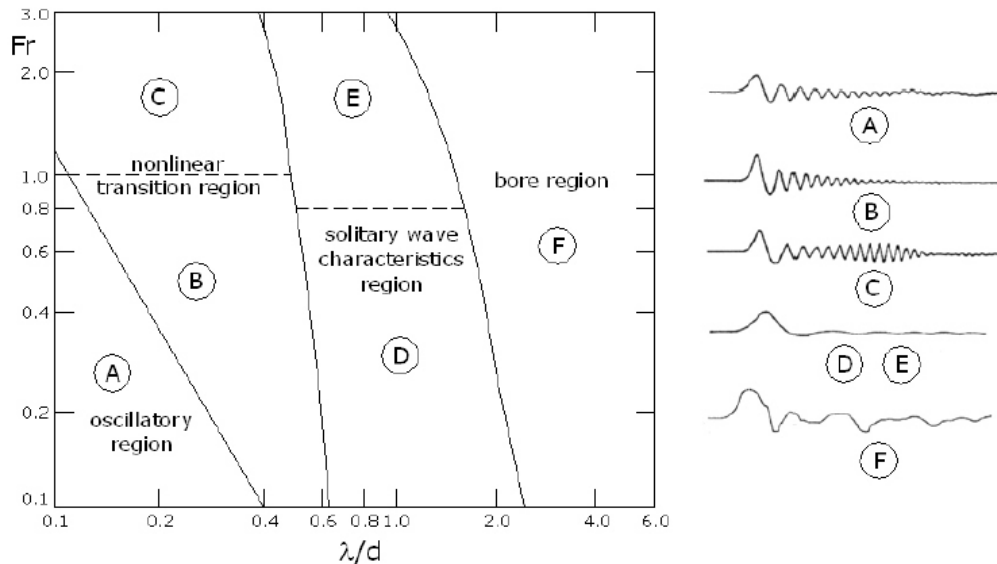


**Figure 4-3** – Different types of impulse waves (Noda, 1970)

$\lambda$ : box width

$d$ : local depth

$Fr$ : dimensionless box falling velocity

Scientists use different methods like numerical modeling with different commercial codes like FLOW-3D (Montana et. al., 2011), COULWAVE (Geist et. al., 2009), GEOWAVE & FUNWAVE (Poisson and Pedreros, 2010) or models developed by themselves like LS<sub>3</sub>D (Ashtiani and Ramshe, 2011), analytical models (Sammarco and Renzi, 2008), empirical formulations derived through physical experiments (Huber & Hager, 1997, Panizzo et. al., 2005) to forecast impulse wave parameters generated by landslides. These models can be based on depth integrated mild slope equations or non-linear Boussinesq equations etc. Most of the efforts are validated with either physical experiments or comparison

with real cases in which wave characteristics are known. The outputs of these different studies are generally appropriate and idealized in certain boundary conditions. Although physical modeling of the case gives the most realistic outputs, this may not be possible due to time and budget constraints. The development of 3D modeling recently makes it easier to make hazard assessment for different situations.

## **CHAPTER 5**

### **COMPARISON OF NUMERICAL MODEL WITH EMPIRICAL FORMULATIONS**

An empirical equation to determine the maximum wave amplitude due to the landslide dimensions in the dam lakes in relation to the slope of the shore and distance from the landslide is given in Panizzo et. al. (2005) during a research program funded by the Italian National Dam Office for forecasting landslide generated water waves. The empirical formulation is developed by using a physical model and it is verified by applying the formulation to three real cases (1959 Pontesei, 1960 & 1963 Vajont) occurred in Italian artificial reservoirs caused by sub-aerial landslides. The relation can also be checked by using the numerical model. For this purpose the tsunami numerical model NAMI DANCE is applied to a regular shaped dam lake with a certain coastal slope. NAMI DANCE simulates tsunami generation and propagation by solving nonlinear form of shallow water equation. The numerical results of NAMI DANCE are compared with the results obtained from an empirical equation developed by Panizzo et. al. (2005).

The computer program NAMI DANCE is developed for to simulate and visualize tsunamis and to understand and investigate the tsunamis from generation area to the coast. It is developed in collaboration with Special Research Bureau of Automation of Sciences Russian Academy of Sciences, Russia and METU Department of Civil Engineering, Ocean Engineering Research Center Turkey. The code is authored by Dr. Andrey Zaytsev in C++ programming language by following the leap frog scheme numerical solution procedure for faster simulation

and better visualizations (Zaytsev et. al. (2008)) in regard to the famous tsunami numerical code TUNAMI N2.

### 5.1 Model Set – Up

Two different set-ups with different inclination angles shown in Figure 5-1 & Figure 5-2 are used for both numerical model & empirical formula and the maximum wave amplitudes near the coast are compared. Figure 5-3 shows the top view of these bathymetries, boundary dimensions and spatial grid sizes in both directions.

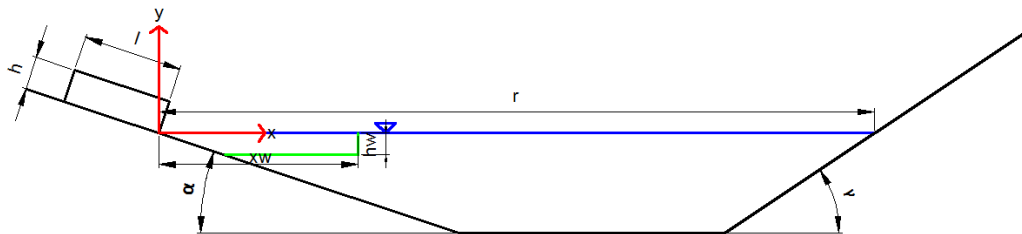


**Figure 5-1** - Cross-section of the inclined coastal slope (1/3) set-up

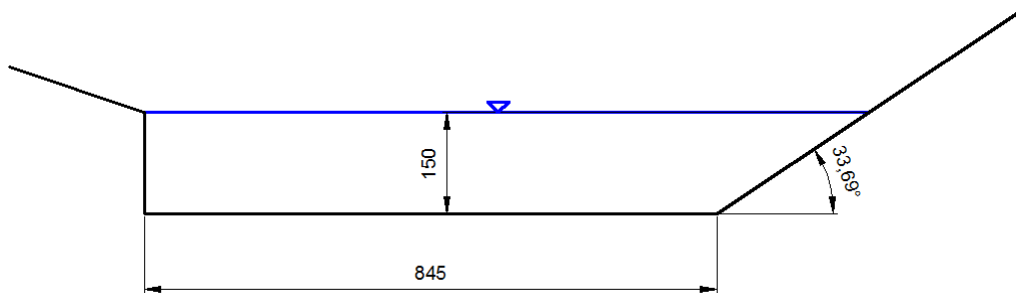


**Figure 5-2** - Cross-section of the vertical coastal slope set-up

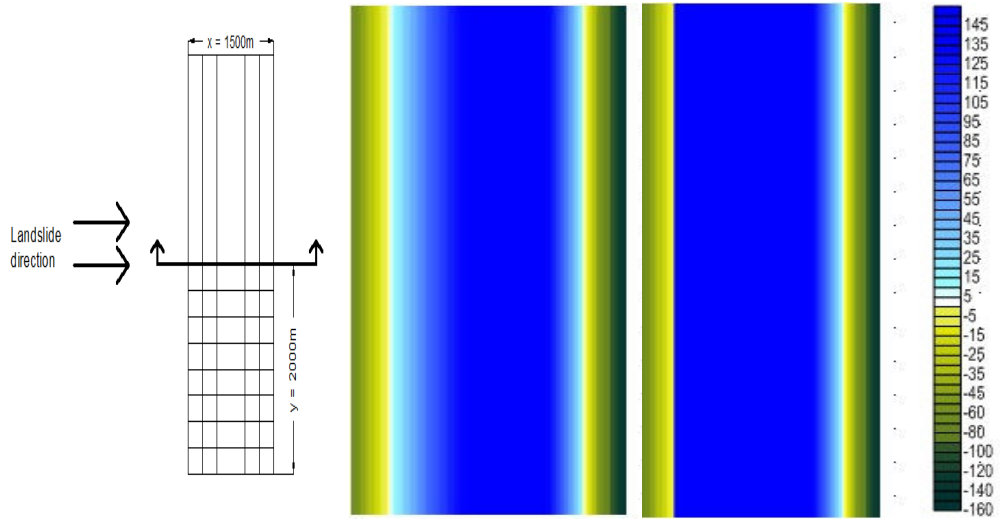


Figure 5-3 – Top view of the set-ups

## 5.2 Empirical Formulation

The empirical formulation used for model verification is taken from Panizzo et al. (2005). In this method the layout given in Figure 5-4 is used to derive 4 formulations as shown below;

$$t_s^* = 0.43 \left( \frac{wh}{d^2} \right)^{-0.27} \left( \frac{v}{\sqrt{gd}} \right)^{-0.66} (\sin\alpha)^{-1.32} \quad (1)$$

$$\frac{H_{max}}{d} = 0.07 \left( \frac{t_s^*}{A_w^*} \right)^{-0.45} (\sin\alpha)^{-0.88} \exp(0.6 \cos \theta) \left( \frac{r}{d} \right)^{-0.44} \quad (2)$$

$$T_{max} \sqrt{\frac{g}{d}} = 2.50 t_s^{*-0.22} (\sin\alpha)^{-0.25} \left( \frac{r}{d} \right)^{0.17} \quad (3)$$

$$\frac{r_u}{d} = 1.37 \left( \frac{H_{max}}{d} \right)^{1.51} \left( T_{max} \sqrt{\frac{g}{d}} \right)^{0.47} (\sin\gamma)^{0.26} \quad (4)$$

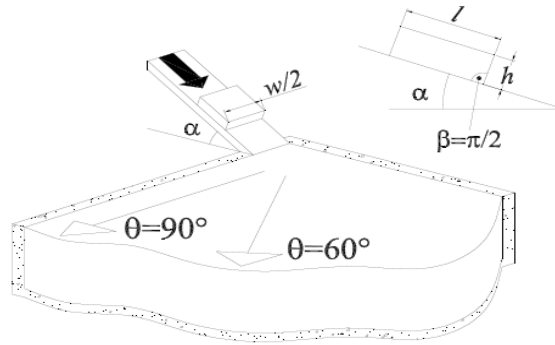


**Figure 5-4** - The layout of the experiments. (Panizzo et. al., 2005)

Figure 5-5 shows the sketch of the physical model used to study the run up of landslide generated water waves on plane slopes where  $L_p$  is the distance between the slope end and the impact point.

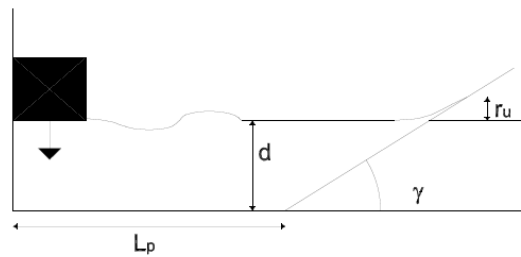


**Figure 5-5** - Sketch of the physical model used to study the run up of landslide generated water waves on plane slopes. (Panizzo et. al., 2005)

### 5.3 Numerical Modeling

For comparison, an initial wave width parallel to shoreline ( $y_w$ ) of 2000m is chosen for 7 different initial wave lengths perpendicular to the shoreline ( $x_w$ ) (50m, 150m, 300m, 350m, 400m, 450m and 500m) and 5 different initial wave amplitudes ( $h_w$ ) (-10m, -20m, -30m, -40m and -50m). Since initial wave length is not taken into account in the empirical formula, only one  $H_{max}$  value is computed for each initial wave amplitude. The input data is given in Table 5-1 .

**Table 5-1** - Input data of the bathymetry & landslide, used for comparison

$y_w$	2000	initial wave width (m)
$v$	5	impact velocity (m/s)
$x_w$	Variable (50-500m)	initial wave length (m)
$\theta$	0	angle from the landslide velocity vector
$d$	150	local water depth (m)
$\alpha$	18.4	inclination angle
$r$	1070	distance from landslide impact point
$\gamma$	33.7	slope inclination angle

### 5.3.1 Numerical modeling with NAMI-DANCE without Flux

In numerical modeling the effect of different initial wave amplitudes on the maximum amplification at the distant shore is investigated. For this reason in total of 35 simulations are carried out. The spatial grid spacing is selected as 2m for achieving more accurate results. The simulation duration is selected as 90 seconds with the time step of 0.025 seconds which are sufficient to determine the maximum wave amplitude before reflection from the distant shore. In the simulations the maximum amplitudes of wave at every grid points are obtained. The change of maximum amplitude (computed in simulation) of the wave towards distant shore is taken from the cross-section line perpendicular to shore (from the landslide origin to the distant shore). The change along the cross section is plotted distance  $X$  versus maximum amplitude  $H_{max}$ . Different cross-section is obtained for a certain initial wave length and they are plotted on a single graph for different initial wave amplitude in different color. The respective graphs are given in Figure 5-6, Figure 5-7 and Figure 5-8.

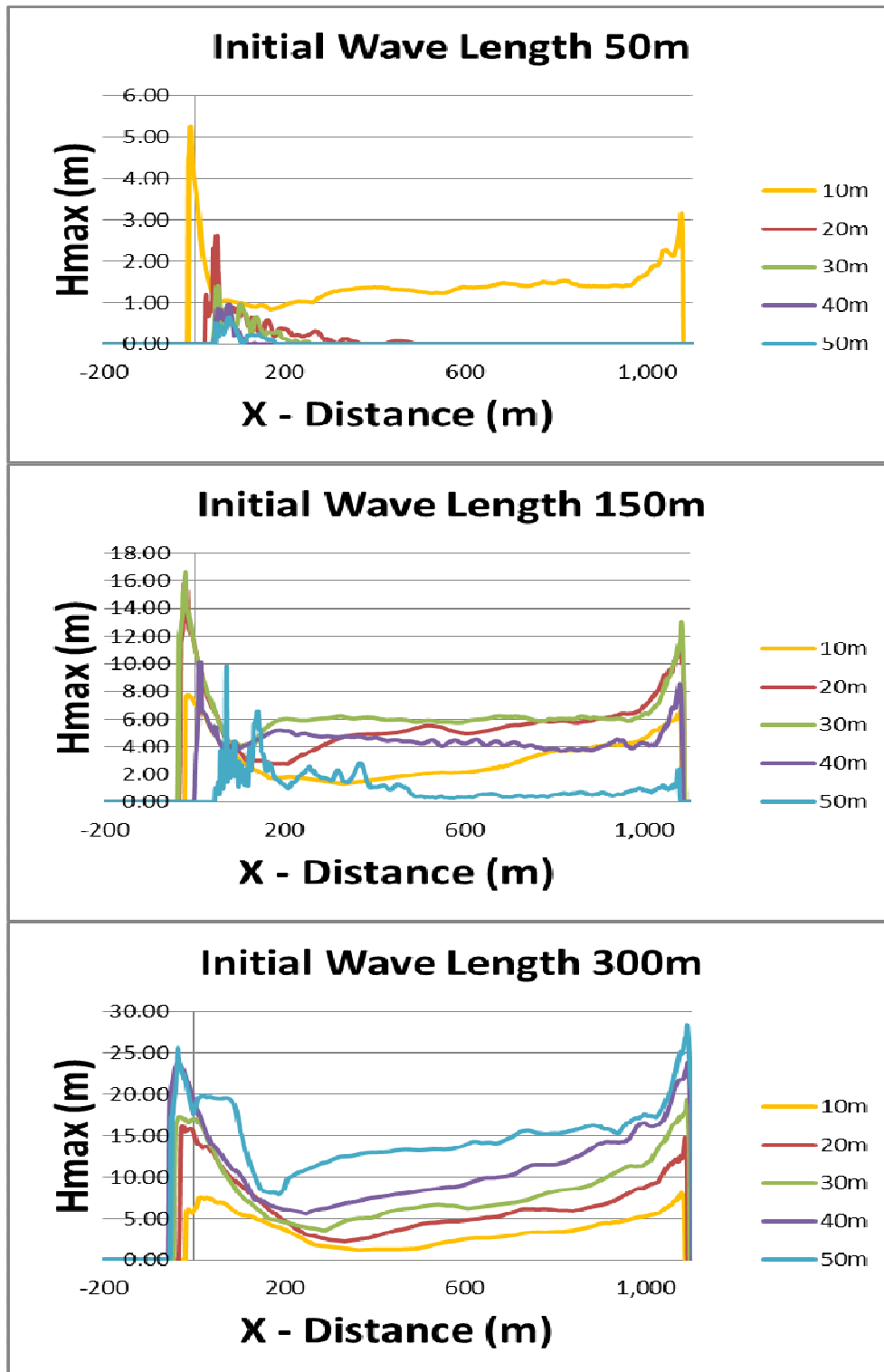


Figure 5-6 – Change of  $H_{max}$  along propagation distance for different initial wave lengths without flux

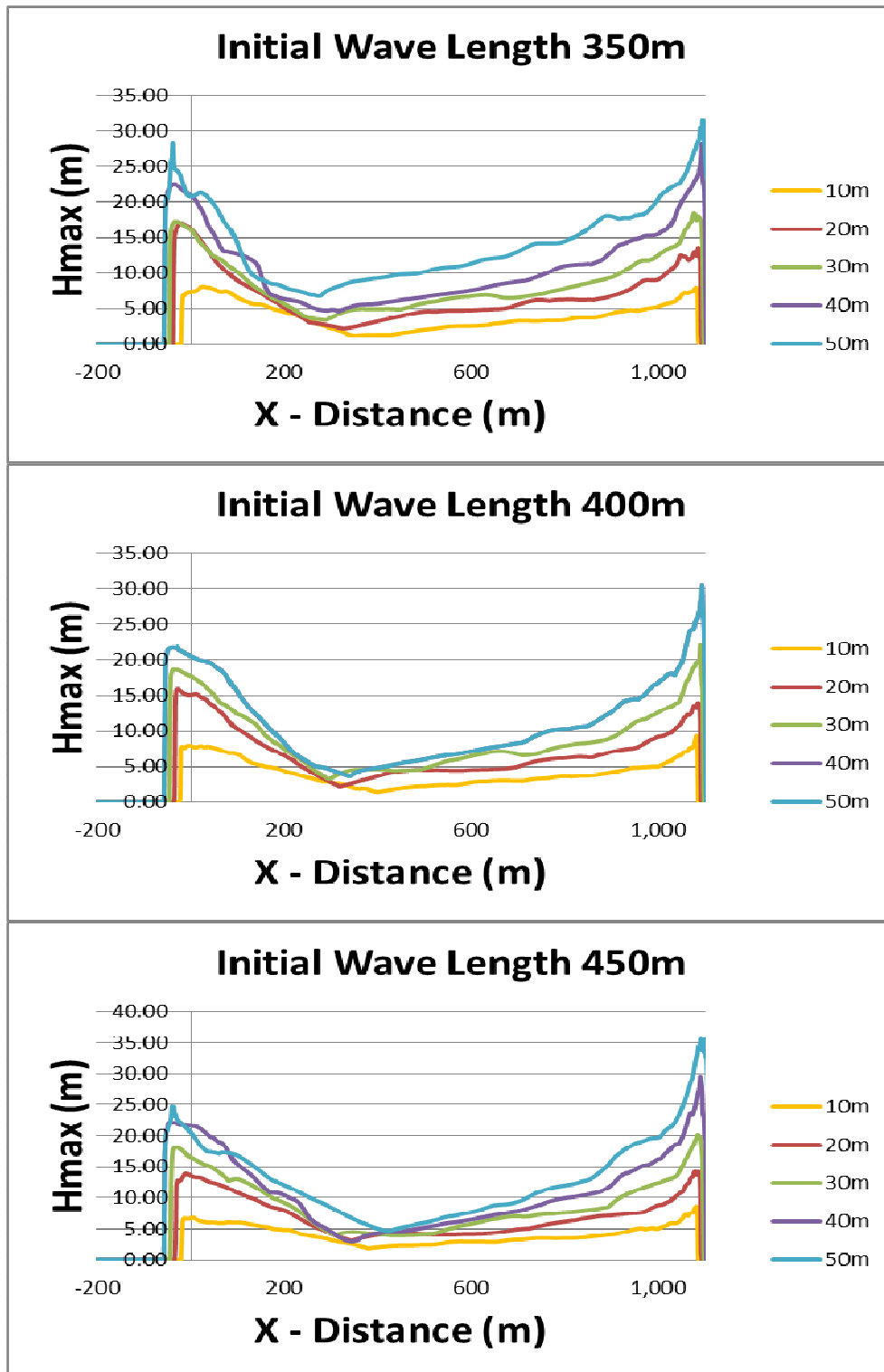
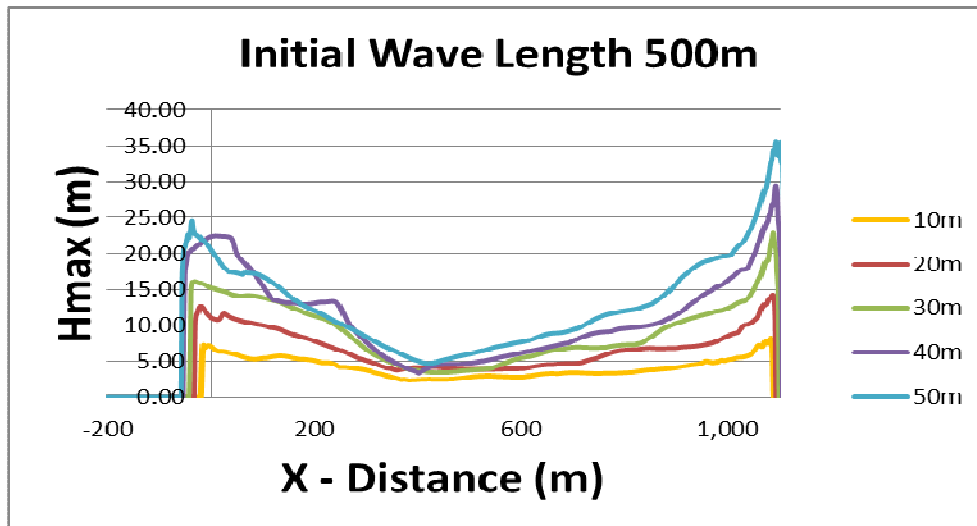


Figure 5-7 - Change of  $H_{max}$  along propagation distance for different initial wave lengths without flux



**Figure 5-8** - Change of  $H_{max}$  along propagation distance for different initial wave lengths without flux

As a result, the outputs with 50 meter initial wave length can be discarded because of its short length and inconsistent results. In other cases where initial wave length is equal to or higher than 150m, maximum wave amplitudes tend to increase up-to 400m initial wave length. But further increase in the initial wave length doesn't increase or even decrease the  $H_{max}$ .

### 5.3.2 Numerical modeling with NAMI-DANCE with Flux

The effect of flux can be modeled in NAMI-DANCE. For the flux in x-direction;

$$M = \text{Flux} = U \text{ (m/s)} * \text{depth (m)}$$

Since the landslide velocity is assumed as 5 m/s, U is generated as 5m/s for landslide dimensions.

For depth, the source file is subtracted from bathymetry file and the negative values are assigned as 0.

Then by multiplying this with U, M.grd file is generated. There is no flux in y-direction.

For initial wave lengths of 300m & 450m and for initial wave amplitudes of 30m & 50m a total of 4 simulations are carried out with NAMI-DANCE. Again from the center cross-sections are taken and these are compared with the simulations without using flux (Figure 5-9 & Figure 5-10).

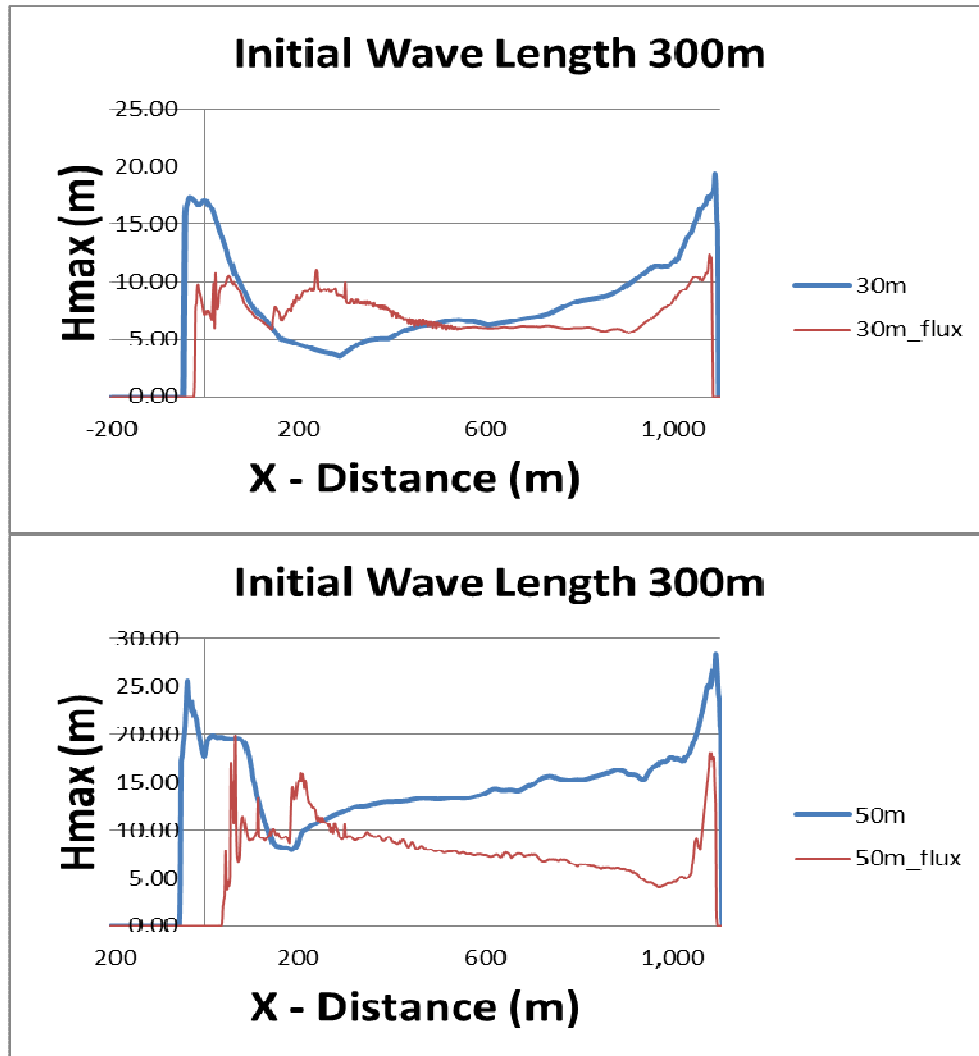


**Figure 5-9** - Change of  $H_{max}$  along propagation distance for initial wave amplitudes with flux

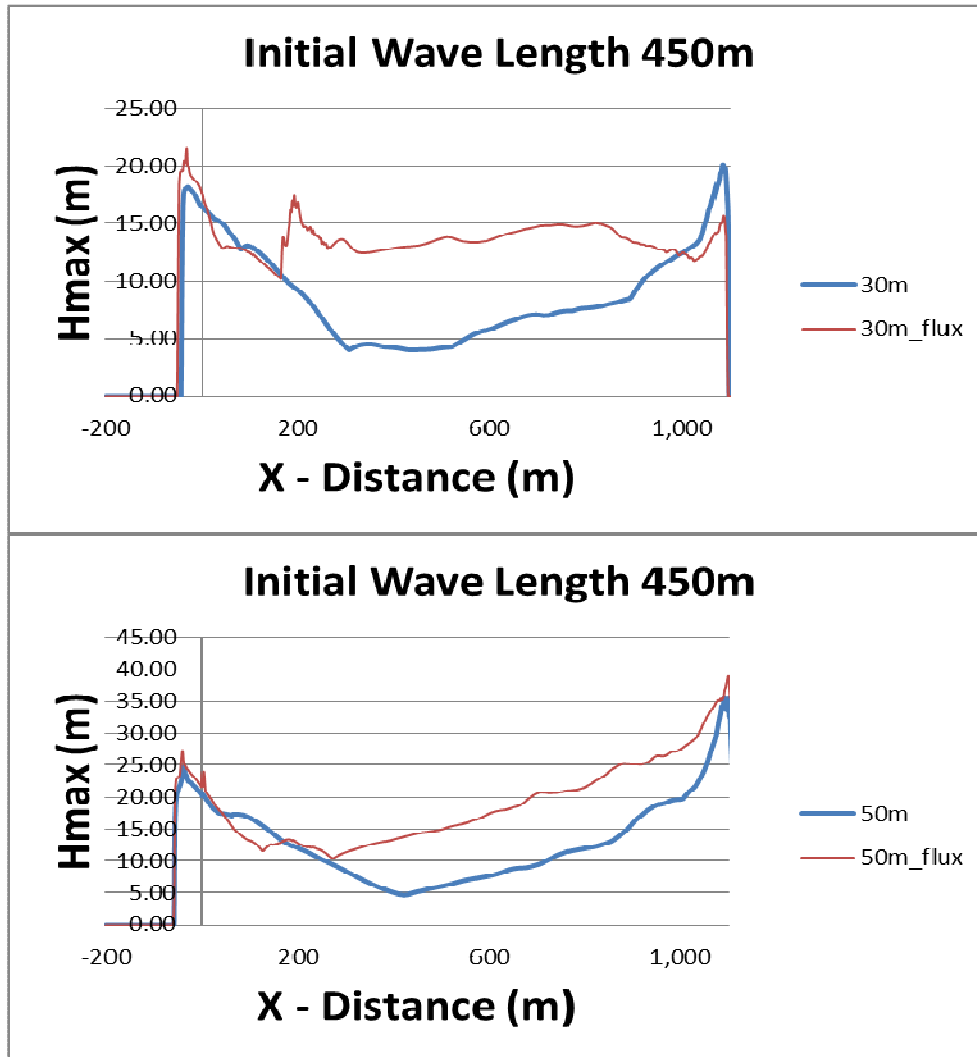


**Figure 5-10** - Change of  $H_{max}$  along propagation distance for initial wave amplitudes with flux

Considering the flux effect, a clear correlation cannot be established according to the model outputs. For example for a initial wave amplitude 30m and initial wave length 300m in inclined coastal slope, addition of flux decreases the maximum wave amplitude by 36%. On the other hand for initial wave length of 450m under same conditions cause 7% increase in the maximum wave amplitude at the distant shore under the condition inputting flux to initial conditions.

### **5.3.3 Numerical modeling with NAMI-DANCE with vertical coastal slope ( $\alpha = 90^\circ$ )**

For this case, 8 runs are carried out having 90 seconds as simulation duration these are;

- i) 300m initial wave length, 30m initial wave amplitude with no flux
- ii) 300m initial wave length, 30m initial wave amplitude with flux
- iii) 300m initial wave length, 50m initial wave amplitude with no flux
- iv) 300m initial wave length, 50m initial wave amplitude with flux
- v) 450m initial wave length, 30m initial wave amplitude with no flux
- vi) 450m initial wave length, 30m initial wave amplitude with flux
- vii) 450m initial wave length, 30m initial wave amplitude with no flux
- viii) 450m initial wave length, 30m initial wave amplitude with flux
- ix) 450m initial wave length, 30m initial wave amplitude with flux

The comparison of results is given in Figure 5-11, Figure 5-12, Figure 5-13, Figure 5-14.

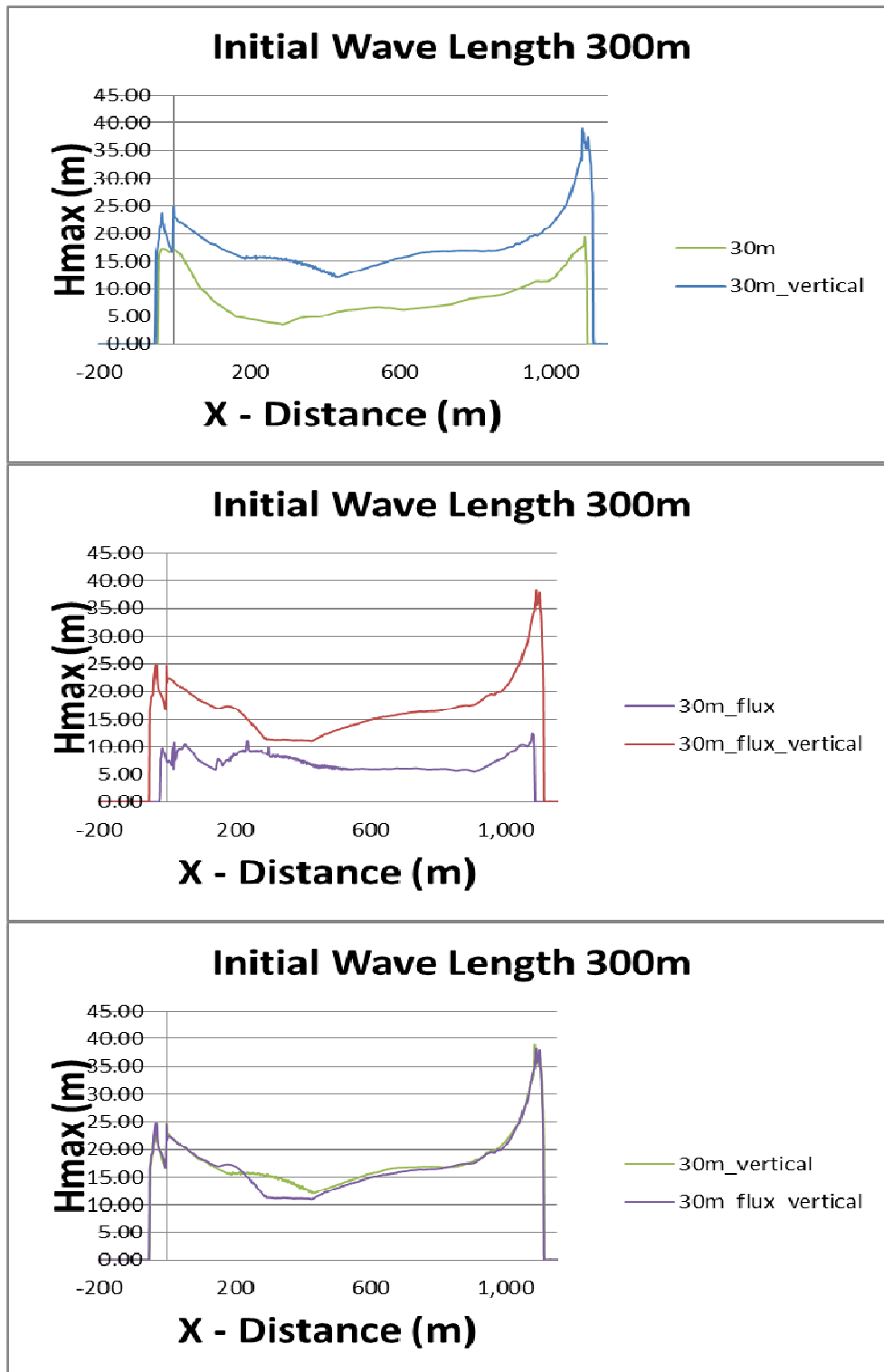


Figure 5-11 - Change of  $H_{max}$  along propagation distance for the case of vertical coastal slope ( $\alpha = 90^\circ$ )

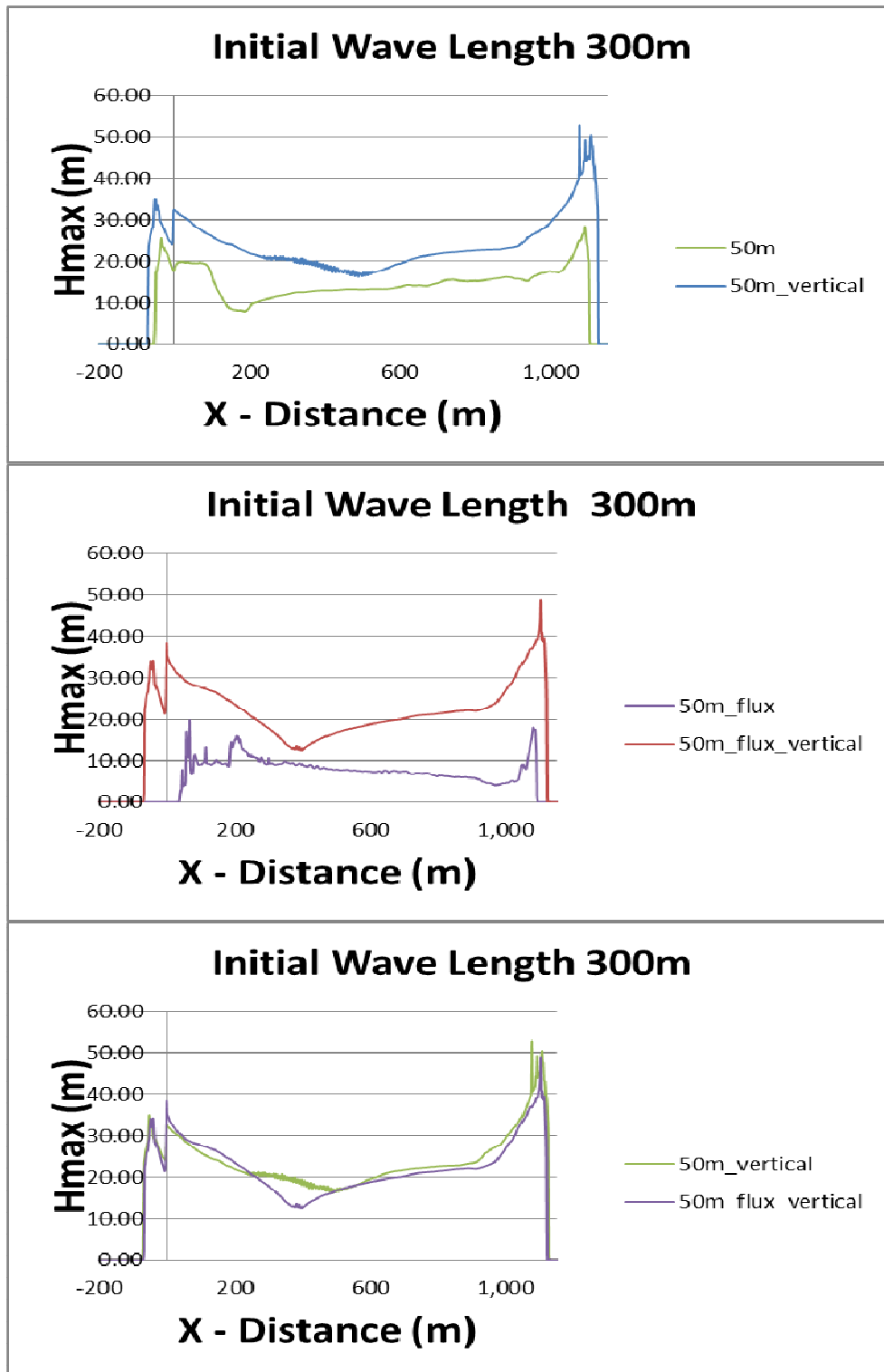


Figure 5-12 - Change of  $H_{max}$  along propagation distance for the case of vertical coastal slope ( $\alpha = 90^\circ$ )

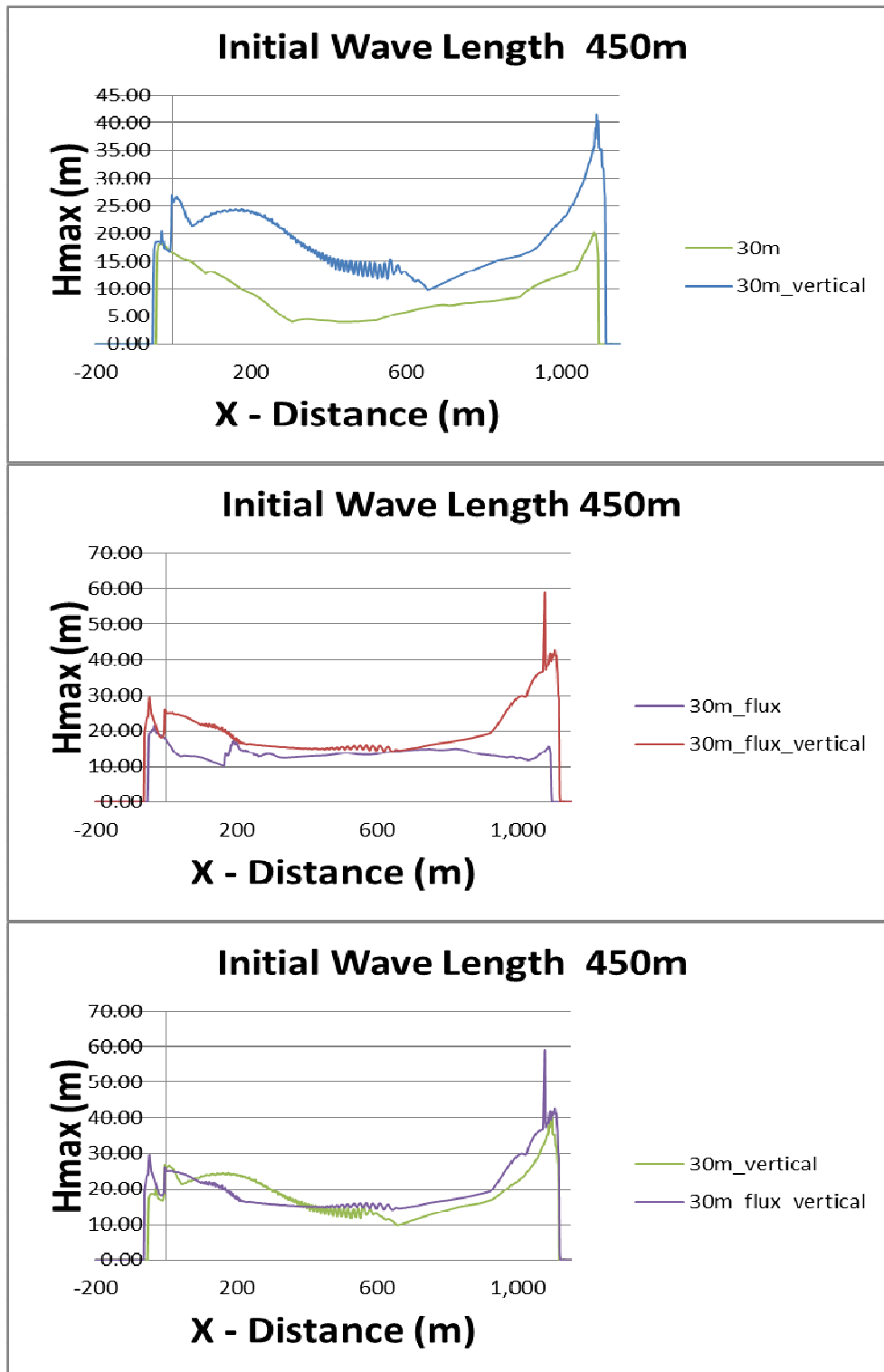


Figure 5-13 - Change of  $H_{max}$  along propagation distance for the case of vertical coastal slope ( $\alpha = 90^\circ$ )

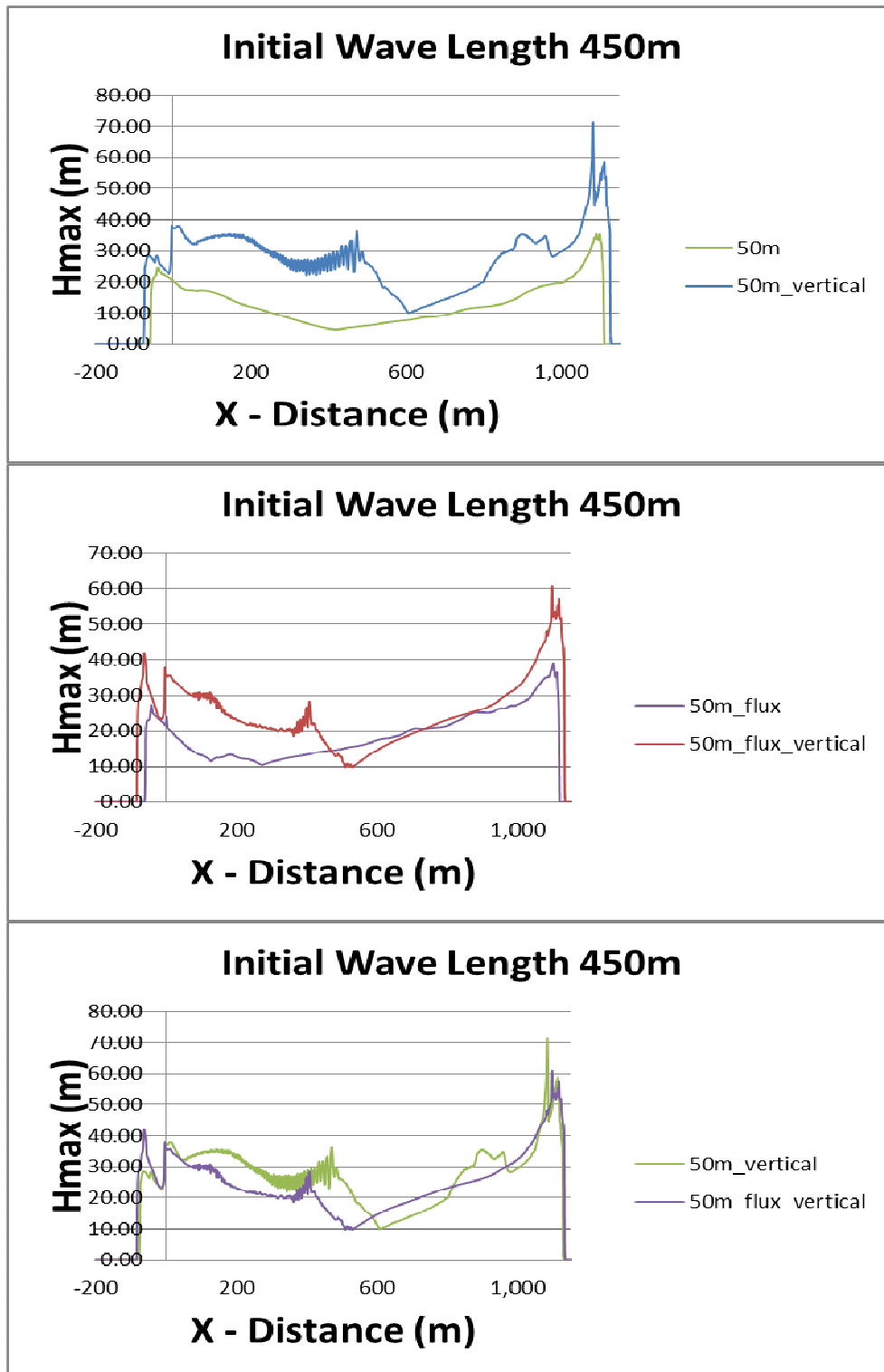


Figure 5-14 - Change of  $H_{max}$  along propagation distance for the case of vertical coastal slope ( $\alpha = 90^\circ$ )

By changing the coastal slope from inclined to vertical, it is expected to see higher maximum wave amplitudes since the subsidence volume increases in the order of double. As expected  $H_{max}$  observed in the wall bathymetry is nearly 2 – 2.5 times of the  $H_{max}$  value in the inclined coastal slope.

#### 5.4 Determination maximum wave amplitude with empirical formulation

The maximum wave amplitudes for initial wave amplitudes of 10m, 20m, 30m, 40m and 50m are computed by empirical formula generated by Panizzo et. al. (2005). Since in this study single initial wave width is used ( $y_w=2000m$ ) and initial wave length is not taken into account by this method only one  $H_{max}$  value for each initial wave amplitude will be computed. The results are given in Table 5-2 . Impact velocity parameter in the formula is taken 5m/s.

**Table 5-2** - Maximum wave amplitudes by empirical formulation

<b>Initial Wave Amplitude (m)</b>	10m	20m	30m	40m	50m
<b>Maximum Wave Amplitude (m)</b>	8.36	12.42	15.67	18.47	20.98

#### 5.5 Comparison of maximum wave amplitudes obtained from numerical modeling

A total of 47 runs are performed by NAMI-DANCE.  $H_{max}$  near the shore values for each case are shown in Table 5-3, the empirical formulation outputs are calculated using the input parameters given in Table 5-2 . All the simulation durations are selected as 90 seconds in order to observe the maximum amplitude of first wave before coming the re-reflected wave from landslide side. This is because the effect of the reflecting wave is not taken into account in empirical formulation. Therefore the simulation duration is taken limited to 90 seconds.

Table 5-3 shows that the outputs with 50 meter initial wave length can be discarded because of its short length and inconsistent results. In those cases, as initial wave height increases,  $H_{\max}$  value decreases. One of the reasons can be the high steepness of the initial wave with short length. In other cases where initial wave length is equal to or higher than 150m, maximum wave amplitudes tend to increase up-to 400m initial wave length. But further increase in the initial wave length doesn't increase or even decrease the  $H_{\max}$  value because of the short distance of the source to distant shore which cannot permit proper evolution of the wave.

Considering the flux effect, a clear correlation cannot be established according to the model outputs. For example for initial wave amplitude of 30m and initial wave length 300m in inclined coastal slope, addition of flux decreases the maximum wave amplitude by 36%. On the other hand for initial wave length of 450 under same conditions cause 7% increase in the maximum wave amplitude at the distant shore under the condition inputting flux to initial conditions. Simulations in vertical coastal slope and simulations with 50 meter initial wave amplitude give similar results, so it can be said that addition of flux in the simulation doesn't cause changes as expected in terms of determining maximum wave amplitude at the distant shore.

By changing the coastal slope from inclined to vertical, it is expected to see higher maximum wave amplitudes since the subsidence volume increases in the order of double. As expected  $H_{\max}$  observed in the wall bathymetry is nearly 2 – 2.5 times of the  $H_{\max}$  value in the inclined coastal slope.

To sum up, increasing initial wave amplitude results in higher maximum wave amplitudes initial wave length higher than 150m. Also the coastal slope has an important effect on maximum wave amplitude since the volume of displaced water is highly dependent on bathymetry. Flux effect cannot be established very

successfully. It is suggested that further investigations are necessary to decide whether it is relevant to take into account in numerical modeling.

**Table 5-3** –  $H_{\max}$  Value from Modeling & Empirical Formulation for each case

Initial Wave Amplitude	Set-Up	Flux	Hmax for Different Initial Wave Lengths							Empirical Hmax (m)
			50	150	300	350	400	450	500	
10	Inclined	No	5.2	7.7	8.1	8.1	9.3	8.6	8.2	8.4
20	Inclined	No	2.6	15.7	16.1	17.0	15.9	14.3	14.2	12.4
30	Inclined	No	1.4	16.6	19.4	18.4	22.0	20.1	22.9	15.7
30	Inclined	Yes	-	-	12.4	-	-	21.6	-	15.7
30	Inclined	Yeni	-	-	36.0	-	-	67.7	-	15.7
30	Vertical	No	-	-	38.9	-	-	41.6	-	15.7
30	Vertical	Yes	-	-	38.3	-	-	58.6	-	15.7
40	Inclined	No	1.0	10.1	24.3	28.1	30.4	29.5	29.4	18.5
50	Inclined	No	0.6	9.8	28.4	31.5	30.4	35.5	35.5	21.0
50	Vertical	No	-	-	52.8	-	-	71.2	-	21.0
50	Vertical	Yes	-	-	48.8	-	-	60.8	-	21.0
50	Inclined	Yes	-	-	19.8	-	-	39.0	-	21.0

### 5.6 Comparison of maximum wave amplitudes obtained from numerical modeling and empirical formulation

The empirical formulation developed by Panizzo et. al (2005), doesn't take initial wave length into account, because of that although numerical modeling is done with 7 different initial wave lengths for each initial wave amplitude, only one empirical  $H_{\max}$  is found for each initial wave amplitude.

In Table 5-4 the comparison of  $H_{\max}$  from modeling to maximum wave amplitude calculated by empirical formulation can be found. In this table % ERROR ( $\epsilon$ ) values are given which are computed as shown in the following;

$$\epsilon = \frac{H_{max \text{ from numerical modeling}} - H_{max \text{ from empirical relation}}}{H_{max \text{ from empirical relation}}} \times 100$$

**Table 5-4** -  $\epsilon$  of maximum wave amplitude values

Initial Wave Amplitude	Set-Up	Flux	Initial Wave Length						
			50	150	300	350	400	450	500
10	Inclined	No	-37%	-7%	-3%	-3%	10%	3%	-1%
20	Inclined	No	-79%	26%	29%	36%	27%	14%	14%
30	Inclined	No	-91%	6%	23%	17%	40%	28%	45%
30	Inclined	Yes	-	-	-21%	-	-	37%	-
30	Vertical	No	-	-	148%	-	-	165%	-
30	Vertical	Yes	-	-	144%	-	-	274%	-
40	Inclined	No	-94%	-45%	31%	51%	64%	59%	59%
50	Inclined	No	-96%	-53%	35%	50%	44%	69%	69%
50	Vertical	No	-	-	151%	-	-	239%	-
50	Vertical	Yes	-	-	132%	-	-	189%	-
50	Inclined	Yes	-	-	-5%	-	-	85%	-

In Table 5-4 , the % ERROR values that fall in the range of  $\pm 15\%$  is highlighted in green and the values fall in the range of  $\pm 15-30\%$  is highlighted in yellow. It can be clearly seen that with 10 meter to 30 meter initial wave lengths, the results of the numerical model are acceptable by comparing the maximum wave amplitude values with empirical relations.

### 5.7 Alternative Flux & Initial Wave Conditions

As previously described in this Chapter, a good correlation could not be achieved for the flux effect. Also an alternative method for determining the initial wave conditions is selected to compare the results with empirical equations. The initial wave conditions can also be estimated by following the experimental results of

Fritz et. al. (2003). Unlike the previous sections Chapter this time leading waves are also inputted in the simulation in addition to depression waves, and the flux effect in x-direction is modeled using “ $\sqrt{gd}$ ” without flux in (lateral) y-direction. For initial wave length of 300 meters for depression waves and 150 meters for leading waves 4 different simulations are performed;

- a) Depression wave amplitude 10m, leading wave amplitude 5m.
- b) Depression wave amplitude 10m, leading wave amplitude 5m with flux.
- c) Depression wave amplitude 20m, leading wave amplitude 10m.
- d) Depression wave amplitude 20m, leading wave amplitude 10m with flux.

Similar to previous sections of this Chapter, the changes of maximum wave amplitude along the propagation distance are plotted and these values are compared with the empirical equations. These graphs are shown in Figure 5-15 without flux and in Figure 5-16 with flux.

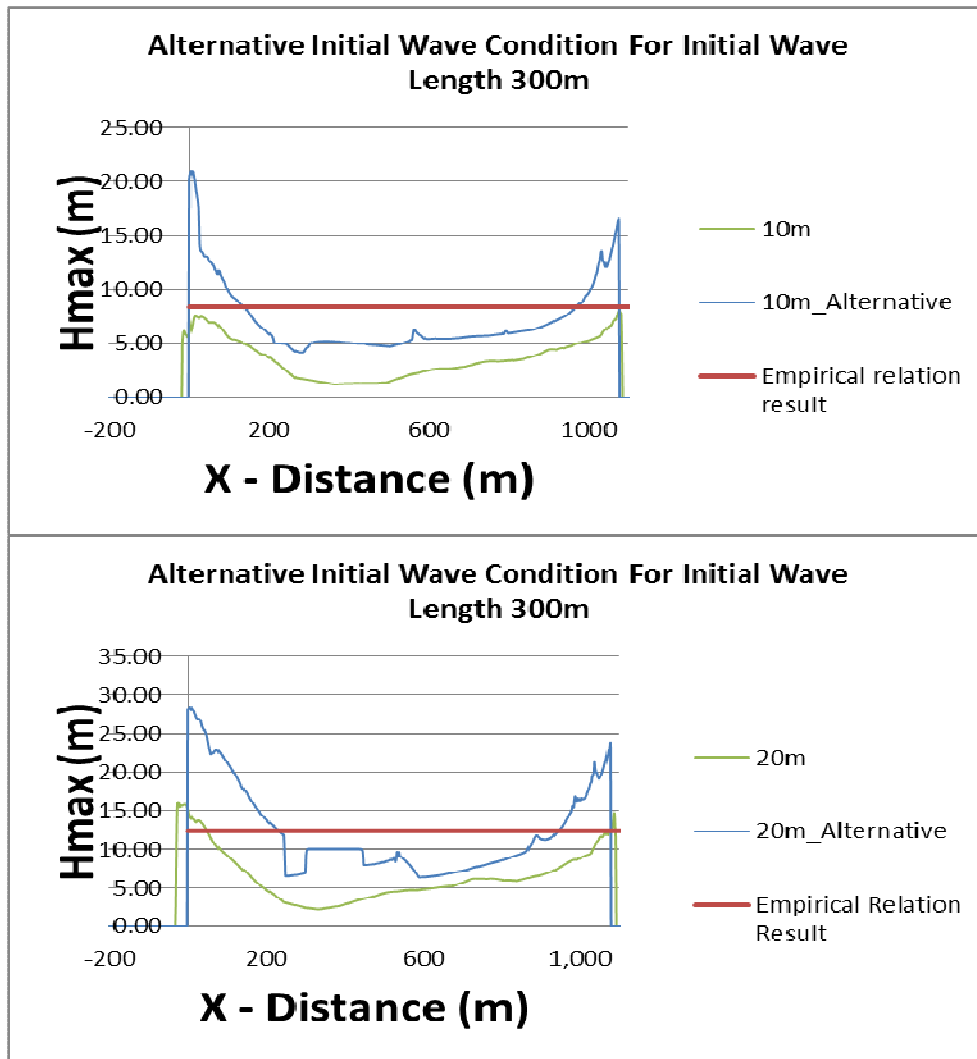
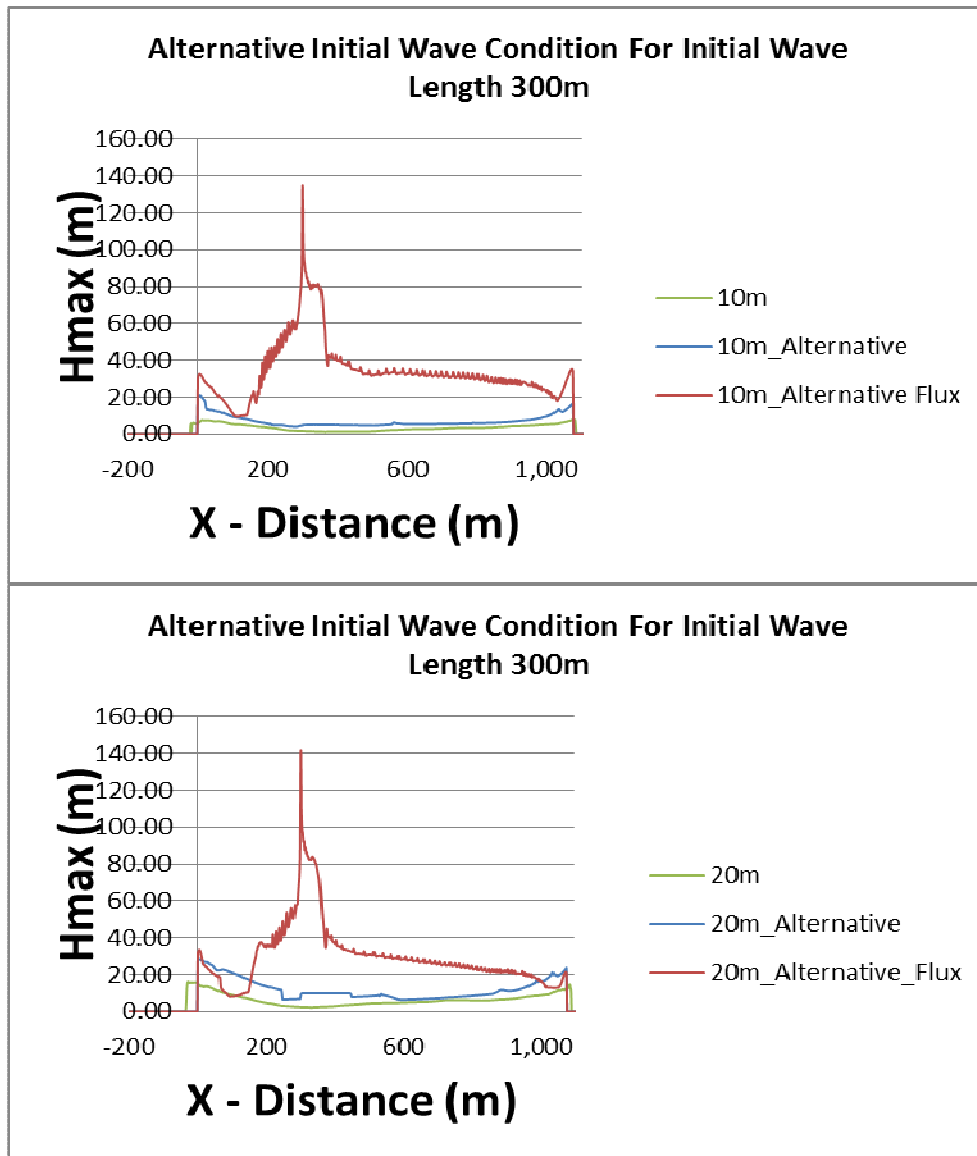


Figure 5-15 - Change of  $H_{max}$  along propagation distance for alternative initial wave conditions without flux



**Figure 5-16 - Change of  $H_{max}$  along propagation distance for alternative initial wave conditions with flux**

The output graphs given in Figure 5-15 and their comparison with the results of empirical formulation relations (Panizzo et. al. 2005) shows that, better correlation can be obtained using only depression waves as initial wave condition for the studies in this chapter.

Also it can be seen from Figure 5-16 that flux effect can't be established using this alternative approach either, since the maximum amplitude values are extremely higher to empirical formulation outputs.

In conclusion, the evaluation of the numerical results and their comparison with the empirical relations, show that the empirical relations can be satisfied if the initial wave amplitude is selected as depression type in the range of 10–30 meters for inclined cross section under the basin conditions used in this Chapter without inputting the initial flux of water.

One of the reason of this result may come from the absence of dispersion term in nonlinear shallow equations since the dispersion can better simulate the highly steep waves which occur in landslide tsunami sources.

## CHAPTER 6

### A CASE STUDY: LANDSLIDE IN PERVARI DAM RESERVOIR

In order to understand the propagation of landslide generated waves in a dam, the Pervari Dam is selected as a case study. A potential landslide's effects on the reservoir of Pervari Dam are modeled in NAMI-DANCE. The maximum wave amplitudes at critical sections of the reservoir and at the dam location are computed and the possibility of overtopping is evaluated. The results from the numerical modeling are compared with the results obtained with the empirical formulation.

The Pervari Dam and Hydroelectric Power Plant (HEPP) will be constructed on the Botan creek, a tributary of the Tigris River, approximately 5 km from the town of Pervari, on Siirt Province, Southeastern Turkey. A 175 m tall RCC dam will be built and the installed capacity will be 400 MW. The project location (Figure 6-1) and project layout (Figure 6-2 ) given below are taken from "Pervari Dam and HEPP Project Consolidated Basic Design Engineering Report" prepared by Intertechne & Temelsu in 2009.

The maximum water level in the dam is 980, whereas the crest elevation is 985 with 5 meters of freeboard. The cross-section of the dam body is given in Figure 6-3.



**Figure 6-1 - Project Location**



**Figure 6-2 – Project Layout (Intertechne & Temelsu, 2009)**

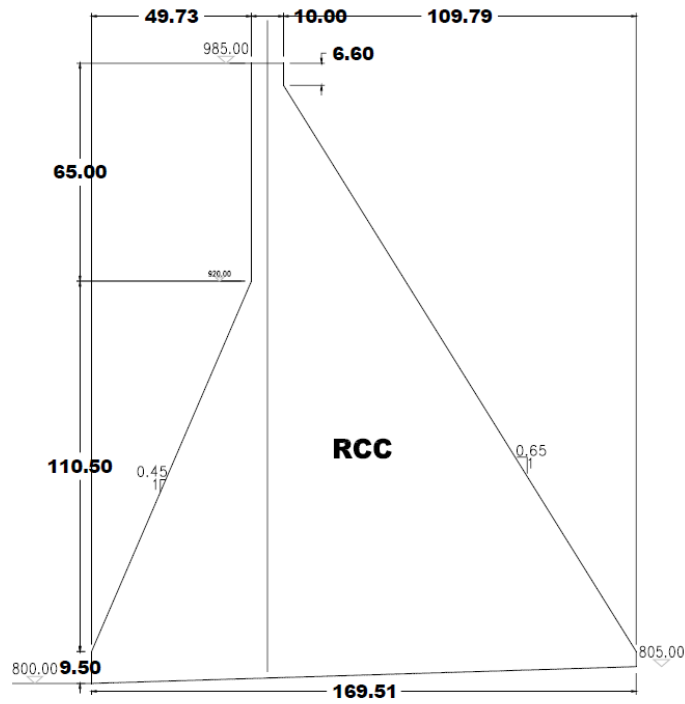


**Figure 6-3 - Cross-Section of the Dam Body**

### **6.1 History of Earthquakes in the Region**

Earthquakes may trigger landslides. Since the study area is at the first degree earthquake zone, Pervari Dam and its nearby area are subject to the threat of experiencing earthquakes and associated phenomena. Table 6-1 shows a list of earthquakes with a magnitude of 6.0 and higher in a diameter of 200km around study area in the last century. Figure 6-4 shows the location of these earthquakes with respect to the study area.

**Table 6-1** - List of nearby earthquakes in the last century

(<http://www.sayisalgrafik.com.tr/deprem>)

Date	Time (GMT)	Latitude	Longitude	Depth (km)	Magnitude
06.09.1975	09:20	38.51	40.77	32	7.8
06.05.1930	22:34	37.98	44.48	70	7.6
19.08.1966	12:22	39.17	41.56	26	6.9
28.04.1903	23:46	39.1	42.5	0	6.3
24.11.1976	12:22	39.05	44.04	10	6.1
28.09.1908	06:28	38	44	0	6

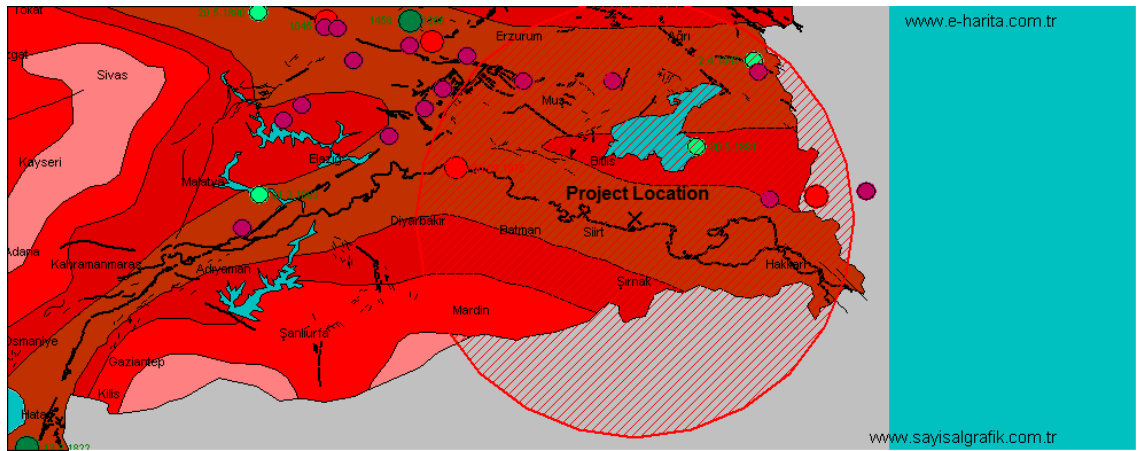


**Figure 6-4** - Location of nearby Earthquakes ([www.sayisalgrafik.com.tr](http://www.sayisalgrafik.com.tr))

## 6.2 Landslide into the Pervari Dam Reservoir

The possible landslide's parameters such as; position, dimensions, velocity, direction etc. are estimated with the help of geology department of Enerjisa Enerji Üretim A.Ş. From a number of alternatives, the most probable set of parameters is selected. The possible landslide location is at the left bank of the river above the maximum water level of the dam and approximately at 400m away from dam body at upstream side (Figure 6-5 ).

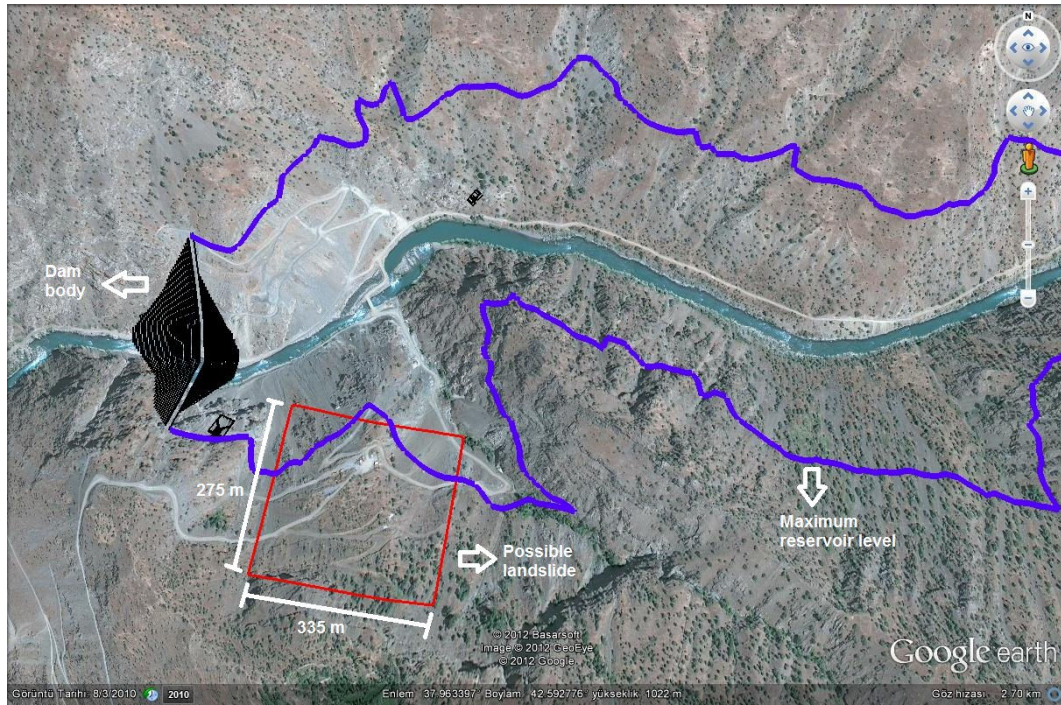


**Figure 6-5** – Landslide layout from Google Earth View

Estimated landslide and determined coastal slope parameters are given in Table 6-2 . The geological experts of Enerjisa have chosen the impact velocity as extremely rapid according to the classification of landslide velocity scale determined by Cruden and Varnes (1996).

**Table 6-2** – Estimated landslide and determined coastal slope parameters

<b>w</b>	335	landslide width (m)
<b>h</b>	30	landslide height (m)
<b>l</b>	275	landslide length (m)
<b>v</b>	5	impact velocity (m/s)
<b>d</b>	150	local water depth (m)
<b><math>\alpha</math></b>	25.7	inclination angle
<b><math>\gamma</math></b>	33.7	slope inclination angle (right bank)

## 6.3 Modeling with NAMI-DANCE

### 6.3.1 Bathymetry & Mapping

The bathymetry is constructed using digitized versions of 1/25000 scale maps. After the merging of digitized maps, the elevation of 980masl which corresponds to maximum water level is considered as 0m elevation. The elevations under this level are the water depths (+) and the elevations that are above this level are corresponding to land (-). The bathymetry is prepared considering maximum water level because the landslide generated waves are most critical at that case.

Spatial grid sizing is selected as 5m in both x and y directions. In total the modeling area is covered with 558x2520 grid notes corresponding to an area of 2790x12600 m<sup>2</sup>. Since dam body has a freeboard of 5m elevation, the crest of the dam is set to -5m with the width of 15m. Hence the overflow and overtopping can be monitored correctly in simulation.

52 gauge points are selected along the dam coast and at the dam crest. The computed water and flow conditions are presented with discussion at selected critical locations among those gauge points. The gauge points are located closer at more critical locations such as dam axis, areas close to landslide, narrow sections of the reservoir etc. The gauge locations are shown in Figure 6-6, and their depths and coordinates are given in Table 6-3. As seen from this Table the gauge locations are near the coast either at land or in the lake.

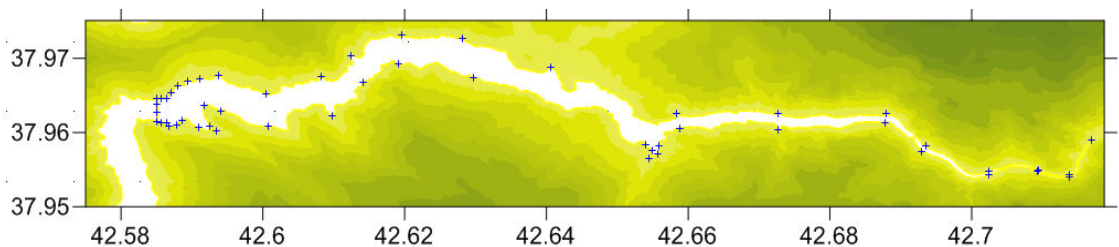


**Figure 6-6** – The locations of the Gauge points to observe time histories of water level fluctuations at different locations of the dam reservoir

**Table 6-3 - Gauge Point Coordinates and their Water Depth**

No.	X Coordinate	Y Coordinate	Depth (m)	No.	X Coordinate	Y Coordinate	Depth (m)
1	42.58505	37.96153	-5.0	27	42.70249	37.95431	-3.4
2	42.58505	37.96266	-5.0	28	42.69295	37.95743	-0.1
3	42.58506	37.96372	-5.0	29	42.69362	37.95816	6.1
4	42.58503	37.96462	-5.0	30	42.68782	37.96136	-1.3
5	42.58573	37.96457	6.4	31	42.67276	37.96038	-11.9
6	42.58640	37.96463	0.8	32	42.65891	37.96049	0.1
7	42.58713	37.96530	0.4	33	42.65594	37.95813	2.1
8	42.58803	37.96625	0.6	34	42.65577	37.95706	-1.7
9	42.58937	37.96697	0.8	35	42.65451	37.95650	0.1
10	42.59117	37.96727	2.3	36	42.65487	37.95749	-0.2
11	42.59376	37.96767	5.8	37	42.65401	37.95833	0.0
12	42.60048	37.96515	3.5	38	42.62970	37.96739	-1.7
13	42.60817	37.96753	3.5	39	42.61913	37.96927	-1.4
14	42.61244	37.97038	1.5	40	42.61411	37.96673	1.1
15	42.61960	37.97309	-0.5	41	42.60976	37.96226	-0.3
16	42.62817	37.97267	3.6	42	42.60078	37.96081	-1.1
17	42.64058	37.96872	1.4	43	42.59411	37.96288	-4.1
18	42.65835	37.96260	1.7	44	42.59178	37.96364	-2.3
19	42.67262	37.96257	2.5	45	42.59244	37.96086	6.4
20	42.68790	37.96253	4.9	46	42.59340	37.96027	0.5
21	42.70241	37.95472	6.1	47	42.59099	37.96069	-2.2
22	42.70941	37.95498	5.4	48	42.58867	37.96155	0.0
23	42.71379	37.95431	6.1	49	42.58778	37.96099	2.4
24	42.71697	37.95901	0.5	50	42.58679	37.96083	-2.2
25	42.71380	37.95405	-16.2	51	42.58646	37.96136	-2.3
26	42.70924	37.95480	-5.8	52	42.58559	37.96136	-3.9

### 6.3.2 Modeling of the landslide case for Pervari Dam

In order to investigate the effects of possible landslide in Pervari the tsunami simulation and visualization code NAMI-DANCE is applied to four different alternatives of initial wave form of the landslide. The initial wave form is obtained from the user-defined source generation module of the code.

For the selection of initial wave parameters a number of studies in the literature are reviewed. Some of these studies that cover submerged landslides are discarded and only the ones studying subaerial landslides are investigated. Some of these studies are already mentioned in Chapter 2 of this thesis study. Finally it is decided that the initial wave parameters for a potential landslide can be determined by using the outputs of the study of Fritz et. al. (2003). This study which is explained in Chapter 2 of this study is modified because of the following reasons;

- The experiments are done for an inclination angle of  $45^{\circ}$  but the inclination angle of the potential landslide angle in Pervari dam reservoir is  $25.7^{\circ}$ .
- The landslide volume in the experiments of Fritz et. al. (2003) reach the toe because of the higher inclination angle which is not applicable in the landslide studied in this Chapter due to a less steep inclination angle.
- The topography of Pervari dam reservoir area is a narrow one and the study of Fritz et. al. (2003) is not focusing on especially landslide generated waves in narrow basins.

Also in this Chapter the outputs of the simulations will be compared with the empirical formulation developed by Panizzo et. al. (2005) which is used for determining the wave parameters of landslide generated waves based on landslide parameters, which was explained previously in this study. Panizzo et. al. (2005) verified their study by applying their study to three historical landslide generated events that occurred in dam reservoirs and comparing the outputs with the observed wave parameters.

The determined initial wave conditions caused by a potential landslide in Pervari dam reservoir are as listed below;

Case (a): Only depression waves with 30m amplitude.

Case (b): 30m amplitude depression waves with 20m amplitude leading waves having smaller major and minor axis lengths than depression waves

Case (c): 30m amplitude depression waves with 30m amplitude leading waves having same major and minor axis lengths with depression waves

Case (d): 30m amplitude depression waves with 20m amplitude leading waves having same major and minor axis lengths with depression waves

The selected forms of initial water surface at the source (near the landslide) for these cases are plotted and shown in Figure 6-7 and the determined parameters are given in Table 6-4, where  $a_1$  is the wave amplitude of the depression wave and  $a_c$  is the wave amplitude of the leading wave.

**Table 6-4 – Determined initial water surface parameters**

		Case (a)			Case (b)			Case (c)			Case (d)		
		Left	Center	Right	Left	Center	Right	Left	Center	Right	Left	Center	Right
Depression Wave ( $a_1$ )	$L_{major}$ (m)	110	70	150	110	70	150	110	70	150	110	70	150
	$L_{minor}$ (m)	40	30	50	40	30	50	40	30	50	40	30	50
	Wave Amplitude	30	30	30	30	30	30	30	30	30	30	30	30
Leading Wave ( $a_c$ )	$L_{major}$ (m)	-	-	-	80	60	125	110	70	150	110	70	150
	$L_{minor}$ (m)	-	-	-	30	25	35	40	30	50	40	30	50
	Wave Amplitude	0	0	0	20	20	20	30	30	30	20	20	20

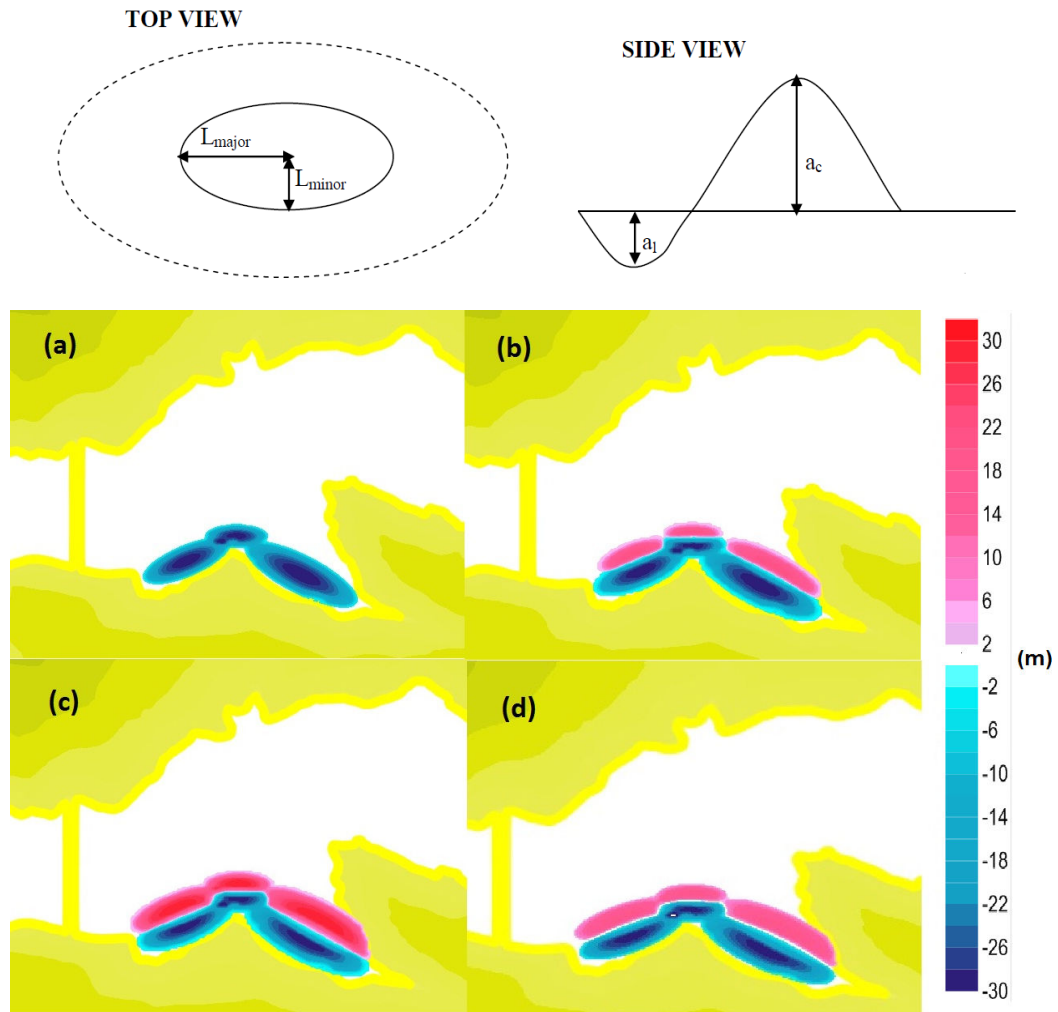


**Figure 6-7** – Initial water surfaces for cases (a), (b), (c) & (d)

### 6.3.3 Simulation & discussion of the results

The simulation duration is defined as 35 minutes which is sufficient to monitor the maximum wave amplitude even at the farthest point of the reservoir area. Time step for the simulation is selected 0.05 seconds for ensuring numerical stability with 5m grid size. The output files of the water surface form are stored at every 10 seconds for better visualization of the wave motion.

In each simulation the maximum water elevations at each grid points “OUT-ZMAX.grd”, are computed together with the arrival time of maximum amplitude

“OUT-TIME-MAX-WAVE.grd” and time histories of the water surface fluctuations at selected gauge points “OUT-TIME-HISTORIES\_ETA.dat”. The sea state at selected time steps are also stored during simulation in order to observe the wave propagation in time in the basin.

The maximum wave amplitude distributions for the simulated four cases are given in Figure 6-8. As it can clearly be seen from that figure, the most critical wave amplitudes (in the order of nearly 12 meters) are observed near dam body location and at the right bank just across the landslide. At other parts of the reservoir, maximum wave amplitudes are 2 meters or even less. This is reasonable as the landslide is modeled just upstream of the dam. Evaluation of the wave motion at or near dam body location is of high importance so a closer look to dam body location for all four cases is provided in Figure 6-9.

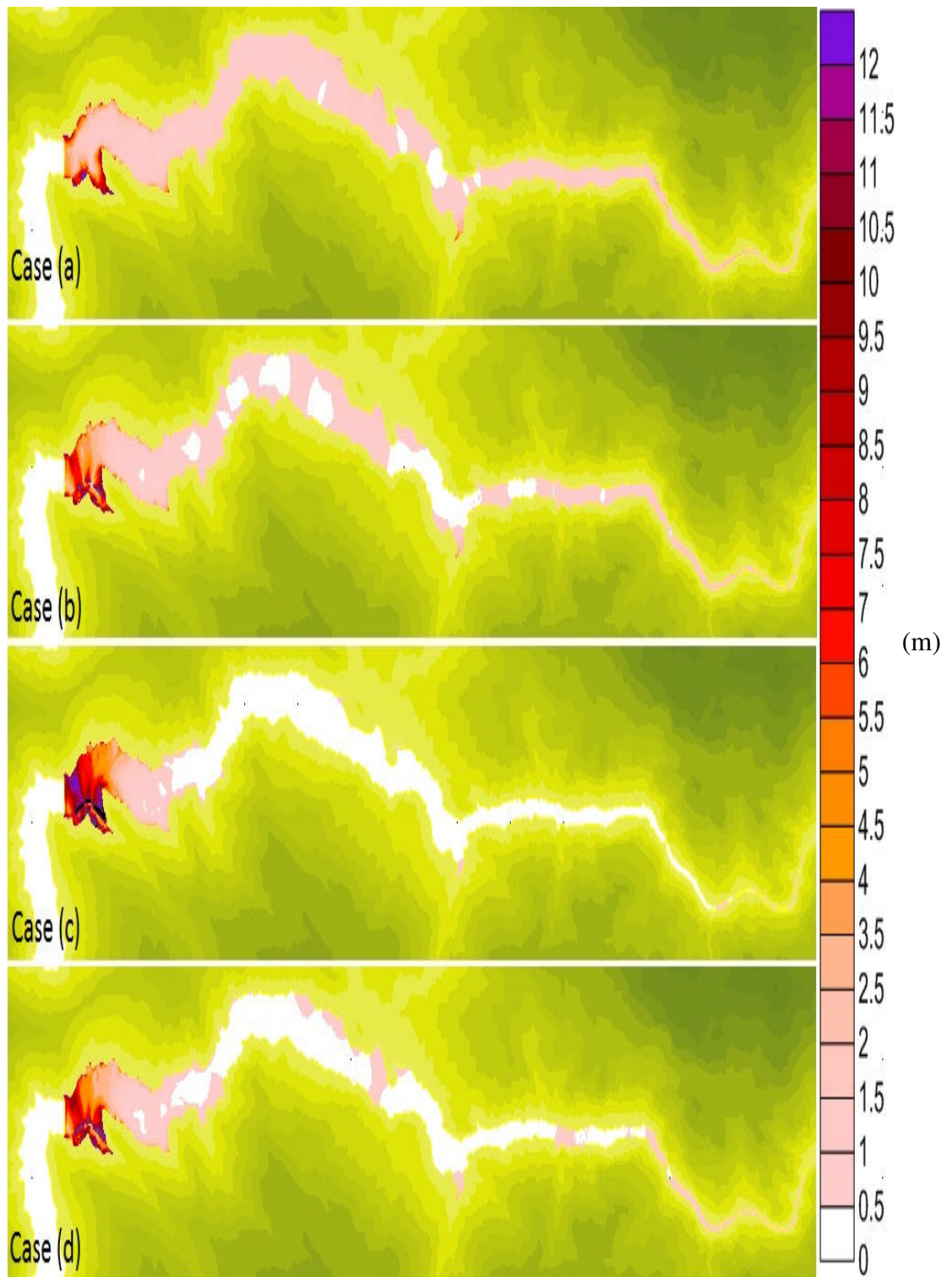


**Figure 6-8** – Maximum wave amplitude distributions along the reservoir for the four cases

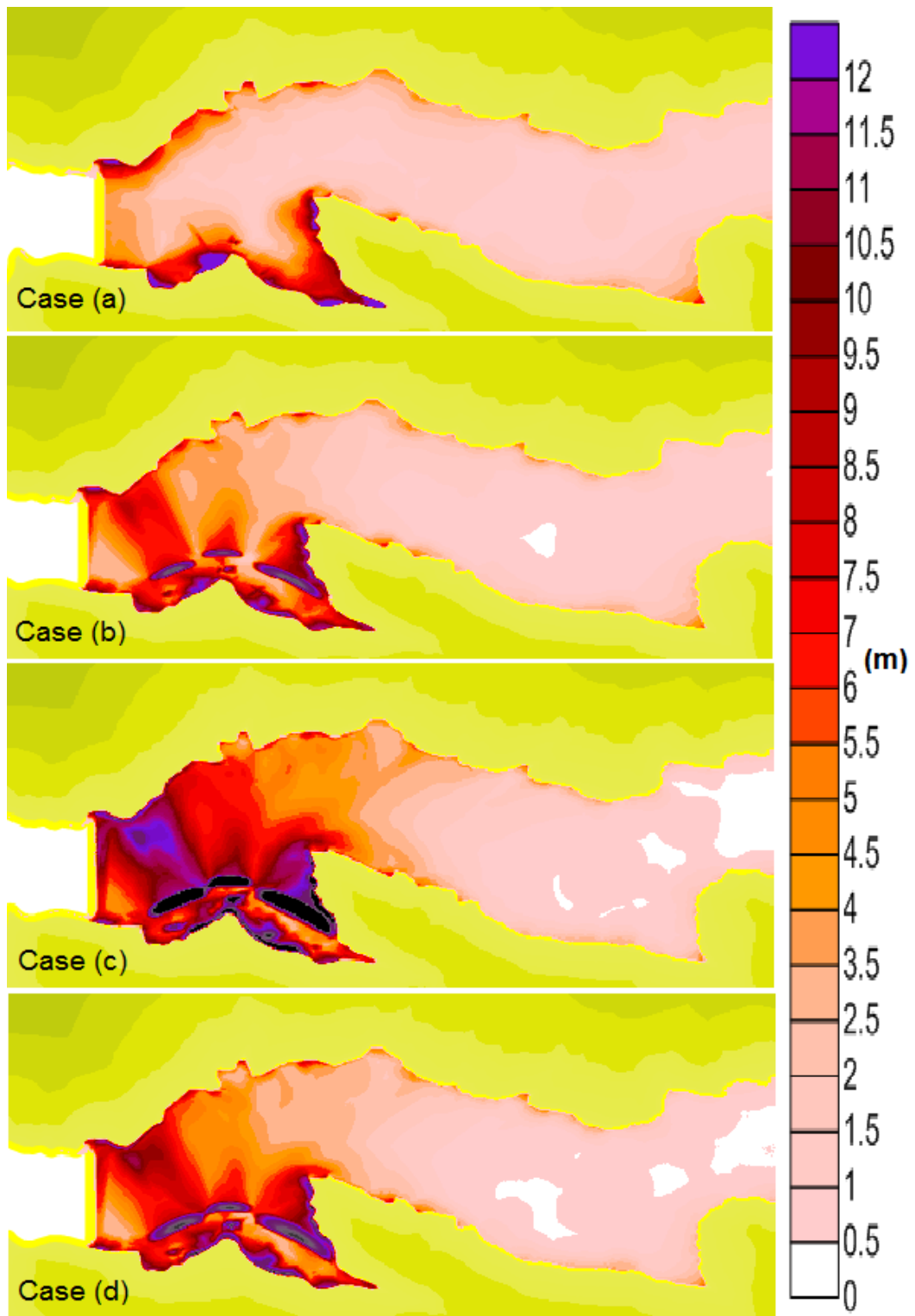


**Figure 6-9** - Maximum wave amplitude distributions near dam body location for the four cases

As it can be seen from the figures maximum wave amplitude values are highest in Case (c), and lowest in Case (a). This is expected as the volume of the water displaced follows the same order. To have a better understanding of the results, the time histories of water surface fluctuations at selected gauge points (Figure 6-10) is given in Figure 6-11, Figure 6-12, Figure 6-13, Figure 6-14 & Figure 6-15. In these graphs the duration of the wave amplification can be seen.

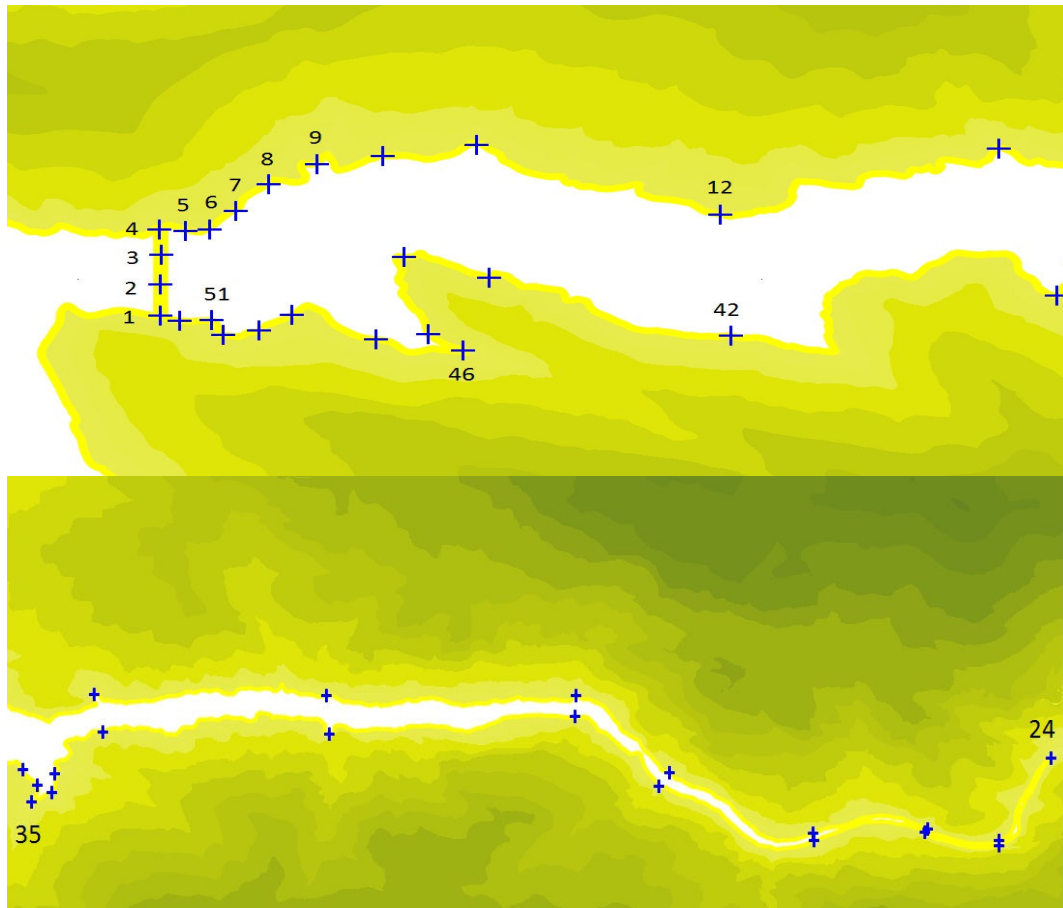


**Figure 6-10** – Location of chosen gauge points

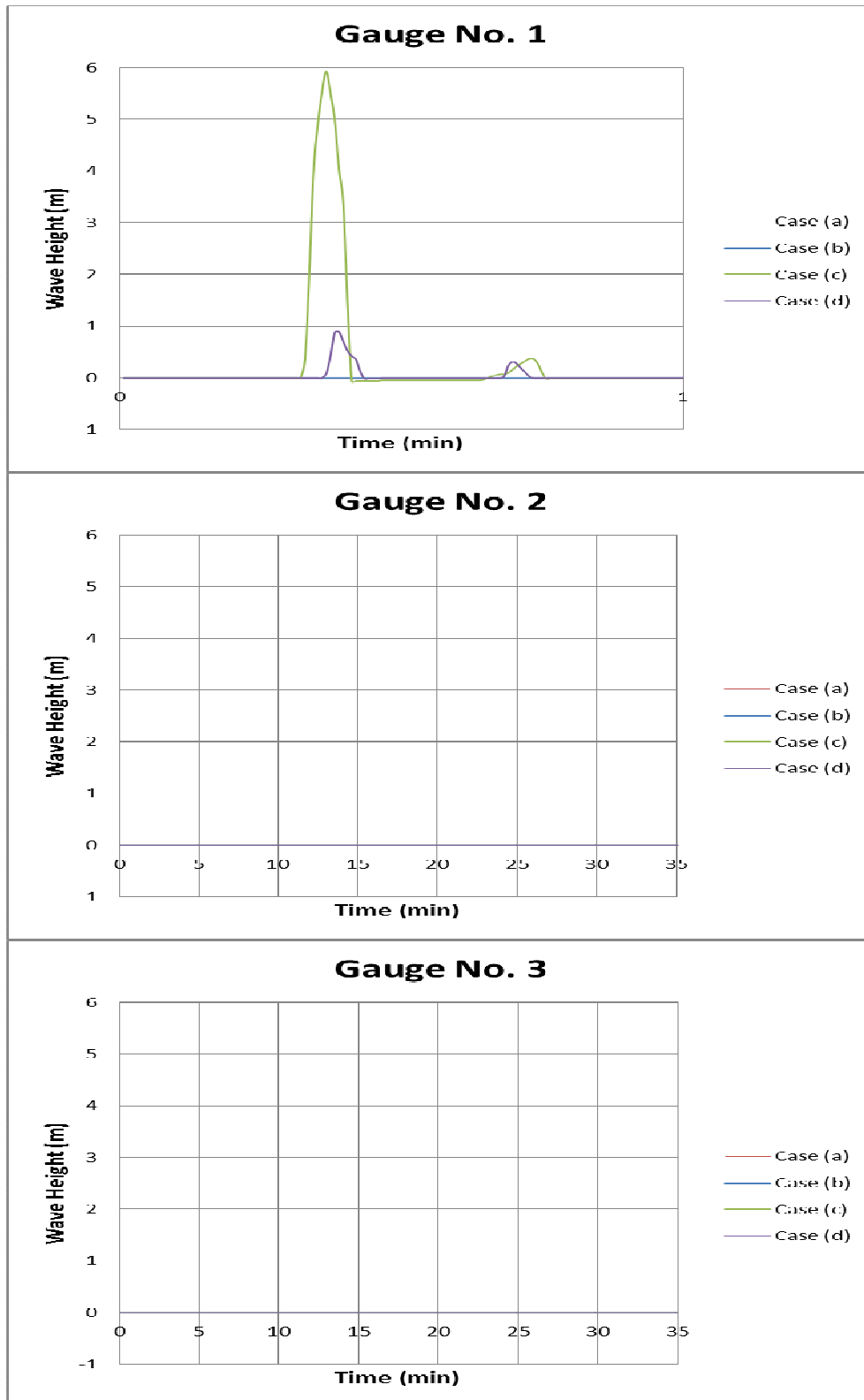


Figure 6-11 – Time histories of water surface fluctuations at gauge points

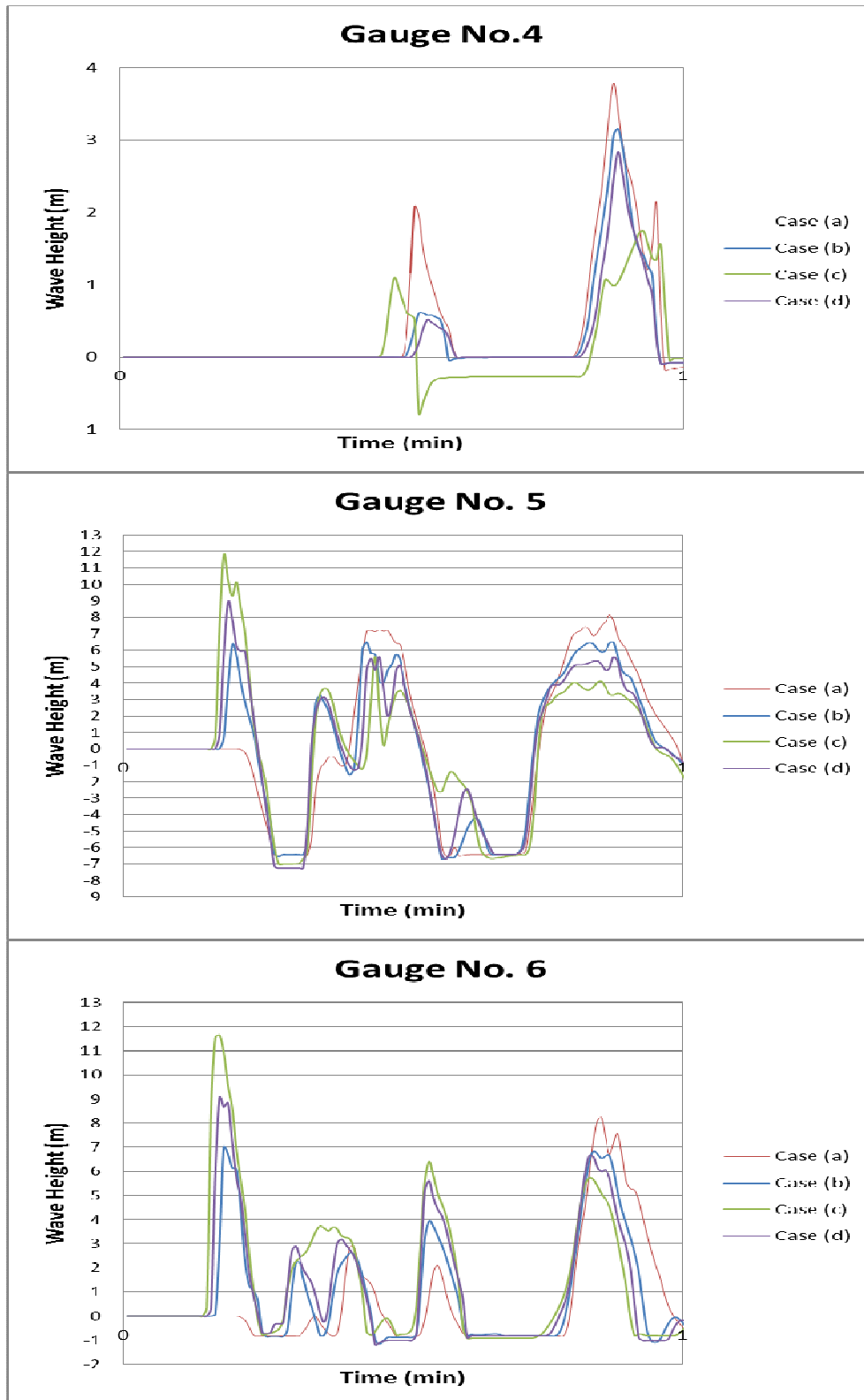


Figure 6-12 – Time histories of water surface fluctuations at gauge points

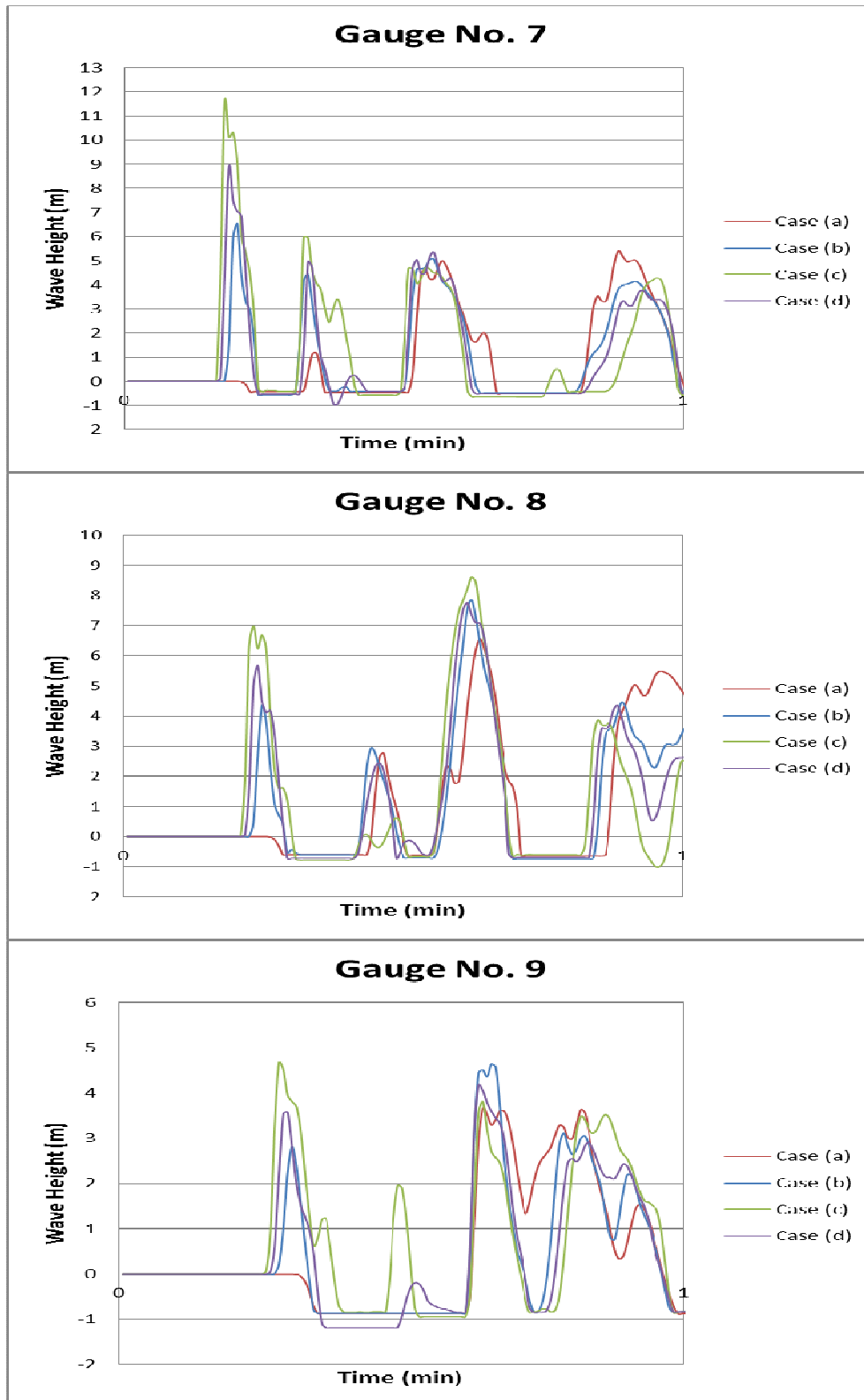


Figure 6-13 – Time histories of water surface fluctuations at gauge points

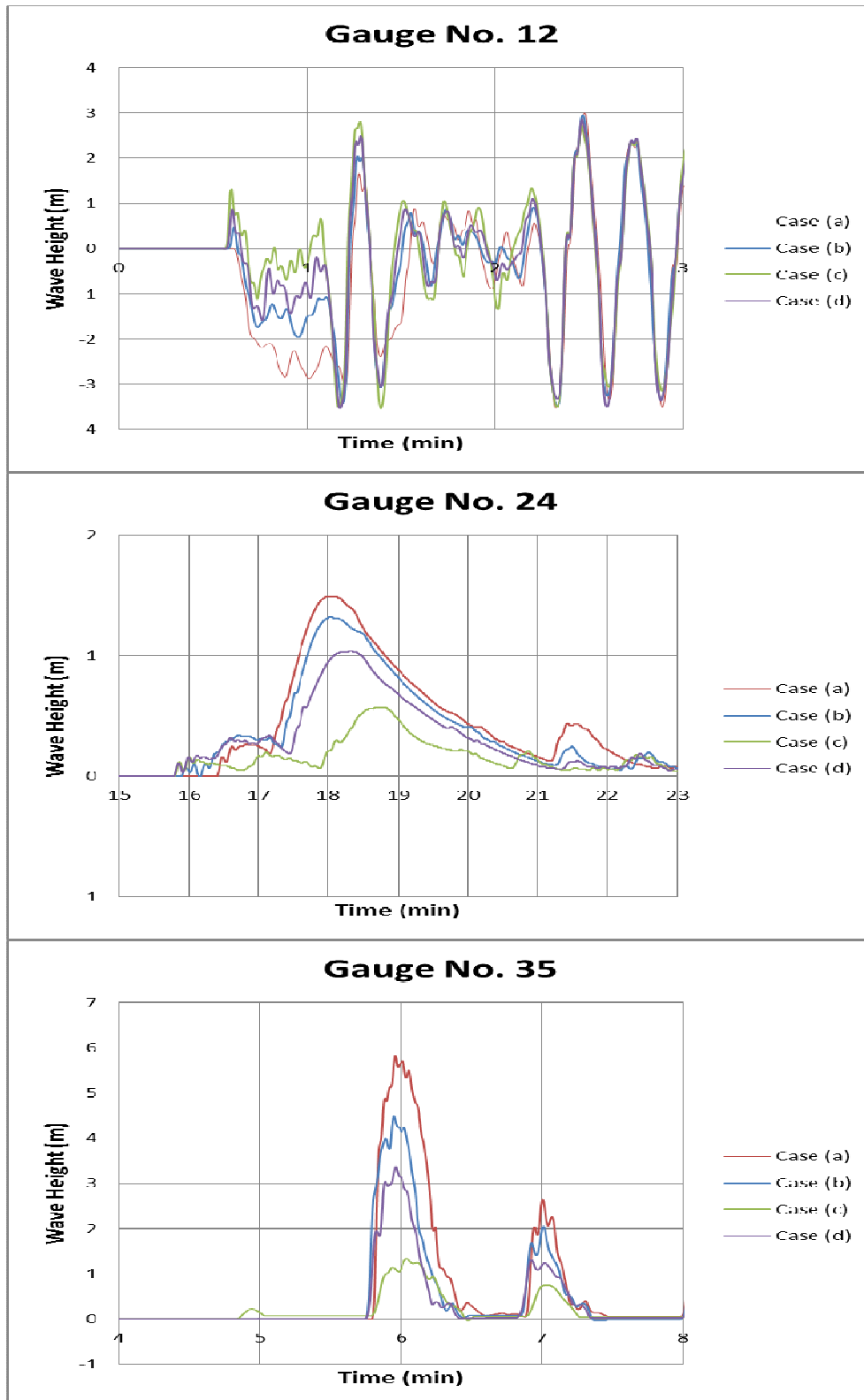


Figure 6-14 – Time histories of water surface fluctuations at gauge points

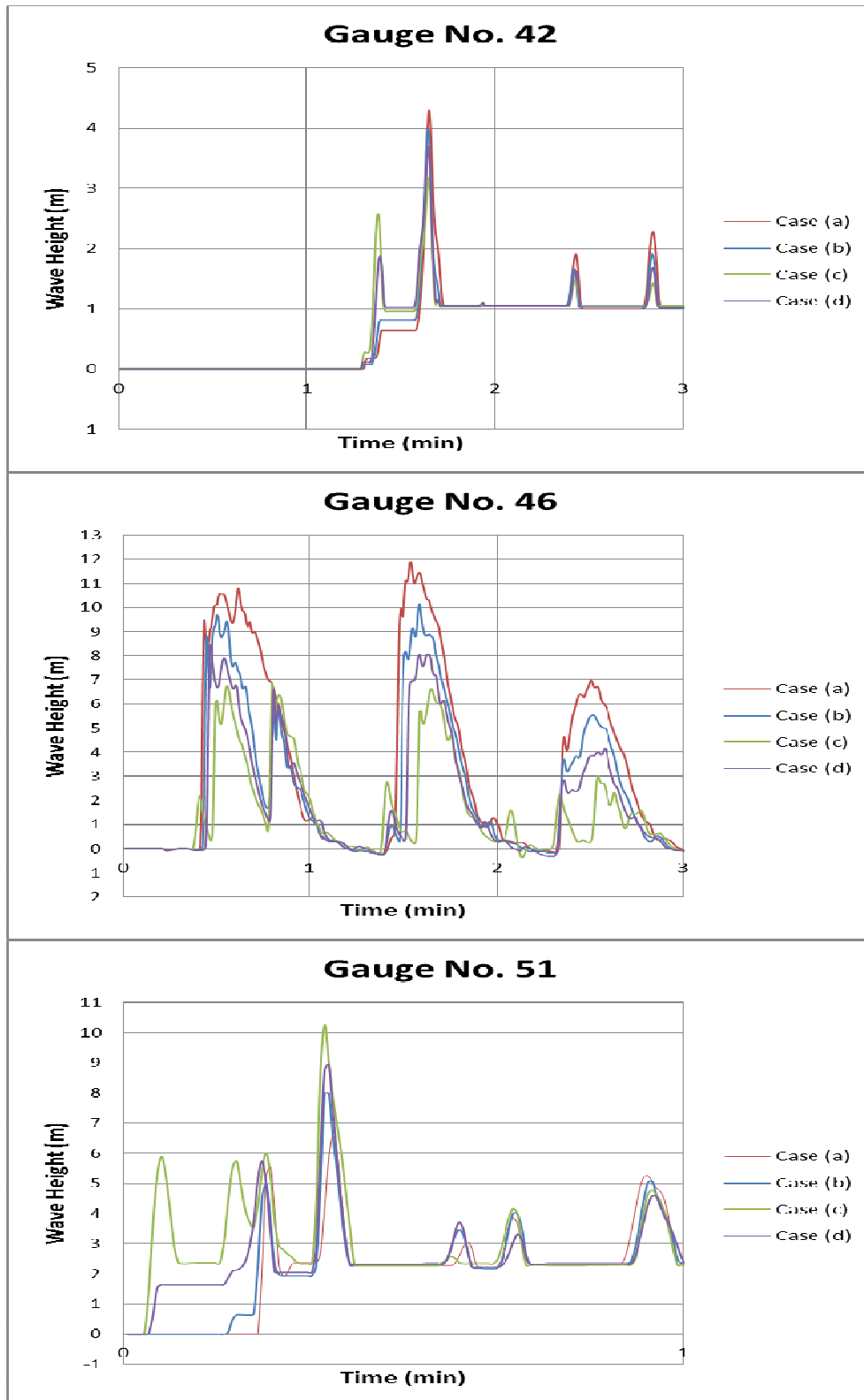


Figure 6-15 – Time histories of water surface fluctuations at gauge points

The first four gauge points are the most critical ones as they are placed at the crest of the dam body and the possibility of overtopping can be evaluated from these gauge points. Gauge no. 2 & 3 which are located at the middle section of the dam records some overtopping in all cases. Gauge no. 1 shows significant overtopping in Cases (c) & (d), whereas gauge no. 4 shows overtopping in all of the 4 cases.

The gauge points close to the dam body at the right bank, which are in the scope of empirical relation, give reasonable outputs. For Case (c), maximum wave amplitude is 11.77 meter in gauge no.5 which is the closest gauge point to the dam body and it decreases to 8.62 meter in gauge no.8 which is almost 500 meters away from the dam body. Maximum wave amplitude follows nearly the same pattern for other three cases also, but as one would expect the observed wave amplitudes are lower.

#### **6.4 Comparison of model outputs with empirical formula results**

The outputs of the modeling are compared to the results obtained from empirical formulations. There are a number of empirical formulations developed by Panizzo et. al (2005), Murty (2003), Huber & Hager (1997) etc. The outputs are evaluated with these formulations but only the comparison with Panizzo et al. (2005) is mentioned in this section because it is the most recent and detailed one giving more realistic results.

The developed empirical formulation is described in detail in Chapter 5.2. This formulation is applied to selected gauge points the results are given in Table 6-5. The gauges that are shaded grey are the gauges located at the dam body which will be studied in more detail. Also the yellow shaded gauges are outside of the scope of the empirical relation so their values will not be compared with empirical relation results.

**Table 6-5** – Comparison of model outputs with empirical relation results

Gauge No.	Maximum Wave Amplitude (m)				Empirical
	Case (a)	Case (b)	Case (c)	Case (d)	
1	0.0	0.0	5.9	0.9	5.7
2	0.0	0.0	0.0	0.0	5.2
3	0.0	0.0	0.0	0.0	4.4
4	3.8	3.2	1.7	2.8	3.6
5	8.1	6.5	11.8	8.9	5.8
6	8.2	7.0	11.7	9.1	6.5
7	5.4	6.5	11.6	8.9	7.0
8	6.6	7.9	8.6	7.8	7.1
9	3.7	4.6	4.7	4.2	6.8
12	3.0	3.0	2.8	2.9	3.1
24	1.5	1.3	0.6	1.0	0.9
35	5.8	4.5	1.3	3.4	1.2
42	4.3	4.0	3.2	3.7	2.6
46	11.9	10.1	6.9	8.5	3.2
51	6.6	8.0	10.3	8.9	4.3

In Table 6-6, the ratio of wave amplitudes from modeling to maximum wave amplitudes calculated using the empirical formulation for the selected gauge points is given. The  $\epsilon$  values (as it is defined in Chapter 5.6) that fall in the range of  $\pm 15\%$  is highlighted in green and the values fall in the range of  $\pm 15 - 30\%$  is highlighted in yellow.

**Table 6-6** -  $\epsilon$  of maximum wave amplitude values

Gauge No.	Case (a)	Case (b)	Case (c)	Case (d)
5	39%	11%	101%	52%
6	27%	8%	80%	40%
7	-23%	-6%	64%	26%
8	-7%	10%	21%	9%
9	-46%	-32%	-31%	-39%
12	-1%	-3%	-8%	-6%

The results clearly show that the wave amplitudes in the right bank of the reservoir, (just opposite of the landslide side) are in correlation with the results obtained from empirical formulation especially for the Case (b). Only in gauge no. 9 where the computed wave amplitudes are nearly the half of the wave amplitude expected from empirical formulation. The location of that gauge point (9) is somewhat sheltered by a peninsula compared which is not taken into account in the development of the empirical formulation. It can be concluded that the computational results under the selected input conditions are in correlation with the empirical results.

The maximum wave amplitude decreases at the gauge points located far (almost 14 km away) from the landslide location at upstream direction as expected.

It can further be said that the result of model application to Pervari reservoir are compatible with the empirical relation when the initial wave is inputted as depression with leading waves as described in **Case (b)**. Any other landslide to any other closed basin can be modeled in a similar way and the results may be compared for more accurate conclusions.

The gauge points from 1 – 4 are located on the dam body to observe overtopping if occurs. Those gauges are located 5 meters above the still water level at the dam crest. Since the basin is very narrow and the landslide location is located very close to the dam body the difference between the modeling and the empirical formulation may be acceptable since the empirical formulation is not developed for such basin especially.

It can be summarized that the maximum amplitude of the landslide generated wave can be 12 m in Pervari Dam Reservoir according to the simulated cases with 5 meter grid size. It is also shown that the risk by wave impact at the area of dam body is much higher than at the upstream side due to landslide at the selected locations with selected initial source.

## 6.5 High resolution simulation of Landslide at Pervari Dam

In order to investigate the level of wave motion and impact near the dam body higher resolution modeling focusing on this region is necessary. To do this the new bathymetry with 1m resolution is processed and a smaller domain covering the dam body and landslide area is selected for the modeling. The map of the smaller 1m resolution domain is given in Figure 6-16. Although the main map is digitalized from 1/25000 scale maps, since dam body is not present in these maps 1m grid resolution defines the future location of the dam body more precisely than 5m grid resolution hence giving more accurate overtopping results.

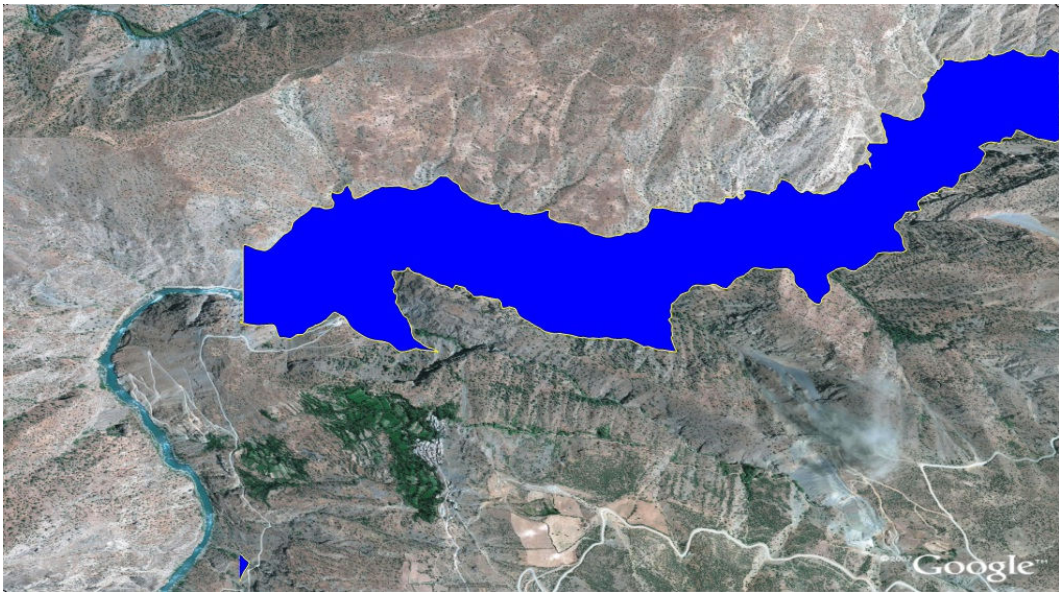


**Figure 6-16** – Map of 1m resolution domain

Higher resolution simulation is performed for the most extreme case, Case (c). In this simulation, the time step is chosen as 0.01 second and the simulation duration is determined as 1 minute which is sufficient to observe the arrival of maximum amplitude waves.

For better understanding of the wave motion, gauges that are on the top over the dam are moved closer to the edge and 4 additional gauge points are also located

just at upstream of the dam body to observe the maximum wave amplitude in front of the dam body together with on top of the crest. The coordinates and the water depths of the gauge points are given in Table 6-7 and the location of the gauge points are given in Figure 6-17.

**Table 6-7** – Gauge points used in 1m grid size simulation

No.	X Coordinate	Y Coordinate	Depth (m)	No.	X Coordinate	Y Coordinate	Depth (m)
1	42.58517	37.96153	-5	1-1	42.58522	37.96153	14.7
2	42.58517	37.96266	-5	2-2	42.58522	37.96266	154.9
3	42.58517	37.96372	-5	3-3	42.58522	37.96372	83.2
4	42.58517	37.96462	-5	4-4	42.58522	37.96462	14.1

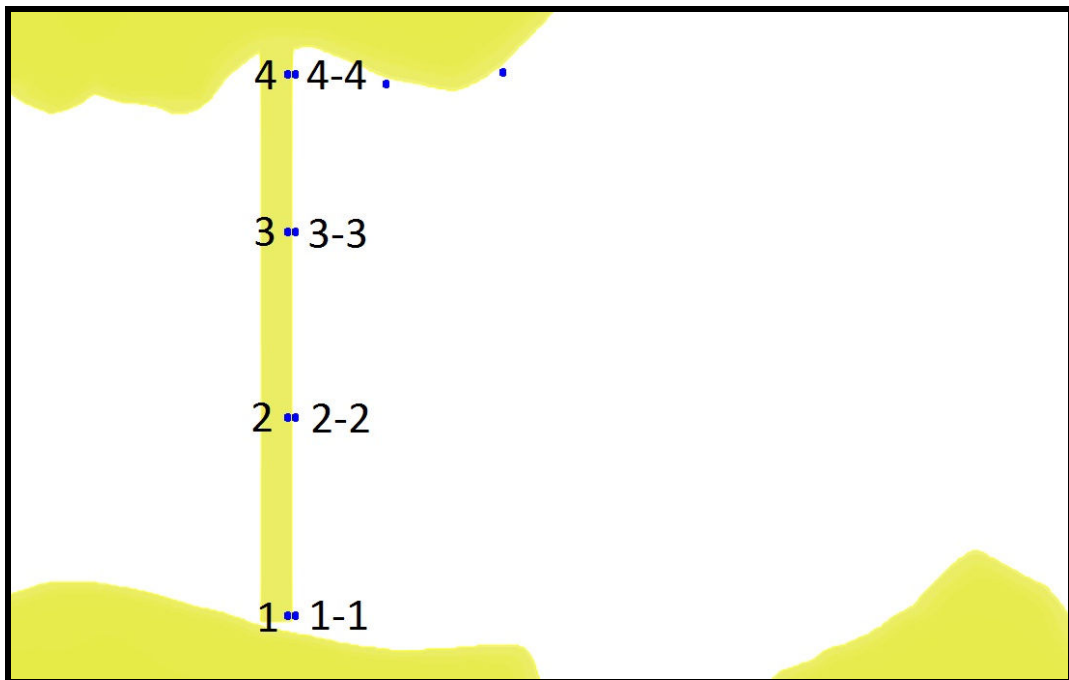


**Figure 6-17** – Location of the gauges used in 1m grid size simulation

Wave overtopping is compared with the maximum wave amplitude in the upstream of the dam by time histories of water surface fluctuation graphs which are given in Figure 6-18 & Figure 6-19.

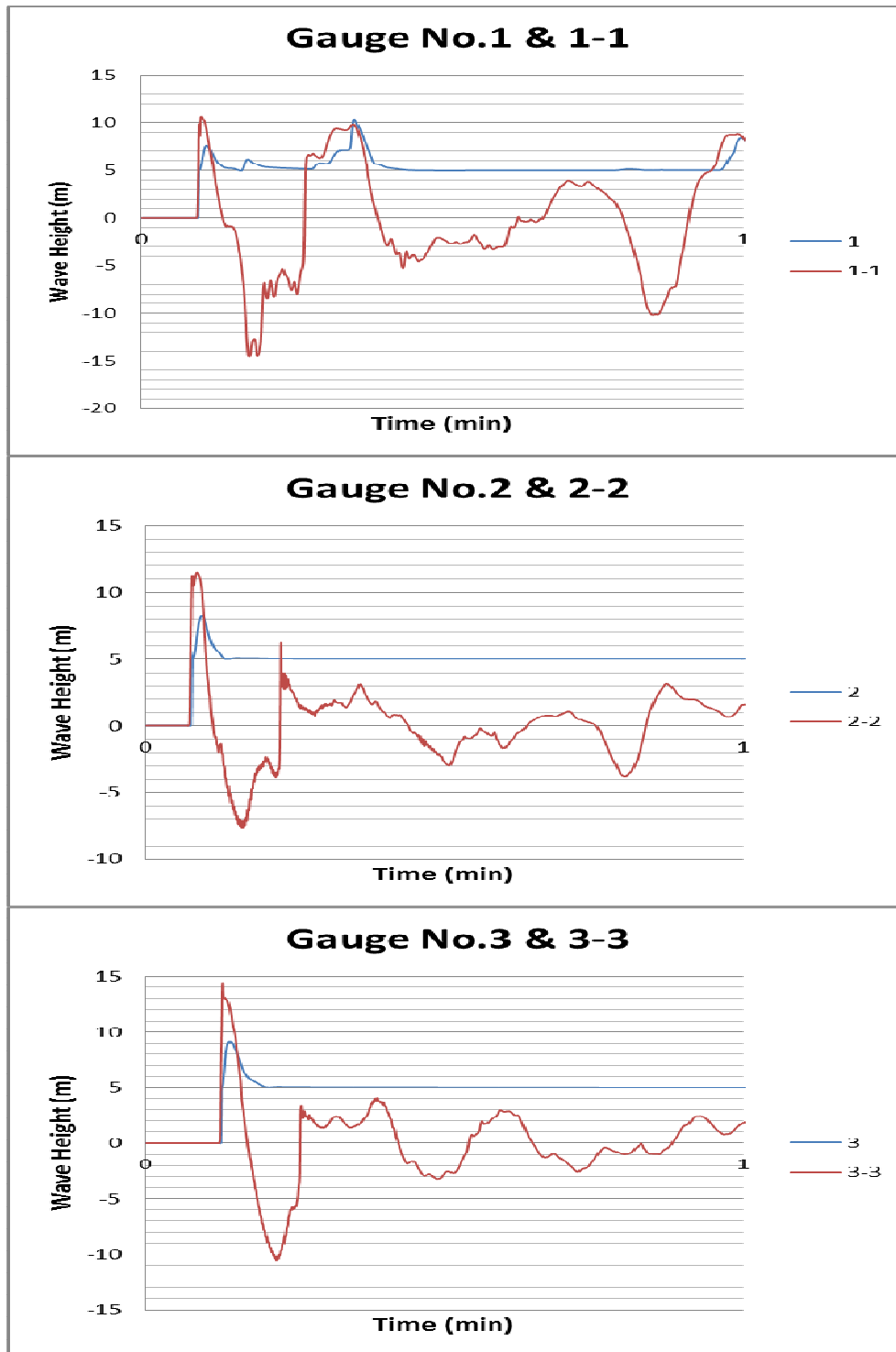


**Figure 6-18** - Time change of wave amplitude at the gauges for 1m grid size simulations

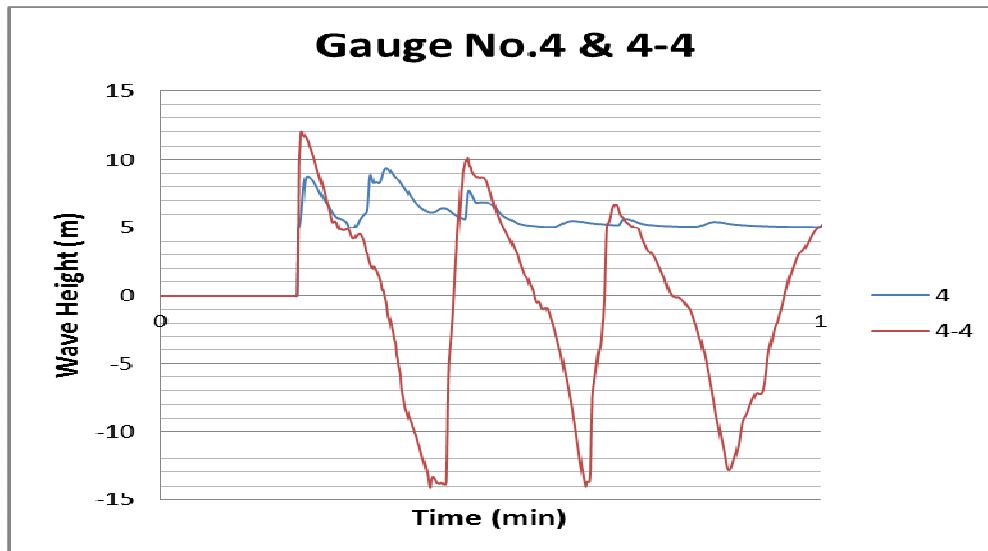


**Figure 6-19** – Time change of wave amplitude at the gauges for 1m grid size simulations

The difference between the outputs of the 1m grid size simulations from the outputs of 5m grid size simulations at the dam crest comes from the resolution difference since the 1m grid simulation is more accurate to compute the flow parameters accurately. 3.2 and 4.2 meters flow height of the overtopping at the crest are computed at gauges 2 and 3 by 1m grid size simulation. These values were small (even zero) in 5m grid size simulation where their locations were farther from the upstream edge of crest. Maximum wave amplitude in upstream face of the dam body for gauge points 2 and 3 are 11.5m and 14.4m respectively which is because of reflection from the dam body. At the locations of the gauge points (1 and 4) the depth of the overtopping flow are 5.4m and 4.4m respectively. The maximum wave amplitudes at the face of the dam body are 10.7m and 12m at same locations. From 1m grid size simulation it can be concluded that the dam can be overtopped about 5.5 meter flow depth.

The current speeds at selected gauge points are given in Figure 6-20 & Figure 6-21.

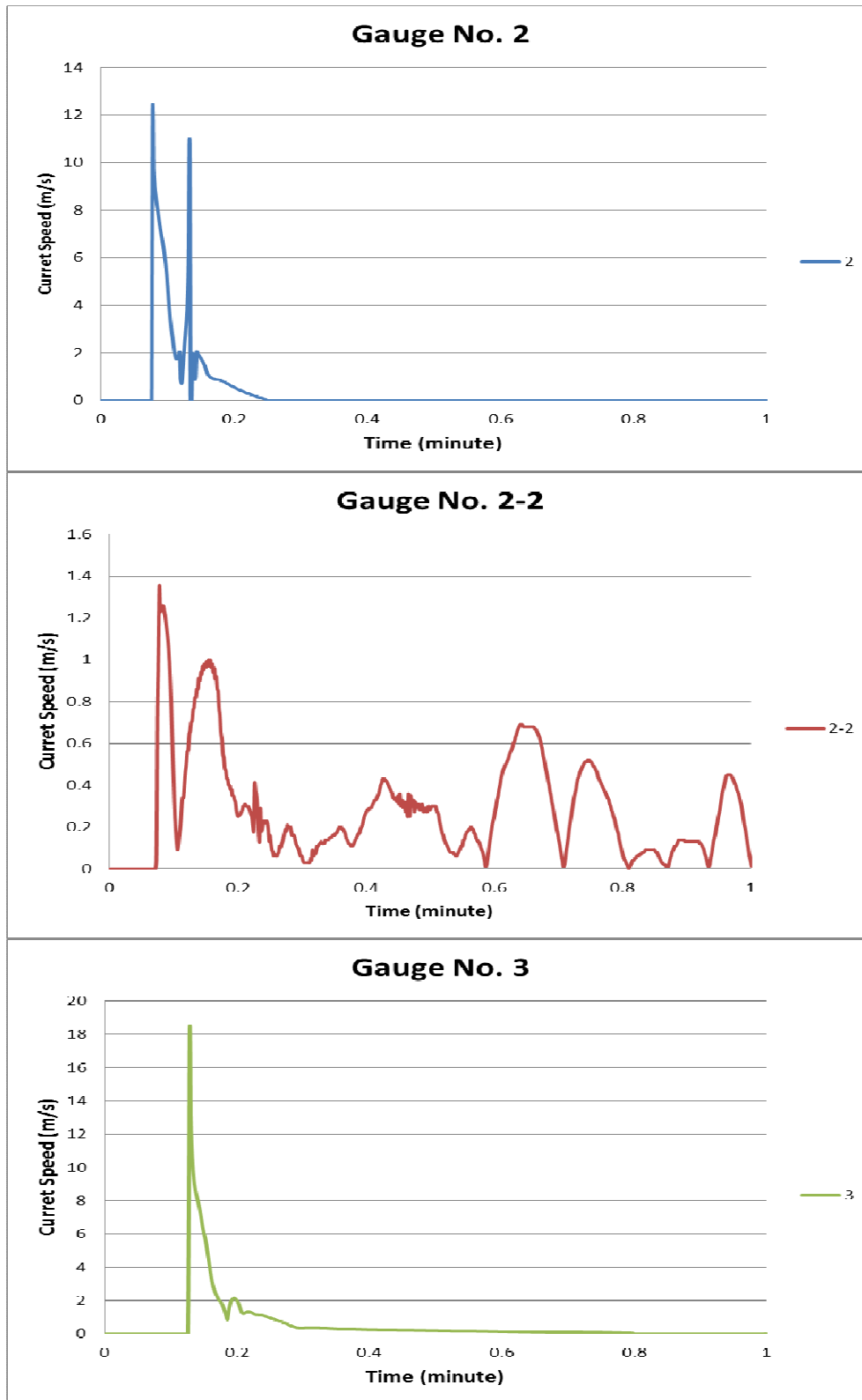


**Figure 6-20** – Time change of current speeds at selected gauge points

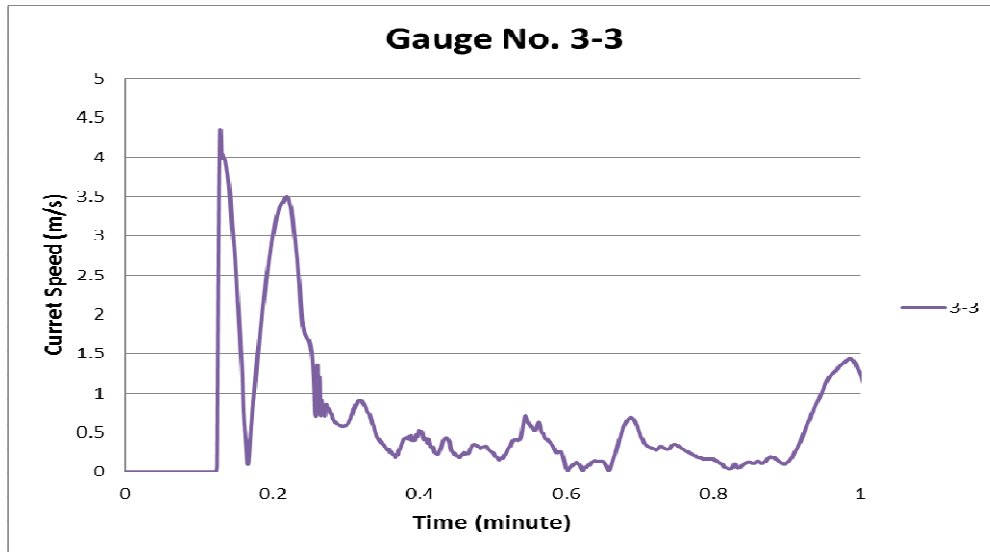


**Figure 6-21** – Time change of wave amplitude at the current speeds at selected gauge points

In the upstream face of the dam current speeds are 1.4 m/s and 4.3 m/s for gauge points 2-2 and 3-3, respectively. These values increase to 12.2 m/s and 18.4 m/s at the gauge points on the top of the dam since the flow depth decreases at the top of the dam body during the overtopping.

The duration of overtopping can be less than 1 minute with 2 or 3 repetitions. It can be suggested that the freeboard of the dam (crest elevation) should be raised to 10.5 – 11 meter in order to fully prevent overtopping. However further detailed analysis are necessary to reduce this height by computations and hence to permit partial overtopping. This is a sensitive issue needs to ensure the stability of the dam body and control the excess flow at the downstream side.

The land connection part of the freeboard will have more wave impact according to reflections from the both sides of the reservoir which may be important to review design considerations of the connection structures of the dam body to the main rock.

According to the selected landslide conditions and initial conditions simulated in this study, an overtopping is expected at the dam body. But it is also recommended here that the stability of dam body under overtopping conditions should be taken into account during design stages.

Further analysis of the initial wave due to landslide parameters is necessary for better modeling applications in Dam Reservoirs.

## CHAPTER 7

### DISCUSSIONS AND CONCLUSIONS

This study focused on landslide generated tsunamis, especially tsunamis generated by subaerial landslides caused by slope instabilities in closed basins like artificial reservoirs of dams. Different approaches of determining the parameters of impulse waves are mentioned and special attention is drawn to computer modeling.

The information on the landslide generated tsunami events is summarized. The importance of landslide characteristics (i.e. landslide volume, speed, Froude number, dimensionless slide thickness, still water depth, bulk slide density, slide impact angle, grain diameter etc.) are discussed. In order to evaluate the maximum wave amplitude generated by the landslide in closed basins the numerical modeling is performed using NAMI-DANCE and the outputs of the simulations are compared with empirical formulation proposed by Panizzo et. al. (2005). After making a total of 47 simulations with two different regular shaped bathymetries (inclined and vertical coastal slope), in a simulation duration of 90 second with different dimensions of initial wave (as 50m, 150m, 300m, 350m, 400m, 450m, 500m length and 10m, 20m, 30m, 40m, 50m subsidence) under with and without initial fluxes, the empirical formula is tested to discuss its generalization. For landslide lengths higher than 150 meter, an increase in landslide height results in higher maximum wave amplitudes. The effect of coastal slope on maximum wave amplitude is evaluated, it is understood that inclined coastal slope gives more accurate outputs. The effect of flux could not be established very successfully. For 10 meter to 30 meter landslide heights, % ERROR values fall in the range of  $\pm 15-30\%$ . Panizzo et. al. (2005) results are correlated with numerical simulation

outputs for landslide heights between 10 – 30 meters for inclined cross section without considering the initial flux of water.

The model is also applied to a case study and the effects of the potential landslide in Pervari Dam artificial reservoir is simulated using NAMI-DANCE. The landslide parameters such as landslide width, height, length and the velocity of the landslide are acquired from geological engineers for the region of landslide possibility. Since the outputs of the model highly dependent on the definition of the initial wave in the model, four different cases of initial wave are tested in simulations by using the outputs of the study of Fritz et. al. (2003) and modifying them for better application. In all of these cases the reservoir level is modeled to be at maximum level since it is the most critical stage. The distribution of maximum amplitude at different location in the dam reservoir is computed by modeling and compared with the results of empirical relation Panizzo et. al. (2005). Furthermore the possibility of wave overtopping at the crest of dam body is also investigated.

All of the four simulated input cases produced the result of maximum amplitude distribution in acceptable level. Better correlation in empirical relation is obtained for a case of initial leading elevation wave. In that case the effect of the landslide is assumed to generate a leading elevation wave with a negative amplitude in the order of landslide height and positive amplitude in the order of  $2/3$  of landslide height, where leading waves have smaller major and minor axis lengths than the depression waves. The correlation between the computed maximum amplitudes with the empirical estimations suggests that the shape of the inputs used in this study can be one of the input alternatives of the landslide generated tsunamis in enclosed basins. For further analysis and verification of the empirical relation, other input alternatives can be tested and compared with the empirical relation.

In the analysis of overtopping possibility, the higher resolution bathymetry is developed and used in the simulations. The input case which generated highest

maximum amplitude is used in the high resolution simulations. The maximum wave amplitudes computed in front of the dam body and at the dam crest are compared. According to the evaluation of the simulation results, the additional 5.5 – 6 m increase of dam crest elevation is suggested.

The artificial reservoirs created by dams are under the threat of facing landslide generated tsunamis, especially if there is slope instability. Since such a hazard can be very destructive and may result in loss of life, property and agricultural land, proper assessment becomes necessary at planning stages of the dams. The modeling study is an efficient tool in the assessment of the effects of landslide generated tsunami hazard in the enclosed basins. Hence it provides valuable information to take the necessary precautions for preventing the destructive effect. The precautions may vary from raising the freeboard or to change the dam axis to operating the dam in lower elevations. But as in any other case, sooner the issue is investigated it would be easier and cheaper to solve the problem.

The final concluding remarks for understanding the effects of the possible landslide generated tsunami in Pervari dam are;

1. Empirical relation and numerical results are compatible under the selected input conditions.
2. Risk near dam body is more than the upstream part of the reservoir. But if there is any settlement or social activities at reservoir coast, the risk must be evaluated and should be taken into account.
3. Wave amplitude near dam body cause overtopping of the dam body.
4. Higher resolution simulation outputs show that in the most extreme case, Case (c), maximum wave amplitude in the upstream face of the dam is 14.4m, on top of the dam overtopping height is 5.4m. Maximum current speed in the upstream face is 4.3m/s and at the top of the dam 18.4 m/s.
5. It can be suggested that the freeboard of the dam (crest elevation) should be raised to 10.5 – 11 meter in order to fully prevent overtopping.

However further detailed analysis are necessary to reduce this height by computations and hence to permit partial overtopping.

## REFERENCES

Alpar, B., Yalçın, A.C., Özbay, I., 2000, Marmara Denizinde potansiyel heyelan alanları ve bunlara ilişkin depreşim dalgası (tsunami) oluşum ve hareketleri, III. Ulusal Kıyı Mühendisliği Sempozyumu, TMMOB İnşaat Mühendisleri Odası, 5–7 Ekim 2000, Bildiriler Kitabı, Çanakkale, ISBN: 975-395-3999-2, pp. 17–31.

Ashtiani, B.A, Ramshe, S.Y., 2011, Numerical simulation of wave generated by landslide incidents in dam reservoirs, Landslides DOI 10.1007/s10346-011-0258-8.

Assier-Rzadkiewicz, S., Heinrich, P., Sabatier, P. C., Savoye, B., And Bourillet, J. F. (2000), Numerical modelling of landslide-generated tsunami: The 1979 Nice Event, Pure Appl. Geophys. 157, 1707–1727.

Bardet, J.P., Synolakis, C.E., Davies, H.L, Imamura, F., Okal, E.A., 2003, Landslide Tsunamis: Recent Findings and Research Directions, Pure appl. geophys. 160, 793–1809.

Bruggemann M.A., 2012, Composite Modeling of the Influence of Geometry on Landslide Generated Impulse Waves, 1st Civil and Environmental Engineering Student Conference, 25-26 June 2012, Imperial College London

Brune, S., Babeyko, A.Y., Ladage, S., Sobolev, S.V., 2010, Landslide tsunami hazard in the Indonesian Sunda Arc, Nat. Hazards Earth Syst. Sci. 10, 589–604.

Cecioni, C., Bellotti, G., 2010, Inclusion of landslide tsunamis generation into a depth integrated wave model, *Nat. Hazards Earth Syst. Sci.*, 10, 2259-2268.

Cruden D.M. & Varnes D.J. (1996), *Landslides Types and Processes*, Turner A.K. & Schuster R.L. (Eds.) *Landslides: Investigation and Mitigation*. Transportation Research Board Special Report 247, National Academy Press, WA, 36-75.

Di Risio, M., Bellotti, G., Panizzo, A., De Girolamo, P., 2008, Three-dimensional experiments on water waves generated by landslides at a sloping coast, *Coastal Engineering*, Vol. 56, No. 5-6. (May 2009), pp. 659-671.

Di Risio, M., De Girolamo, P., Bellotti, G., Panizzo, A., Aristodemo, F., Molfetta, M.G., Petrillo, A.F., 2009, Landslide generated tsunamis runup at the coast of a conical island: new physical model experiments, *J Geophys Res*, 114:C01009.

Fine, I.V., Rabinovich, A.B., 2003, Thomson, R.E., Kulikov, E.A., Numerical Modeling of Tsunami Generation by Submarine and Subaerial Landslides, A. C. Yalçiner, E. Pelinovsky, E. Okal, C. E. Synolakis (eds.), *Submarine Landslides and Tsunamis* 69-88.

Fine, I.V., Rabinovich, A.B., Bornhold, B.D., Thomson, R.E., Kulikov, E.A., 2005, The Grand Banks landslide-generated tsunami of November 18, 1929: preliminary analysis and numerical modeling, *Marine Geology* 215, 45–57.

Fritz, H.M., Hager, W.H., Minor, H.E., 2004, Near Field Characteristics of Landslide Generated Impulse Waves, *Journal Of Waterway, Port, Coastal, And Ocean Engineering*, 287-302.

Fritz, H.M., Mohammed, F., Yoo, J., 2009, Lituya Bay Landslide Impact Generated Mega-Tsunami 50th Anniversary, *Pure appl. geophys.* 166, 153–175.

Geist, E.L., Lynett, P.J, Chaytor, J.D, 2009, Hydrodynamic modeling of tsunamis from the Currituck landslide, *Marine Geology* 264, 41–52.

Geist, E.L., Jakob, M., Wieczorek, G.F., Dartnell, P., 2003, Preliminary Hydrodynamic Analysis of Landslide-Generated Waves in Tidal Inlet, Glacier Bay National Park, Alaska, Open-File Report 03-411

Giachetti, T., Paris, R., Kelfoun, K., Torrado, F.J.P., 2011, Numerical modeling of the tsunami triggered by the Güimar debris avalanche, Tenerife (Canary Islands): Comparison with field-based data, *Marine Geology* 284, 189–202.

Fritz, Hermann M., Hager W. H., Minor, H. E., 2003, Landslide generated impulse waves, *Experiments in Fluids* 35, 505–519.

Fritz, Hermann M., Mohammed, F., Yoo, J., 2009, Lituya Bay Landslide Impact Generated Mega-Tsunami 50th Anniversary, *Pure appl. geophys.* 166, 153–175.

Haeussler, P., Lee, H., Ryan, H., Labay, K., Kayen, R., Hampton, M., Suleimani, E., 2007, Submarine slope failures near Seward, Alaska, during the M9.2 1964 earthquake. Lykousis, V., Sakellariou, D., Locat, J. (eds) *Submarine Mass Movements and their consequences*, pp 269–278.

Harbitz, C.B., Løvholt, F., Pedersen, G. & Masson, D.G., 2006: Mechanisms of tsunami generation by submarine landslides: a short review. *Norwegian Journal of Geology*, Vol. 86, pp. 255-264.

Heller, V. & Hager, W.H., 2010, Impulse product parameter in landslide generated impulse waves. *Journal of Waterway, Port, Coastal, and Ocean Engineering*, 136(3), pp.145-155

Huber, A., Hager, W.H., 1997, Forecasting impulse waves in reservoirs, Commission Internationale Des Grands Barrages C.31, 993–1005.

ICOLD, 2002, Reservoir Landslides: Investigation and Management – Guidelines and case histories

Jing, D., Wang, G., 1988, The Tangyanguang landslide of Zaxi reservoir, Typical slopes in China, Science Publication House, China (in Chinese), p.301-307.

L’Heureux, J.S., Glimsdal, S., Longva, O., Hansen, L., Harbitz, C.B., 2011, The 1888 shoreline landslide and tsunami in Trondheimsfjorden, central Norway, Mar Geophys Res 32: 313–329.

Mattioli, G. S., Voight, B., Linde, A. T., Sacks, I. S., Watts, P., Widiwijayanti, C., Young, S. R., Hidayat, D., Elsworth, D., Malin, P. E., Shalev, E., Van Boskirk, E., Johnston, W., Sparks, R. S. J., Neuberg, J., Bass, V., Dunkley, P., Herd, R., Syers, T., Williams, P., and Williams, D., 2007, Unique and remarkable dilatometer measurements of pyroclastic flow-generated tsunamis, Geology, 35, 25–28.

Liu, G., 1988, Environmental geologic investigation of Xintan landslide, Environmental Geology, Volume 12, Number 1, 11-13.

Mazzanti, P., Bozzano, F., 2011, Revisiting the February 6th 1783 Scilla (Calabria, Italy) landslide and tsunami by numerical simulation, Mar. Geophys Res. 32: 273–286.

Montagna, F., Bellotti, G., Di Risio, M., 2011, 3D numerical modeling of landslide-generated tsunamis around a conical island, Nat. Hazards 58, 591–608.

Murty, T.S., 2003, Tsunami Wave Height Dependence on Landslide Volume, *Pure appl. geophys.* 160, 2147–2153.

Noda E., 1970, Water waves generated by landslides, *Journal of Waterway, Harbours, and Coastal Engineering Division-ASCE* 835-855.

Okal, E.A., Plafker, G., Synolakis, C.E. & Borrero, J.C., 2003, Near-field survey of the 1946 Aleutian tsunami on Unimak and Sanak Islands, *Bull. seism. Soc. Am.*, 93, 1226–1234.

Panizzo A., 2004, Physical and numerical modeling of subaerial landslide generated waves, PhD Thesis,

Panizzo, A., Girolamo, P. De, Risio, M. Di, Maistri, A., Petaccia, A., 2005, Great landslide events in Italian artificial reservoirs, *Natural Hazards and Earth System Sciences* 5, 733–740.

Pelinovsky, E., Zahibo, N., Dunkley, P., Edmonds, M., Herd, R., Talipova, T., Kozelkov, A., Nikolkina, I., 2004, Tsunami Generated by the Volcano Eruption on July 12-13, 2003 at Montserrat, Lesser Antilles. *Sciences of Tsunami Hazard* Vol. 22, No. 2, pages 44-57.

Plafker G., 1969, Tectonics of the March 27, 1964 Alaska Earthquake, U.S. Geological Survey Professional Paper, 543-I, 74 pp.

Poisson, B., Pedreros, R., 2010, Numerical modelling of historical landslide-generated tsunamis in the French Lesser Antilles, *Nat. Hazards Earth Syst. Sci.*, 10, 1281–1292

Rabinovich, A.B., Thomson, R.E., Bornhold, B.D, Fine, I.V., Kulikov, E.A., 2003, Numerical Modelling of Tsunamis Generated by Hypothetical Landslides in the Strait of Georgia, British Columbia, *Pure appl. geophys.* 160, 1273–1313.

Ruff, L.J., 2003, Some Aspects of Energy Balance and Tsunami Generation by Earthquakes and Landslides, *Pure appl. geophys.* 160, 2155–2176.

Sammarco, P., Renzi, E., 2008, Landslide tsunamis propagating along a plane beach, *J. Fluid Mech.* vol. 598, pp. 107–119.

Semenza, E., 2002, La storia del Vajont, raccontata dal geologo che ha scoperto la frana., Tecomproject, Ferrara.

Soloviev, S. L., Go, C. N., Kim, K. S., 1992, Catalogue of Tsunamis in the Pacific 1969-1982. Academy of Sciences of the USSR, Soviet Geophysical Committee, Moscow, Translated by Amerind Publishing Co. Pvt. Ltd, New Delhi (1988 210 pp).

Stephenson, F. E., Rabinovich, A. B., 2009, Tsunamis on the Pacific Coast of Canada recorded in 1994-2007, *Pure and Applied Geophysics*, v. 166, no. 1-2, p. 177-210.

Suleimani, E., Nicolsky, D.J., Haeussler, P.J. Hansen, R., 2011, Combined Effects of Tectonic and Landslide-Generated Tsunami Runup at Seward, Alaska During the MW 9.2 1964 Earthquake, *Pure Appl. Geophys.* 168, 1053-1074

Tinti S., Maramai A., Armigliato, A., Graziani, L., Manucci, A., Pagnoni, G., and Zaniboni, F., 2005, Observations of physical effects from tsunamis of 30 December 2002 at Stromboli volcano, Southern Italy, *Bull. Volcanol.*, in press.

Tinti, S., Pagnoni, G., Zaniboni, F., 2006, The landslides and tsunamis of the 30th of December 2002 in Stromboli analysed through numerical simulations, *Bull Volcanol* 68: 462–479.

Tinti, S., Chiocci, F.L., Zaniboni, F., Pagnoni, G., Alteriis, G., 2011, Numerical simulation of the tsunami generated by a past catastrophic landslide on the volcanic island of Ischia, Italy, *Mar Geophys Res* 32: 287–297.

Valentin H., Willi H.H., 2010, Impulse Product Parameter in Landslide Generated Impulse Waves, *Journal of Waterway, Port, Coastal, and Ocean Engineering-ASCE* May-June 2010, 145–155.

Walder, J. S., Watts, P., Sorensen, O. E., Janssen, K., 2003, Tsunamis generated by subaerial mass flows. *Journal of Geophysical Research* 108, B5, 2236.

Watts, P., Grilli, S.T., Kirby, J.T., Fryer, G. J., Tappin, D.R, 2003, Landslide tsunami case studies using a Boussinesq model and a fully nonlinear tsunami generation model, *Natural Hazards and Earth System Sciences* 3, 391–402.

Zaytsev, A., Karakus, H., Yalciner, A.C., Chernov, A., Pelinovsky, E., Kurkin, A., Ozer, C., Dilmen, D.I., Insel, I and Ozyurt, G. (2008). Tsunamis in Eastern Mediterranean, Histories, Possibilities and Realities. COPEDEC VII. Dubai. Paper No:Z-01.